Contract Report ITL-98-1
September 1998

US Army Corps of Engineers
Waterways Experiment Station

Stochastic Fatigue Crack Growth in Steel Structures Subjected to Random Loading

by Ruohua Zheng, Bruce R. Ellingwood, The Johns Hopkins University

Prepared for Headquarters, U. S. Army Corps of Engineers

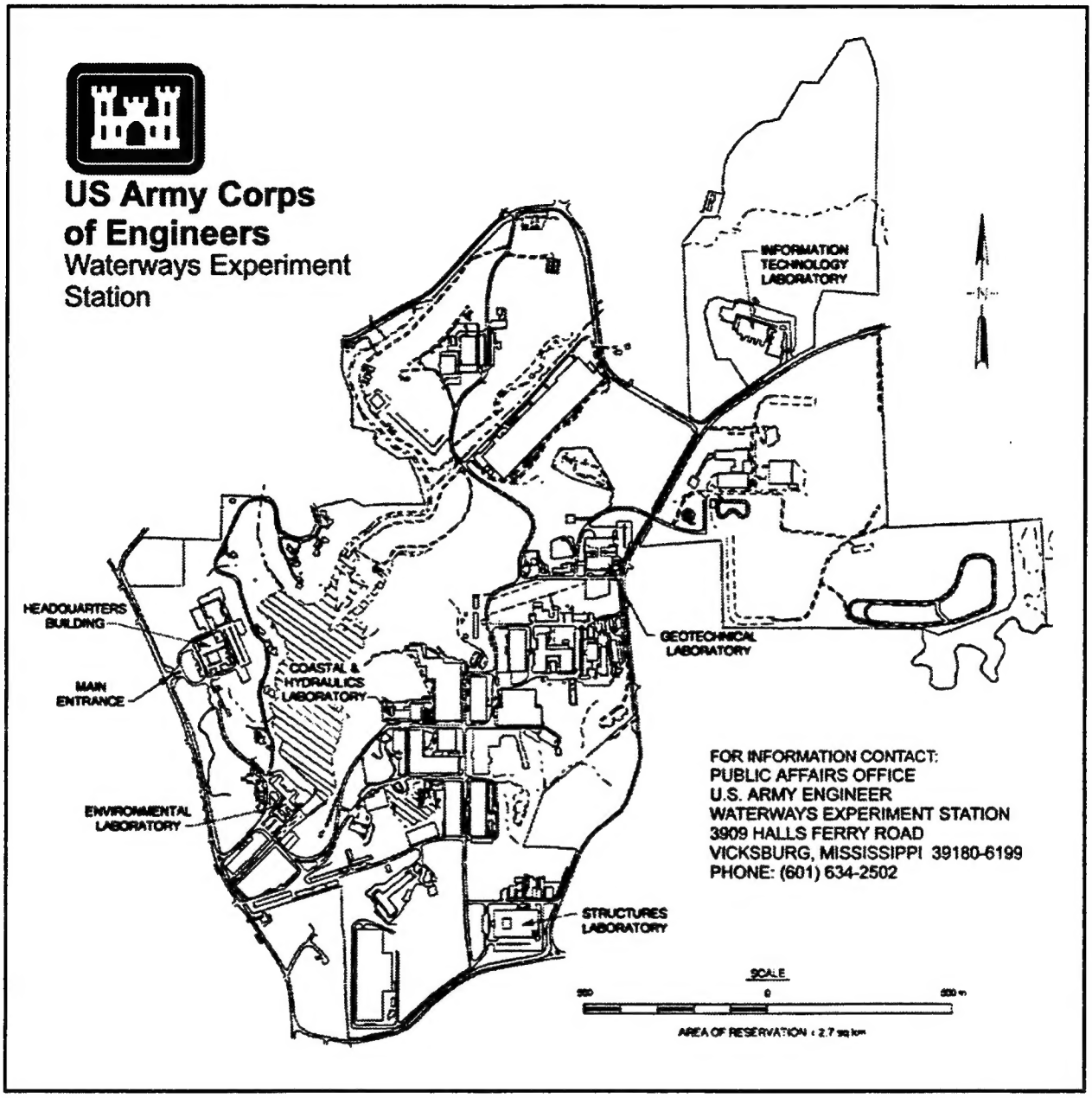

Waterways Experiment Station Cataloging-in-Publication Data

Zheng, Ruohua.

Stochastic fatigue crack growth in steel structures subjected to random loading / by Ruohua Zheng, Bruce R. Ellingwood ; prepared for U.S. Army Corps of Engineers.

157 p. : ill. ; 28 cm. — (Contract report ; ITL-98-1)

Includes bibliographical references.

1. Fracture mechanics. 2. Steel — Stress corrosion — Testing. 3. Steel, Structural —Fatigue — Testing. I. Ellingwood, Bruce R. II. United States. Army. Corps of Engineers. III. U.S. Army Engineer Waterways Experiment Station. IV. Information Technology Laboratory (U.S. Army Engineer Waterways Experiment Station) V. Computer-aided Structural Engineering Project. VI. Title. VII. Series: Contract report (U.S. Army Engineer Waterways Experiment Station) ; ITL-98-1.

TA7 W34c no.ITL-98-1

Preface

The work reported herein was performed at The Johns Hopkins University by Ruohua Zheng and Dr. Bruce R. Ellingwood. It was funded under the Risk Analysis for Water Resources Investments Research & Development Program at the U.S. Army Engineer Waterways Experiment Station (WES). The work was coordinated with Headquarters, U.S. Army Corps of Engineers (HQUSACE), by Messrs. Jerry Foster and Don Dressler of the Engineering Division, Directorate of Civil Works. Technical monitors were Dr. Mary Ann Leggett, Information Technology Laboratory (ITL), WES, and Dr. Doug B. Cleary, Black and Veatch, Federal Division. The work was performed under the general supervision of Mr. H. Wayne Jones, Chief, Computer-Aided Engineering Division, ITL, and Dr. N. Radhakrishnan, Director, ITL.

At the time of publication of this report, Director of WES was Dr. Robert W. Whalin. Commander was COL Robin R. Cababa, EN.

Contents

List of Tables

List of Figures

Chapter 1

Introduction

Fatigue is a phenomenon involving progressive damage accumulation and failure of materials under cyclic loads, the peak values of which are usually considerably smaller than the static failure load. Fatigue damage can lead to sudden failure of a structure if not controlled through proper in-service inspection and maintenance programs. According to the report of the ASCE Committee on Fatigue and Fracture Reliability (ASCE, 1982), 80% to 90% of failures in metallic structures are associated with fatigue and fracture. Deterioration and damage due to fatigue have become a significant problem in aging steel structures that are part of the nation's infrastructure, such as highway or railway bridges, gates on locks and dams on inland waterways, and offshore structures, which may be subject to a large number of load cycles during their service lives. For example, an average daily truck traffic (ADTT) count of one thousand over a bridge would impart 3.65 million load cycles to the bridge in ten years (Yen et al, 1990); an average of 18 daily hydrostatic cycles on steel miter gates at locks and dams along the Ohio River resulting from normal lockages of barges leads to about 65,700 load cycles in ten years (US Army Corps of Engineers, 1995).

The fatigue damage process occurs in two phases: crack initiation and crack propagation. In fatigue analysis of civil engineering structures, the point of demarcation between crack initiation and propagation is somewhat arbitrary, and often is determined by the capabilities of the particular non-destructive evaluation (NDE) equipment used to detect flaws in the structure. In many steel structures with welded, bolted or riveted connections, which may contain flaws as a result of normal fabrication, the total fatigue life is dominated by the fatigue crack growth phase. The traditional S-N approach (Basquin, 1910), which relates the total number of cycles (crack initiation plus propagation) to failure with stress range and is commonly used to design against structural fatigue (e.g. AASHTO, 1989), neither considers the propagation life explic-

itly nor provides information on structural parameters such as crack size or reduction of component resistance. A fracture mechanics-based approach is a more informative tool for condition assessment when crack propagation is the dominant damage accumulation mechanism; however it may lead to a conservative appraisal of service life when the structure is initially essentially flaw-free.

Deterministic fracture mechanics models based on experiments (Barsom and Rolfe, 1987) relate the median crack growth rate to stress intensity. However, considerable scatter in crack growth behavior usually is apparent even under carefully controlled experimental conditions due to material uncertainty and other unknown factors (e.g. Virkler et al, 1979). Futhermore, there rarely is any degree of certainty regarding the load cycles and environment (e.g. corrosive environment) in field situations. Uncertainties in these factors can amplify the scatter in crack growth (e.g. Barsom and Rolfe, 1987). Thus, uncertainties in prediction of crack size are unavoidable. Most of the design criteria, condition assessment procedures, and policies for management of engineered facilities subjected to fatigue service have been based on deterministic models and some empirical safety factors to account for uncertainties in fatigue behavior. Probabilistic analysis facilitates a quantitative description of the uncertainty in fatigue damage growth. Since structures are subjected to variable service conditions and no model is perfect, in-service inspection and condition assessment of fatigue damage are necessary for managing risk in an aging structure and for scheduling maintenance or repair. State-of-the-art nondestructive evaluation techniques (NDE) provide an opportunity to obtain data on fatigue crack growth in service without doing any damage to a structure. However, uncertainty exists in the ability of NDE methods to detect and measure flaws accurately. Neglecting these uncertainties not only may result in misinformed decision-making, but also may lead to unnecessary repair or hidden damage which later must be repaired. A rational approach to analyzing these sources of uncertainty is also needed.

1.1 Background

1.1.1 Fatigue

The parameters that affect structural fatigue performance include applied stress, geometry of structural details, properties of the material, and operating environment. A widely accepted empirical crack growth law originally was suggested by Paris, Gomez and Abderson (1961),

$$da/dN = C(\Delta K)^m \tag{1.1}$$

where da/dN is the increment of fatigue crack advance per stress cycle, and ΔK is the range of stress intensity factor, which is related in linear elastic fracture mechanics (LEFM) to the far-field nominal stress range, and component geometry factor. C and m are empirical constants dependent on material property and environment; m is also called the fatigue exponent.

Experimental data on fatigue crack growth are recorded as the crack size a versus the number of elapsed cycles, N. The data subsequently are transformed by numerical data processing techniques into crack growth rate da/dN versus stress intensity factor ΔK, and a graph of $\log(da/dN)$ versus $\log \Delta K$ is plotted. Regression analysis of these data provides estimates of C and m from the intercept and slope of the fitted straight line (Clark and Hudak, 1975). Due to various sources of uncertainty, to be discussed subsequently, the data are dispersed about the regression line. The variance of da/dN increases with ΔK but the standard error of the of the regression of $\log da/dN$ on $\log \Delta K$ remains essentially constant (Clark and Hudak); this standard error approximates the coefficient of variation in da/dN if the noise of $\log da/dN$ is a normal variate.

Statistical nature of crack growth

The regression analysis leading to Eqn 1.1 only describes crack growth rate in the median sense. Investigation of the randomness of fatigue crack growth rate under service load conditions must consider the statistical characteristics of the crack growth law under constant amplitude loadings and the randomness of loadings that gives rise to fatigue under variable amplitude loads.

Numerous experimental studies with a variety of materials reveal the highly variable nature of crack growth, as illustrated in Figure 1.1[1]. In a program which involved 78 tests on a 10Ni-8Co-1Mo steel plate at 15 different laboratories with several test specimen geometries, Clark and Hudak (1975) found that the primary source of variability was not associated with geometry or data processing, but with the experimental techniques to develop the a versus N data and some unknown factors. Virkler et al (1979) conducted an experimental program involving 68 replica tests on 2024-T3 aluminum alloy. They concluded that due to microscopic material inhomogeneities, crack growth rarely follows a smooth curve "unless the process is considered from a very macroscopic viewpoint." Their study also revealed that the growth rates are statistically correlated in the sense that high growth rates early in the fatigue process under constant load are likely to be maintained later in the process. In a later study

[1]Tables and figures are collected at the end of each chapter in which they appear

of small cracks in aircraft fastener holes, Hovey et al (1983) claimed that the correlation of crack growth rates along the crack path is quite important for small cracks. Barsom and Rolfe (1987) found, by comparing the fatigue test data for A36, A588 and A514 steels obtained in both benign and aggressive environments, that aggressive fatigue environments increased scatter in fatigue behavior.

Various theoretical probabilistic models of crack growth have been proposed to model the experimentally observed variability under constant amplitude loading: random variable models (Yang, et al, 1983), crack size-dependent (Ortiz and Kiremidjian, 1987; Madsen, 1985; Madsen et al, 1986; Ditlevsen, 1986) or time-dependent stochastic models (Lin and Yang, 1985; Spencer and Tang, 1988; Spencer, et al, 1989). A more detailed discussion of these models will be presented in Chapter 2. All involve a number of assumptions (e.g. the distribution of the time to failure, the nature of the correlation structures of noise) that limit their applicability. Additional developments are required to enhance these probabilistic models and to make them more generally applicable for modeling structural fatigue stochastically.

Loading uncertainty

Fatigue analysis requires a knowledge of the history of stresses, stress amplitudes or stress ranges. To first order, the development of fatigue damage depends on stress ranges. In civil engineering applications, the amplitude of the stress range is usually not constant with respect to time. Modeling the stress ranges for purposes of fatigue reliability analysis involves two parts: definition of cycles based on stress histories and identification of probabilistic characteristics of those cycles.

The stress range history of a narrow-band stress process can be clearly identified with the individual stress cycles. However, the definition of stress ranges becomes difficult where wide-band stress processes are concerned because of the complexity of the frequency content of the stress process. Different approaches have been proposed for stress range definition, such as track filtering (Veers, 1987; Fuchs et al, 1977; Nelson and Fuchs, 1977) and rainflow counting (Matsuishi and Endo, 1968). The first approach transforms the stress process into an equivalent (from a damage accumulation point of view) narrow band stress process; thus the subsequent fatigue analysis can be conducted as a narrow band stress fatigue problem. But the transformation is performed by trial and error and predictions of fatigue damage can be quite unconservative in some cases (Veers, 1987). The second approach identifies stress range from closed stress-strain loops. It has been widely used in cumulative fatigue damage based on the Palmgren-Miner rule (Miner, 1945), in which it is assumed that the portion of damage in the total fatigue life contributed by a certain stress level

is linearly proportional to the fraction of the number of cycles corresponding to that stress level. The rainflow cycle-counting algorithm has not been have been applied to crack growth analysis.

The probabilistic characteristics of cycles identified by rainflow analysis are not available. An empirical approach, involving trial and error (Wirsching and Light, 1980), or direct simulation, involving a significant computational burden, is generally required. An evaluation of the rainflow cycle counting method for handling a broad-band stress process in analyzing stochastic crack propagation should be conducted. Computationally efficient methods for treating stresses in time or cycle domains require further investigation.

1.1.2 Non-destructive evaluation

Non-destructive evaluation (NDE) can locate and size flaws in structures in service. The most common NDE techniques in civil structures are Visual Inspection (VT), Penetrant Inspection (PT), Magnetic Particle Inspection (MT), Eddy Current (EC), Radiographic Inspection (RT), Ultrasonic Inspection (UT) and Acoustic Emission (AE) (ASM, 1989; Chase, 1994). While NDE plays an essential role in in-service condition assessment, no in-service inspection is perfect. NDE outputs depend on many factors such as the condition of the structure that is inspected, the sensitivity of equipment, material imperfections and operator training and skills. There are two basic types of NDE error- detection error and sizing error- and their mathematical treatments are somewhat different.

The probability of detection ($POD(a)$) expresses the probability of detecting a crack of a given size a. For any but very large defects, there is a finite probability that the flaw escapes detection. Conversely, there is a possibility that NDE indicates a flaw when none is present (a so-called false call); repair actions in such a case not only would be unnecessary but might damage the structure. Typical POD curves are illustrated in Figure 1.2; the threshold of detection, a_{th}, depends on the NDE method chosen.

Sizing error refers to the measurement noise with respect to the true size when a flaw is detected. For example, slopes of regression lines of true size on measured size may deviate from 1 (indicating bias), and the standard error with respect to the the regression line can be as high as 20% of the thickness of the element inspected (Heasler et al, 1990). A typical regression sizing relationship relating actual flaw size, a, to measured size, a_m, is illustrated in Figure 1.3.

Extensive laboratory experiments have been conducted to quantify the NDE detection and measurement uncertainties for cracks in steel or aluminum specimens (e.g. Heasler and Doctor, 1996; Heasler et al, 1993, 1990; Bowen, et al, 1989; Berens, 1989; Rummel et al, 1989; Packman et al, 1969). However, these findings have yet to be built into a time-dependent probabilistic fatigue crack growth analysis for steel civil construction. Most NDE methods have been developed and tested for use in manufacturing, where conditions are clean. Field conditions in civil construction may be more difficult, and POD and sizing error may be more diffuse as a result. The role of uncertainties in NDE on condition assessment and time-dependent reliability analysis of existing structures requires further investigation.

1.1.3 Summary

This brief review has shown that there is significant variability in crack growth even under constant amplitude loading. Current approaches to modeling this uncertainty involve some restrictive assumptions on the statistical nature of the crack growth process. The treatment of variable amplitude loading frequently has been based on either over-simplified loading assumptions or tedious simulation. Finally, uncertainties in NDE are considerable, but have not been included in time-dependent reliability analysis of fatigue damage. Research to broaden the applicability of stochastic fatigue analysis is needed to provide a basis for developing guidelines for in-service condition assessment of civil construction.

1.2 Objective and scope

This report will develop a methodology for the reliability evaluation of fatigue crack growth in steel civil structures subject to random loadings. This will be accomplished through the following tasks:

- Generalize the stochastic fatigue crack growth models of previous studies by incorporating a time-dependent noise term described by arbitrary marginal distributions and autocorrelation structures to model the uncertainty in the crack growth under constant amplitude loading;
- Develop a computationally efficient approach for handling wide-band random loadings based on the rainflow method of stress cycle identification;

- Perform reliability analyses of a degrading structure and identify the critical parameters that affect the reliability of the structure through sensitivity studies; and
- Examine the role of NDE in probability-based condition assessment of structures, and conduct a sensitivity analysis to determine how NDE impacts time-dependent fatigue reliability.

The analysis focuses on the growth of a single dominant crack. Interaction of multiple cracks is not considered. Loadings are assumed to be stationary and effects of infrequent extreme overloads on crack growth are not considered (abrupt loadings on civil structures are relatively less frequent than those for aircraft for which the impacts of landing or takeoff are important). The analysis relies on existing experimental data and focuses on the construction of theoretical models to analyze those data. No fatigue crack growth experiments were conducted.

1.3 Organization

Chapter 2 presents background material required for stochastic fatigue analysis and structural condition assessment, including mathematical tools (concepts and calculus of stochastic processes) and deterministic methods for fatigue and fracture analysis.

Chapter 3 presents the method for modeling the uncertainty in the crack growth under constant amplitude loading and for predicting the evolution in the probability distribution of crack size during the service life of the structure. The uncertainty is described by a stationary random noise with an arbitrary autocorrelation structure and marginal distribution. The treatment of this noise is based on a combination of time and frequency domain analysis. Approaches for handling narrow-band non-Gaussian processes based on Gaussian processes and wide-band processes by an approximation based on the rainflow method of stress cycle identification are also discussed.

Chapter 4 illustrates the approaches developed in Chapter 3 through a number of parametric studies, establishing their validity with comparisons to previous analysis. A thorough sensitivity study of crack growth to different factors, such as the variances of noises and loadings, is conducted.

Chapter 5 illustrated the method by a time-dependent reliability analysis with respect to crack growth in a steel miter gate at the Emsworth Lock on the Ohio River. A model for service loadings based on the history data and a model for the

uncertainty of crack growth based on literature are proposed. A comparison is made between the predictions and the actual service history of the gate.

Chapter 6 introduces probability methods for characterizing NDE and discusses procedures for updating flaw size information using NDE techniques and Bayesian analysis. The impact of NDE on condition assessment and reliability of structures is examined. A guideline for repair decision is suggested. Examples of condition assessment based on MT and UT are illustrated.

Chapter 7 summarizes the main conclusions and contributions of this report, and recommends some topics for future research.

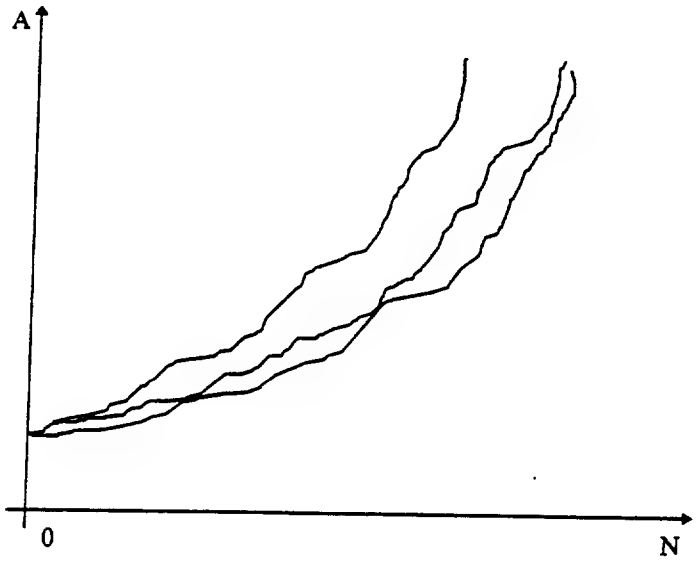

Figure 1.1: Illustration of crack growth uncertainty

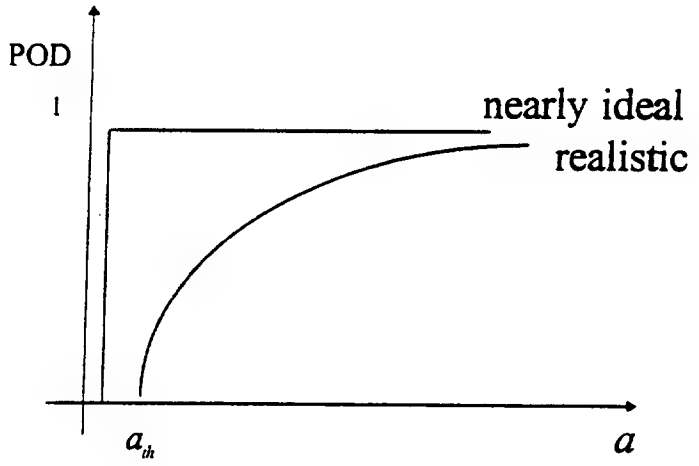

Figure 1.2: Illustration of probability of detection

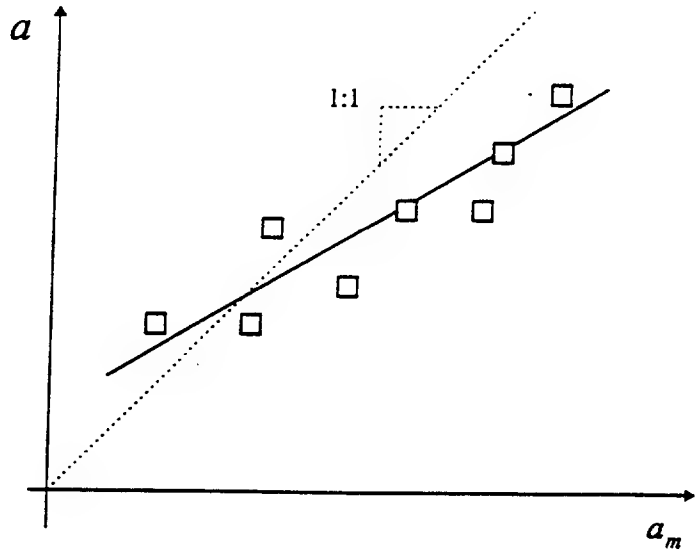

Figure 1.3: Illustration of sizing error

Chapter 2

Mathematical Tools for Stochastic Fatigue Analysis

This chapter starts with a brief overview of some basic concepts of stochastic processes and stochastic calculus. Classical deterministic approaches to fatigue and fracture analysis as well as state-of-art stochastic models to crack growth are then surveyed.

2.1 Stochastic processes

The basic mathematical tool underlying the analysis of crack growth in this report is the stochastic differential equation. In order to have a better understanding of subsequent developments, some knowledge of stochastic processes is required.

A stochastic process (s.p.) $X(t)$ is a time (or other parameter)-dependent family of random variables whose possible values at any time are governed by probabilistic laws. It becomes a random variable (r.v.) when index parameter, t, is fixed.

2.1.1 Moments and spectral density

Let $X(t)$ be a continuously valued and continuously parametered stochastic process with probability density function (PDF) $f_n(x_1, x_2, ..., x_n; t_1, t_2, ..., t_n)$. The nm^{th} joint

moment is defined by,

$$E[X^n(t_1)X^m(t_2)] = \int_{-\infty}^{\infty} x_1^n x_2^m f_2(x_1, x_2; t_1, t_2) dx_1 dx_2 \tag{2.1}$$

When $m = 0$ and $n = 1$, Eqn 2.1 defines the mean at t_1; when $m = n = 1$, it defines the autocorrelation function $R_X(t_1, t_2)$.

A stochastic process is mean-square differentiable at time t if and only if the second generalized derivative of its correlation function, defined by (Soong and Grigoriu, 1993),

$$\lim_{\tau_1,\tau_2 \to 0} \frac{1}{\tau_1 \tau_2}[R(t+\tau_1, s+\tau_2) - R(t+\tau_1, s) - R(t, s+\tau_2) + R(t, s)] \tag{2.2}$$

exists at (t,t) and is finite.

A s.p. $X(t)$ is weakly stationary if $E[X(t)]$ is constant and $R_X(t_1, t_2) = R(\tau)$, where $\tau = t_2 - t_1$. In this case, the two-sided power spectral density function (PSD) of $X(t)$ is (Parzen, 1965)

$$S_X(\omega) = \lim_{T \to \infty} \frac{1}{2\pi} \int_{-T}^{T} e^{-i\omega\tau} R_X(\tau) d\tau \tag{2.3}$$

$$= \lim_{T \to \infty} \frac{1}{\pi} \int_{0}^{T} cos(\omega\tau) R_X(\tau) d\tau \tag{2.4}$$

The relationship between the correlation function and power spectral density is defined by the Wiener-Khintchine relations,

$$R_X(\tau) = \int_{-\infty}^{\infty} e^{i\omega\tau} S_X(\omega) d\omega \tag{2.5}$$

$$= 2\int_{0}^{\infty} cos(\omega\tau) S_X(\omega) d\omega \tag{2.6}$$

The power spectral density of the n_{th} derivative of $X(t)$ is,

$$S_{X^{(n)}}(\omega) = (i\omega)^n S_X(\omega) \tag{2.7}$$

The spectral moments of a power spectral density are defined as,

$$\lambda_m = 2\int_{0}^{\infty} \omega^m S_X(\omega) d\omega \tag{2.8}$$

Parameter λ corresponds to the variance of the m^{th} derivative of $X(t)$ (Lutes and Sarkani, 1997), for example, σ_X^2, $\sigma_{\dot{X}}^2$ and $\sigma_{\ddot{X}}^2$, when m equal to 0, 2 and 4. A family of bandwidth parameters, measures of bandwidth, are described as,

$$\alpha_m = \frac{\lambda_m}{\sqrt{\lambda_0 \lambda_{2m}}} \tag{2.9}$$

which have their values between $[0, 1]$. The one that is most widely used in practice is α_2. The process is narrow band if α_2 is close to 1, and wideband if 0.

2.1.2 Mean upcrossing rate and peak distribution

The mean upcrossing rate and peak distribution are useful descriptors for structural fatigue loading, and will be used in the following chapter. The mean upcrossing rate $\nu^+(u,t)$ is the measure of the average frequency that a process crosses a certain level u with positive slope. In other words, it is the mean rate of the occurrence of the event $E = (\mathrm{X(t)=u} \cap \dot{X}(t) > 0)$ at time t. Assuming that the joint density function of $X(t)$ and $\dot{X}(t)$ is $f_{X\dot{X}}$, we have (Rice, 1945),

$$\nu^+(u,t) = \int_0^\infty w f_{X\dot{X}}(u,w,t)dw \tag{2.10}$$

The peak occurrence rate is the rate of occurrence of the event $E = (\dot{X}(t) = 0 \cap \ddot{X}(t) < 0)$. It is the zero down crossing rate of $\dot{X}(t)$,

$$\nu_p(t) = \int_{-\infty}^0 |w| f_{\dot{X}\ddot{X}}(0,w)dw \tag{2.11}$$

where $f_{\dot{X}\ddot{X}}$ is the joint density function of $\dot{X}$ and $\ddot{X}$.

The cumulative distribution function (CDF) of a peak intensity is (Rice, 1945),

$$F_p(t)(u) = \lim_{\Delta t \to 0} P(X(t) \le u | \text{peak during}(t, t+\Delta t)) \tag{2.12}$$

$$= \frac{\int_{-\infty}^0 |w| f_{X\dot{X}\ddot{X}}(u,0,w)dw}{\nu_p} \tag{2.13}$$

2.1.3 Some special stochastic processes

Gaussian process

A s.p. $X(t)$ is said to be Gaussian if for any integer n and any subset $t_1, t_2, ..., t_n$ of T, the r.v.s $X(t_1)$, $X(t_2)$,...,$X(t_n)$ have a joint Gaussian distribution. A Gaussian process is entirely determined by its mean and autocorrelation function, and all the linear transformations of $X(t)$ are also Gaussian. As a result, the derivative of a Gaussian process is still Gaussian. The original process and its first derivative are independent. The original process and its second derivative have correlation coefficient equal to α_2 (Lutes and Sarkani, 1997). If $X(t)$ has mean zero, all moments can be expressed in terms of the second-order moments by the following formula (Sobczyk, 1991),

$$E(\prod_{s=1}^n X_s) = \begin{cases} 0 & n = \text{odd} \\ \sum E[(X_{i_1} X_{i_2})]...E[(X_{i_{n-1}} X_{i_n})] & n = \text{even} \end{cases} \tag{2.14}$$

The summation is over all possible ways of combining pairs; the total number of the terms summed is $\frac{2m!}{2^m m!}$, where $m = n/2$. The mean zero-crossing rate and mean rate of occurrence of peaks for a zero mean stationary Gaussian random process, $X(t)$, are $\nu^+(t) = \frac{\sigma_{\dot{X}}}{2\pi\sigma_X}$, and $\nu_p(t) = \frac{\sigma_{\ddot{X}}}{2\pi\sigma_{\dot{X}}}$. The peak distribution is given by (Rice, 1945),

$$F_p(u) = \Phi(\frac{u-\mu_X}{\sqrt{1-\alpha_2^2}\sigma_X}) - \alpha_2 \exp(-\frac{(u-\mu_X)^2}{2\sigma_X^2})\Phi(\frac{\alpha_2(u-\mu_X)}{\sqrt{1-\alpha_2^2}\sigma_X}) \tag{2.15}$$

It often is necessary to generate Gaussian processes from a power spectral density, when studies ae conducted that involve time series. There are two widely used approaches, involving deterministic spectral amplitudes (DSA) and random spectral amplitudes (RSA).

Given a two sided power spectral density $S(\omega)$ of a Gaussian process, $X(t)$, a sample function of the discrete sequence, $X(t_i)$, $i = 0, ..., M-1$, can be obtained by the DSA method (Rice, 1954; Shinozuka and Deodatis, 1991),

$$x(t_i) = \sqrt{2}\sum_{k=0}^{N-1} A_k cos(\omega_k t_i + \Phi_k) \tag{2.16}$$

in which $A_k = (2S(\omega_k)\Delta\omega)^{1/2}$, $\omega_k = k\Delta\omega = k\frac{\omega_u}{N}$, ω_u is the cut-off frequency, and Φ_k are uniform variates with $U[0, 2\pi]$. In order to avoid aliasing, the time interval, Δt, should be selected such that $\omega_u \leq \pi/\Delta t$.

A sample function of $X(t_i)$ can be also generated by the RSA method (Rice, 1944; Tucker et al, 1984),

$$x(t_i) = \sqrt{2}\sum_{k=0}^{N-1} A_k cos(\omega_k t_i + \Phi_k) \tag{2.17}$$

in which $A_k = (R_k S(\omega_k)\Delta\omega)^{1/2}$, $\omega_k = k\Delta\omega = k\frac{\omega_u}{N}$, R_k are Rayleigh variates, and Φ_k are uniform variates with $U[0, 2\pi]$.

It may be noted that the DSA only consists of one random factor, the random phase, and the amplitudes of A_i are deterministic. As a result, realizations generated from DSA are artificially regular, and each realization has the same variance as the true random process. This is not realistic for finite length realizations. Furthermore, $x(t_i)$ is bounded as long as the number of summation terms to generate the sample is limited. In other words, the DSA method may not be able to reproduce the extremes of the process unless the value of N is large enough. The bias in extremes associated with the DSA method can be propagated into the mean and variance of the output of a nonlinear system (Ude, 1995). Also, if the power spectral density function is a

Dirac delta function, i.e., there only exists a single frequency, the process produced by the DSA is no longer Gaussian. The RSA method consists of two random factors, the random phase and the random amplitude. A realization from RSA is a more accurate reflection of the "irregularity" of the real process, especially when the m^{th} power of the amplitudes of a process are of major interest. Furthermore, the process generated by the RSA method is always Gaussian. Accordingly, the RSA method is utilized later in this study.

Wiener process

A Wiener process $W(t)$ is defined as a process with independent and stationary Gaussian increments, $\Delta W = W(t+\Delta t) - W(t)$, with $E(\Delta W) = 0$, and $E(\Delta W)^2 = \Delta t$. $W(t)$ is a Gaussian s.p. with zero mean and autocorrelation function $E[W(t)W(t+\Delta t)] = t$, where $\Delta t \geq 0$. Almost all sample functions of $W(t)$ are of unbounded variation in every finite interval (Parzen, 1965).

White noise

A white noise $\xi(t)$ process is a stationary process with zero mean and autocorrelation function $2\pi S_0\delta(t)$, in which $\delta(\bullet)$ is a Dirac delta function. Its (two sided) power spectral density is a constant, S_0, over all frequencies.

Markov and diffusion process

A Markov process $X(t)$ is one in which, given all past and present states, the knowledge of future states is dependent only on the present state. The evolution of a Markov process is described by a transition PDF, $f(y,t|x,s)$, which represents the probability density of $X(t) = y$, given that $X(s) = x$, $t > s$. In other words, all probabilistic information of a Markov process can be determined from its transition probability density function and initial state.

A special case of the Markov process is the diffusion process. A Markov process $X(t)$ is called a diffusion process if, for any $\epsilon > 0$ (Arnold, 1974),

$$\lim_{t\to s} \frac{1}{t-s} \int_{|y-x|>\epsilon} f(y,t|x,s)dy = 0 \tag{2.18}$$

and there exist $m(x,s)$ and $\sigma(x,s)$, such that

$$\lim_{t\to s}\frac{1}{t-s}\int_{|y-x|\le\epsilon}(y-x)f(y,t|x,s)dy = m(x,s) \tag{2.19}$$

$$\lim_{t\to s}\frac{1}{t-s}\int_{|y-x|\le\epsilon}(y-x)^2 f(y,t|x,s)dy = \sigma^2(x,s) \tag{2.20}$$

The first condition means that a large change in $X(t)$ over a short period of time is impossible. The drift coefficient, $m(x,s)$, describes the mean velocity of the increment $X(t)-X(s)$ under the condition $X(s)=x$. The diffusion coefficient, $\sigma^2(x,s)$, measures the local magnitude of the fluctuation of $X(t)-X(s)$ about the mean value. It can be shown (Arnold, 1974) that,

$$X(t)-X(s) \simeq m(X(s),s)(t-s)+\sigma(X(s),s)(W(t)-W(s)) \tag{2.21}$$

where the increments of a Wiener process, $W(t)-W(s)$, have the Gaussian distribution $\mathcal{N}(0,(t-s))$.

A diffusion process can be written as the solution of the Ito stochastic differential equation,

$$dX(t) = m(X,t)dt + \sigma(X,t)dW(t) \tag{2.22}$$

Analogously, a n-dimensional vector Markov diffusion process $\mathbf{X}(t)$ may be generated from a vector Ito differential equation,

$$d\mathbf{X}(t) = \mathbf{M}(\mathbf{X},t)dt + \mathbf{\Gamma}(\mathbf{X},t)d\mathbf{W}(t) \tag{2.23}$$

where $\mathbf{M}$ is a n-dimensional drift vector, $\mathbf{\Gamma\Gamma}^T$ is a nxn diffusion matrix, and $\mathbf{W}$ is a vector of n independent Wiener processes. Note that it is not necessary that all components of the vector be Markovian for the vector to be Markovian.

The transition probability density $f(y,t|x,s)$ of a Markov diffusion process is uniquely determined by the drift vector and diffusion matrix. Suppose f is continuous with respect to s and the derivatives $\partial f/\partial x_i$ and $\partial^2 f/\partial x_i\partial x_j$ exist and are continuous with respect to s. Then f is a solution of the Kolmogorov backward equation (Arnold, 1974),

$$\frac{\partial f}{\partial s}+\sum_{i=1}^{n}m_i(\mathbf{x},s)\frac{\partial f}{\partial x_i}+\frac{1}{2}\sum_{i=1}^{n}\sum_{j=1}^{n}b_{ij}(\mathbf{x},s)\frac{\partial^2 f}{\partial x_i\partial x_j}=0 \tag{2.24}$$

If $\mathbf{X}(t)$ is a homogeneous process, that is, the transition probability is dependent on $\tau = t-s$, not s, then we have,

$$-\frac{\partial f}{\partial \tau}+\sum_{i=1}^{n}m_i\frac{\partial f}{\partial x_i}+\frac{1}{2}\sum_{i=1}^{n}\sum_{j=1}^{n}b_{ij}\frac{\partial^2 f}{\partial x_i\partial x_j}=0 \tag{2.25}$$

If f is continuous with respect to t and the derivatives $\partial(m_i(\mathbf{x},t)f)/\partial x_i$ and $\partial^2(b_{ij}(\mathbf{x},t)f)/\partial x_i \partial x_j$ exist and are continuous, then f is a solution of the Kolmogorov forward (or Fokker-Planck) equation,

$$\frac{\partial f}{\partial t} + \sum_{i=1}^{n} \frac{\partial(m_i(\mathbf{x},t)f)}{\partial x_i} - \frac{1}{2}\sum_{i=1}^{n}\sum_{j=1}^{n} \frac{\partial^2(b_{ij}(\mathbf{x},t)f)}{\partial x_i \partial x_j} = 0 \qquad (2.26)$$

2.2 Fatigue and fracture

2.2.1 Deterministic approaches

Fatigue is understood to be caused by irreversible plastic shear deformation at local inhomogeneities or local stress concentrations in structural details. Research on the fatigue of materials can be traced back to around 1829, when a German mining engineer named W. Albert performed repeated load tests on mine-hoist iron chains (Suresh, 1991). Later on, interest in fatigue grew with the increasing use of metallic structures subjected to fluctuating loads. Basically, there are two different types of approaches to fatigue life prediction: the total life approach and the defect-tolerant approach.

The total life approach relates the total number of cycles to initiate a crack and propagate it until failure occurs to stress range (S-N approach) or strain range. The concept of an S-N curve was first introduced in the 1860s by the German railway engineer Wöhler (Suresh, 1991), but the empirical law which is widely employed nowadays in structural design is credited to Basquin (1910). Models considering non-zero mean stress were contributed by Gerber, Goodman and Soderberg, as reviewed in Suresh (1991). The strain-based approach is used mainly in low cycle fatigue, where behavior is inelastic and strain is a more informative parameter. A strain-cycle model was proposed by Coffin (1954) and Manson (1954) independently; a modification for mean stress was suggested by Rashe and Morrow (1969). These models are all based on constant amplitude loadings. For variable amplitude loadings, the most popular approach to fatigue damage assessment is the Palmgren-Miner rule (Miner, 1945), as mentioned in Chapter 1.

The defect-tolerant approach defines the fatigue life as the number of fatigue cycles or time required to propagate a crack from an initial size to some critical dimension. It involves empirical crack growth laws and utilizes fracture mechanics theory. Fracture can be classified into three modes: tensile opening or Mode I, in-plane sliding and tearing, and anti-plane shear (Suresh, 1991). Mode I is of most interest in civil

structures. The theory of fracture mechanics includes both linear elastic (LEFM) and nonlinear elastic-plastic fracture mechanics (EPFM).

LEFM is applicable for conditions of small scale yielding, where the nonlinear zone at the crack tip is small compared with the crack length. This approach characterizes the crack growth rate in terms of a stress intensity factor range ΔK (Irwin, 1957). EPFM deals with the case where the size of the plastic region at the crack tip becomes large with respect to the crack length, and characterizes the crack advance rate by crack tip opening displacement or J-integral (Suresh, 1991; Dowling and Begley, 1976; Dowling, 1977). Term J is the rate of change of potential energy with respect to crack advance for a nonlinear elastic material, and reduces to the strain energy release rate for a linear elastic material (Rice, 1968). LEFM is more common in structural engineering applications because it is applicable to a vast spectrum of materials and environmental loading conditions, a substantial body of supporting test data exists, and the stress intensity factor range, determined from far-field loading conditions of the cracked component, uniquely characterizes the propagation of the crack. Detailed knowledge of the micro-mechanics of fracture is not required.

Crack growth behavior exhibits three distinct regions, depending on ΔK. In the first region, below threshold ΔK_{th}, cracks remain essentially dormant. As ΔK increases, the region of stable crack growth is entered. In the third or instability region, cracks propagate rapidly, and a tearing mechanism may occur which leaves fatigue striations on the fracture surface. Although crack growth rates in the first and third regions are described in the literature (e.g. Walker, 1970; Forman et al, 1967), the stable region is of most interest for civil engineering applications. In this range, the relationship between the increment of fatigue crack advance per stress cycle, da/dN, and the stress intensity factor range, ΔK, is often modeled as (Paris, et al, 1961),

$$\frac{da}{dN} = C(\Delta K)^m \tag{2.27}$$

(often referred to as the "Paris law") in which,

$$\Delta K = Y \Delta\sigma \sqrt{\pi a} \tag{2.28}$$

and $\Delta\sigma = \sigma_{max} - \sigma_{min}$ is the far-field nominal stress range, a is the crack length, Y is the geometry factor dependent on the size of the crack relative to the component, and C and m are experimentally determined constants which depends on material properties, microstructure, structure details, environment and temperature. The exponent m is typically between 2.0 and 4.0 for ductile steels. C is around $3 \sim 4 \times 10^{-10}$ for austenitic and ferrite-pearlite steels and 0.7×10^{-8} for martensitic steels in room temperature air environment (Barsom and Rolfe, 1987), when the units of crack size and stress are inches and ksi, respectively.

For variable amplitude loading, the crack growth can be calculated on the basis of the summation of crack growth cycle-by-cycle or an equivalent stress intensity factor range ΔK_{eq}. Several proposals have been offered for ΔK_{eq}, the most common being (Hibberd and Dover, 1977; Yen, et al;1990),

$$\Delta K_{eq} = E[\Delta K_i^m]^{1/m} \tag{2.29}$$

This approach does not provide sufficient information to describe the scatter or variance in the crack growth due to the randomness of the stress history, and the extremes of the crack size distribution during the service life remain unknown. Different loading sequences might have different effects on the crack growth; for example, a high-to-low load sequence might resulted in a longer crack propagation life than a low-to-high load sequence. Using the Paris law in a cycle by cycle summation will not distinguish between such load sequence effects. However, they are more important for load histories that contain occasional large overloads, such as may occur in aircraft (Nelson, 1977), than for civil construction. Several semi-empirical prediction models (e.g. Elber, 1970; Wheeler, 1972) have been developed. But load sequence-dependent models for wide-band load histories, in which the definition of a fatigue cycle is not straightforward, are still under development.

2.2.2 Stochastic fatigue crack growth model

A stochastic fatigue crack growth model used in time-dependent reliability analysis and condition assessment of civil structures must have two parts: a description of the statistical characteristics of crack growth under constant amplitude loadings, and a means for incorporating randomness in service loads.

Statistical characteristics of crack growth law

Different stochastic crack growth models have been proposed to model uncertainties. Yang et al (1983), and others (ASCE, 1982) suggested taking the material coefficients C and m as random variables. Such models are sufficient to describe the fluctuations between the mean behavior of different specimens and environment in a very general way, but are not capable of modeling the deviation of crack growth from the mean crack path within each specimen.

Ortiz and Kiremidjian (1987) assumed that C and m are jointly distributed random variables, and introduced a crack size dependent stochastic process $X(a)$ to characterize the irregular crack growth due to micro-inhomogeneities along the crack

path: Eqn 2.27 then becomes, $dA/dN = C(\Delta K)^m X(a)$, in which $X(a)$ was assumed to be stationary with a lognormal marginal distribution and an exponential correlation structure. The mean and variance of the time to failure, that is, the time for a crack to reach a critical size, were calculated but it was claimed that the CDF of time to failure was difficult to determine. Applying their model to the experimental data of Virkler et al (1979), Ortiz and Kiremidjian found that including the autocorrelation function of the noise term $X(a)$ improved the agreement between the fatigue life prediction and the experimental data for very short cracks; for medium cracks, $X(a)$ could be taken as uncorrelated; and for very long cracks, the contribution of $X(a)$ was negligible.

Madsen et al (1986) proposed taking C as $\frac{C_1}{C_2(a)}$ in which C_1 is a positive random variable and $C_2(a)$ is a positive random process with lognormal marginal distribution. The mean and variance of the time to failure were also found, but some difficulty was encountered in determining the distribution of time to failure, and so a normal distribution was simply assumed. Ditlevsen (1986) introduced a noise term that was dependent on crack size and crack size increment, $X(a, \Delta a)$. He modeled it as an weighted integral of white noise and approximated the distribution of time to failure as an inverse Gaussian distribution. Lin and Yang (1985) introduced a time-dependent random process to represent the "combined effect of unknown contributions toward changing the crack propagation rate with time". Spencer et al (1988, 1989) and Sobczyk and Spencer (1992) later adopted this model.

The selection of an appropriate stochastic model for fatigue crack growth depends on the nature of the uncertainty to be interpreted. The application of the stochastic fatigue analysis in this study is directed toward civil infrastructure which often is exposed to a relatively aggressive environment. Time-dependent fluctuation of the crack growth from the deterministic crack growth law appears to be significant. In this study, the crack growth noise process is modeled in the time domain.

The number of loading cycles is a discrete variable with respect to time. When time-dependent stochastic analysis is conducted, the number of loading cycles is modified into a continuous variable by introducing an average cyclic rate $\overline{\nu(t)}$ for each cycle, in which $\overline{\nu(t)}$ equals the inverse of the time interval for a cycle. When the cycle occurrence frequency is large enough, the time interval for a cycle becomes very small, and the $\overline{\nu(t)}$ converges to a instant value $\nu(t)$ with respect to time. In this case, we have,

$$\frac{dA}{dt} = \frac{dA}{dn}\frac{dn}{dt} = \nu(t)\frac{dA}{dn} \tag{2.30}$$

in which A is the random flaw size (upper cases denote random variables or processes)

and $\nu(t)$ is a stochastic process. As a consequence, the Paris law can be expressed as,

$$\frac{dA}{dt} = Q(A)X(t) \tag{2.31}$$

in which $Q(A)$ = function of flaw size, stress, geometry and cyclic rate and $X(t)$ is a non-negative (thus non-Gaussian) random process, which must be selected to in such a way that the growth rate is non-negative. There are two extremes of $X(t)$: one is that $X(t)$ is temporally uncorrelated, and the other is that $X(t)$ is perfectly correlated at any two times, in which case $X(t)$ becomes a random variable and the model becomes similar to that proposed early on by Yang and others (Yang, 1983; Committee, 1982). A realistic $X(t)$ is somewhere in between (Lin and Yang, 1985).

Lin and Yang (1985) re-wrote Eqn 2.31 as,

$$\frac{dA}{dt} = Q(A)(\mu + Y(t)) \tag{2.32}$$

where $Y(t)$ is a random process with zero mean and covariance that is the same as that of $X(t)$. By assuming that the correlation time of $Y(t)$ is relatively short compared with the characteristic time of $A(t)$, they approximated $A(t)$ as a Markov diffusion process which is governed by Ito's stochastic differential equation,

$$dA = m(A,t)dt + \sigma(A,t)dW(t) \tag{2.33}$$

where $W(t)$ is a Wiener process, and the drift and diffusion coefficients, $m(A,t)$ and $\sigma(A,t)$, were obtained as functions of Q and R_Y. A closed-form solution for the transition probability density function $f(a,t|a_0,t_0)$, which determines the evolution of the Markov crack growth process, was obtained from the Fokker-Planck equation, assuming that $Q(a)$ and $\partial Q/\partial a$ vary slowly and R_Y is a triangle function.

This method is an improvement in stochastic fatigue crack growth analysis over previous methods because a transition probability density function of the crack size is found. However, modeling $A(t)$ as a Markov diffusion process requires that the correlation time of $Y(t)$ is short, which may not be realistic in some situations. Also, Eqn 2.33 implies that, since $W(t)$ is a Wiener process, dA could be negative, which is not physically reasonable. Futhermore, the marginal distribution of the noise term is not taken into account. In other words, as long as the means and autocorrelation functions of two noise processes remain the same, this method yields the same transition PDF of the crack size. This may not be appropriate for the analysis of the extremes of crack size, when the tails of the crack size distribution may be sensitive to the distribution of the noise term.

Sobczyk and Spencer (1992) and Spencer et al (1989, 1988) introduced an auxiliary Gaussian process to transform the problem into a vector Markov diffusion process.

Suppose $X(t)$ has a marginal distribution function $F_X(x)$; the (non-negative) random process $X(t)$ can be represented by the transformed process (Grigoriu, 1984)

$$X(t) = F_X^{-1}[\Phi(G(t)/\sigma_G)] \tag{2.34}$$

where $\Phi(\bullet)$ is the standard normal distribution function and $G(t)$ is an auxiliary Gaussian process obtained from the solution of the Langevin stochastic differential equation,

$$\frac{dG}{dt} = -\alpha G + \xi(t) \tag{2.35}$$

in which $\alpha > 0$ and $\xi(t)$ is a white noise with mean and autocorrelation function

$$E(\xi(t)) = 0 \qquad E(\xi(t)\xi(t+\tau)) = 2\pi S_0 \delta(\tau) \tag{2.36}$$

where S_0 is the magnitude of the constant two-sided spectral density function. The autocorrelation and spectral density functions of $G(t)$ are (Lin, 1967),

$$R_G(\tau) = \frac{\pi S_0}{\alpha} e^{-\alpha|\tau|} \tag{2.37}$$

$$S_G(\omega) = \frac{S_0}{\alpha^2 + \omega^2} \tag{2.38}$$

Thus Eqn 2.31 becomes,

$$\frac{dA}{dt} = Q(A) F_X^{-1}(\Phi(\frac{G(t)}{\sigma_G})) \tag{2.39}$$

with initial conditions, $A(0) = A_0; G(0) = G_0$. Eqns 2.35 and 2.39 can be interpreted in the Ito form; the vector $[A(t), G(t)]^T$ is a diffusion Markov process, for which the transition probability density is governed by either the Fokker-Planck equation or Kolmogorov backward equation.

Sobczyk and Spencer's approach takes into account the marginal distribution of the noise term and does not require the correlation time of the noise term to be short since the crack size A is not necessarily a Markov diffusion process. (Recall that A need not be Markovian for the vector $[A, G]^T$ to be a Markov diffusion process). However, their model is valid only if the correlation of the auxiliary process $G(t)$ has the form of Eqn 2.37. When this condition does not hold, the Langevin equation is not sufficient to capture the correlation structure of the noise, $X(t)$. A new approach is required to construct vector Markov diffusion processes with different correlation structures because the crack growth reliability analysis not only relies on the marginal distribution but also on the correlation structure of $X(t)$; different marginal distributions and correlation structures of $X(t)$ result in different correlation structures of $G(t)$. Moreover, none of the above studies considers the stochastic models of wide band loads.

Loading uncertainty

The probabilistic description of stress range required for fatigue analysis depends on the characteristics of the stress history. If the stress is modeled as a stationary narrow band process, the wave form can be expressed in terms of harmonic components, the frequencies of which are concentrated in a narrow range (Cramer and Leadbetter, 1967), and cycles within a stress history can be clearly identified. If the mean stress is zero, the range is approximately twice the value of the peak. For a stationary Gaussian process, the peak is described by a Rayleigh PDF (e.g. Cramer and Leadbetter; 1967). Thus, the stress range can be modeled as a Rayleigh random variable.

If the stress is wide band, the frequency content of the load process becomes complex and sample functions of the process have poorly defined cycles. Although the distribution of peaks of a process can still be obtained (Rice, 1944; 1945), it cannot be directly applied to fatigue analysis because the process is highly irregular. Fatigue cycles cannot be counted simply by local ranges, for numerous small peaks may obscure the large fatigue-critical load cycles.

If load sequence effects can be neglected as discussed previously, several cycle counting techniques are available. Among these, rain-flow counting is considered to be the most reliable. The rainflow counting algorithm is illustrated in Figure 2.1 (Dowling, 1983). The history is plotted with the time axis on the vertical; rain is injected at each point of stress reversal, in order, and flows by gravity down the multiple-roof-like structures according to the following rule:

1. for rain starting from the right and moving toward the left and down, the flow stops if it hits the roof whose right point is farther than or equal to the one from which it started.

2. for rain starting from the left and moving toward the right and down, the flow stops if it hits the roof whose left point is farther than or equal to the one from which it started.

3. the flow stops to avoid meeting rain from the roof above.

Computer programs have been developed (Downing and Socie, 1982) for rain-flow analysis. However, a closed-form description of the loading history is difficult. Wirsching and Light (1980) introduced an empirical correction factor, γ, which is dependent on the fatigue exponent and the irregularity factor, α_2, of the power spectral density of the stress process (cf Eqn 2.9), to associate the mean value of the m^{th} power of the stress range of a wideband Gaussian process, S_W, with that of a narrow

band process, S_N, that is, $E(\Delta S_W^m) = \gamma E(\Delta S_N^m)$, assuming the variance and zero crossing rate of the processes are the same. Later, Lutes et al (1984) showed that the irregularity factor is not sufficient to determine the correction factor and there is a need to use other parameters, but no exact solution was proposed. Lutes' study also indicated that the effect of nonnormality of the stress process on the correction factor may be significant. Therefore, efforts should be devoted to modeling the distribution of stress ranges based on the rainflow analysis. A computationally efficient approach to this problem when simulation in the time domain is involved is presented in the next chapter.

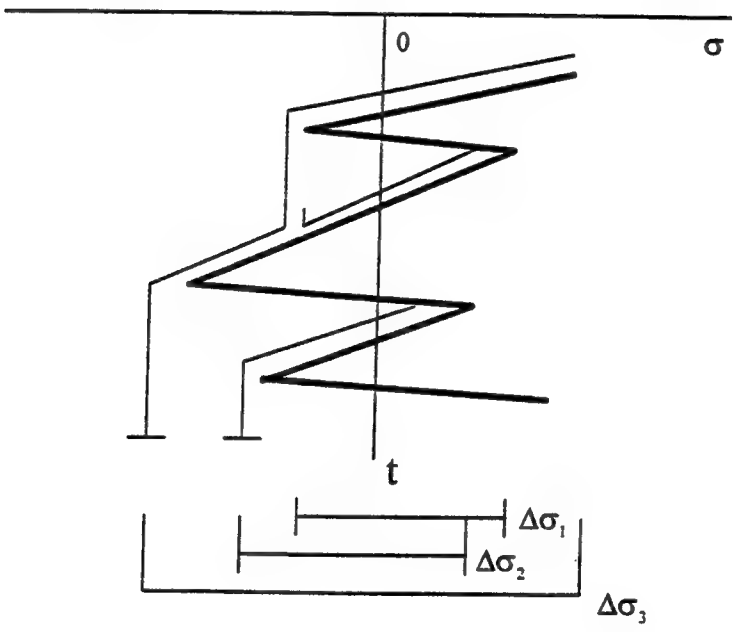

Figure 2.1: Rainflow analysis

Chapter 3

Stochastic Fatigue Crack Growth

This chapter is divided into two sections. Section 3.1 discusses treatment of the noise term that models inherent variability in the crack growth under constant amplitude loading with respect to different marginal distributions and correlation structures, and presents a theoretical model for the analysis of crack growth based on that treatment. Section 3.2 generalizes the stress range modeling beyond the traditional stationary Gaussian narrow band model. The mathematical tools developed in this chapter will be used in Chapters 4 and 5 to analyze stochastic fatigue crack propagation.

3.1 Statistical characteristics of crack growth

The time-dependent uncertainty in crack growth rate is modeled as a non-negative stationary random noise process, $X(t)$, with marginal distribution $F_X(x)$ and correlation structure $R_X(\tau)$ (cf Eqn 2.31):

$$\frac{dA}{dt} = Q(A)X(t) \tag{3.1}$$

in which $Q(A)$ = function of flaw size, stress geometry and cycling rate. The crack growth rate noise, $X(t)$, describes the inherent randomness in crack growth rate at the level of accuracy provided by the Paris equation and its experimental constants in the region where it is valid, and the test procedures that are used to obtain them. This noise generally is non-Gaussian. To facilitate the analysis of this stochastic differential equation, an auxiliary zero-mean stationary Gaussian process, $G(t)$, is introduced to generate $X(t)$ so that crack growth can be modeled as a vector Markov diffusion process (Spencer et al, 1988; 1989). The attractive feature of this approach is

that powerful tools for the analysis of vector diffusion processes have been developed and, unlike the scalar Markov diffusion model for crack growth (e.g., Lin and Yang, 1985), no assumption regarding the correlation length of the noise needs to be made.

Two conditions relating $X(t)$ and $G(t)$ are established to ensure consistency in the first and second moments: the marginal distributions and the correlation structures. The first can be easily satisfied by the transformation (Grigoriu, 1984),

$$X(t) = F_X^{-1}[\Phi(G(t))] \tag{3.2}$$

where $\Phi(\bullet)$ is the marginal distribution of the Gaussian process $G(t)$, with zero mean and standard deviation σ_G. Usually, σ_G is set equal to 1. However, some additional effort is required to accomplish the second, that is, to determine the correlation function, $R_G(\tau)$, in which $\tau = t_2 - t_1$, in order to match $R_X(\tau)$ after the above transformation.

3.1.1 Determination of $R_G(\tau)$

Examining Eqn 3.2, it is noted that an exact form of $R_G(\tau)$ is usually not available due to the complexity of the transformation function, and an approximation must be sought. One might express $G(t)$ in terms of $X(t)$ by expanding the function, $G = \Phi^{-1}F_X(x)$, in a Taylor series if it is differentiable and estimating R_G from the linear approximation. However, this approximation is not satisfactory if the function $\Phi^{-1}F_X$ is highly non-linear, which unfortunately is the usual case. But if more expansion terms are retained, it is difficult to determine the higher order moment terms $E[X(t_1)^m X(t_2)^n]$, $m + n > 2$, unless $X(t)$ is Gaussian.

The dilemma can be solved by approximating the transformation $X = F_X^{-1}\Phi(G)$ by a polynomial,

$$\hat{X}(t) = \sum_{i=0}^{n} b_i G^i(t) \tag{3.3}$$

in which the coefficients b_i are obtained by minimizing the squared errors between the exact and approximate $X(t)$. Theoretically, the highest order, n, of the polynomial can be arbitrary, depending on how small the residual error is required. In most practical cases, a second or third order polynomial is sufficient.

This approach is similar to the Hermite moment model proposed in an earlier study (Winterstein, 1988), in which a non-Gaussian response is approximated by a Gaussian process through a Hermite series based on certain specified response moments. The

order of the Hermite series equals the number of given marginal response moments minus 1. The Hermite moment models are developed for the case when the number of given moments is limited, say, less than or equal to 4, but not for the case when the actual non-Gaussian marginal distribution is available. There are various numerical techniques for polynomial approximation; in this study, least-squares regression method is employed.

Multiplying $\hat{X}(t_1)$ by $\hat{X}(t_2)$ and taking the expectation, we have

$$R_{\hat{X}}(\tau) = E[\hat{X}(t_1)\hat{X}(t_2)] \tag{3.4}$$

$$= \sum_{i=0}^{n}\sum_{j=0}^{n} b_i b_j E[G^i(t_1)G^j(t_2)] \tag{3.5}$$

in which $E[G^i(t_1)G^j(t_2)]$ is determined from the property of Gaussian processes (Grigoriu, 1995; Sobczyk, 1991),

$$E(\prod_{k=1}^{n} G(t_k)) = \begin{cases} 0 & n = \text{odd} \\ \sum E[G(t_{i_1})G(t_{i_2})]...E[G(t_{i_{n-1}})G(t_{i_n})] & n = 2m = \text{even} \end{cases} \tag{3.6}$$

where the summation is over all possible ways of combining pairs and the total number of the terms summed is $\frac{2m!}{2^m m!}$. For example,

$$E(G_1G_2G_3G_4) = E(G_1G_2)E(G_3G_4) + E(G_1G_3)E(G_2G_4) + E(G_1G_4)E(G_2G_3) \tag{3.7}$$

and

$$E[G_1^3G_2^3] = 9\sigma_G^4 R_G + 6R_G^3 \tag{3.8}$$

Eqn 3.6 indicates that $E[G_1^iG_2^j]$ is simply a polynomial function of $R_G(\tau) = E[G(t_1)G(t_2)]$. As a result, R_X can be approximated by a polynomial function of R_G, and R_G can be estimated by one of the roots of this polynomial equation. The coefficients of this equation depend on the marginal distribution of X and R_X.

The question arises as to which root should be chosen. The fact that G is mean-square differentiable requires that $R_G(\tau)$ be differentiable also. This implies that $R_G(\tau)$ should be selected from a consistent root at different time lags τ. Since σ_G is known, the correct root should be the one that satisfies $R_G(0) \simeq \sigma_G^2$. In the case when there are repeated roots at $\tau = 0$, the legitimate root $r(\tau)$ for $R_G(\tau)$ is identified by the following conditions (Soong and Grigoriu, 1993):

- $r(\tau) = r(-\tau)$
- $r^2(\tau) \leq r^2(0)$

- $r(\tau)$ is non-negative definite

The first two conditions are simple to justify. The third one is justified by Bochner's theorem (Cramer and Leadbetter, 1967), which states that $r(\tau)$ is nonnegative definite if and only if it can be represented in the form,

$$r(\tau) = \int_{-\infty}^{\infty} e^{i\tau\omega} dF(\omega) \tag{3.9}$$

where $F(\omega)$ is real, non-decreasing and bounded. In other words, the Fourier transform of r with respect to τ should be a real, non-negative and bounded function.

The method will be illustrated as follows. Suppose that

$$\hat{X} = \mathbf{BG} \tag{3.10}$$

where $\mathbf{B} = [b_0, b_1, ..., b_n]$ and $\mathbf{G} = [1, G, ..., G^n]^T$. The domain of the standard normal variable G is infinite. It is replaced by a large interval, say $(-4, 4)$, over which the least-squares experiment is conducted. The number of experimental points should be greater than $n + 1$ in order to determine $n + 1$ coefficients in $\mathbf{B}$. Suppose that n_e experiments are taken using different values of G_i, with responses X_i being given. Minimization of the squared error between the observed and estimated responses, defined as (Myers, 1971; Box and Draper, 1987),

$$L = (\mathbf{X_L} - \mathbf{BG_L})^T(\mathbf{X_L} - \mathbf{BG_L}) \tag{3.11}$$

where

$$\mathbf{X_L} = [X_1, ..., X_{n_e}]^T \tag{3.12}$$

and

$$\mathbf{G_L} = \begin{bmatrix} 1 & 1 & \cdots & 1 \\ G_1 & G_2 & \cdots & G_{n_e} \\ \vdots & & & \\ G_1^n & G_2^n & \cdots & G_{n_e}^n \end{bmatrix} \tag{3.13}$$

yields the estimator of $\mathbf{B}$,

$$\hat{\mathbf{B}} = (\mathbf{G_L}{\mathbf{G_L}}^T)^{-1}\mathbf{G_L}\mathbf{X_L} \tag{3.14}$$

This is an unbiased estimator, with $E(\hat{\mathbf{B}}) = \mathbf{B}$ and

$$cov(\hat{\mathbf{B}}) = E[(\hat{\mathbf{B}} - \mathbf{B})(\hat{\mathbf{B}} - \mathbf{B})^T] \tag{3.15}$$

$$= \sigma^2(\mathbf{G_L}\mathbf{G_L^T})^{-1} \tag{3.16}$$

where σ is the standard error of the regression, the value of which depends on the value of the highest order of the polynomial, n. It is seen that the matrix $(\mathbf{G_L G_L^T})$ plays an important role in the estimation of b_i, $i = 0, ..., n$, and the covariance between $\hat{b}_i$ and $\hat{b}_j$. The characteristics of this matrix are determined by the experimental layouts of G_i and the value of n_e. For the sake of computational efficiency for obtaining the inverse of this matrix, experimental layouts of G_i are arranged to be symmetric about 0 so that most of the off-diagonal elements in $(\mathbf{G_L G_L^T})$ and $(\mathbf{G_L G_L^T})^{-1}$ are zero (i.e., estimates of b_i and b_j are uncorrelated). The value of n_e is selected so that $cov(b_i, b_j)/\sigma^2$ is sufficiently small, say on the order of 0.1.

Suppose that $n = 2$, i.e., the polynomial is quadratic. Substituting the estimated values of b_i, $i = 0, ..., n$ into Eqn 3.10, we have,

$$\hat{X}(t_1) = b_0 + b_1 G(t_1) + b_2 G^2(t_1) \tag{3.17}$$

$$\hat{X}(t_2) = b_0 + b_1 G(t_2) + b_2 G^2(t_2) \tag{3.18}$$

Thus

$$\begin{aligned} \hat{X}(t_1)\hat{X}(t_2) &= b_0^2 + b_0 b_1 G(t_1) + b_0 b_2 G^2(t_1) \\ &+ b_0 b_1 G(t_2) + b_1^2 G(t_1)G(t_2) + b_1 b_2 G^2(t_1)G(t_2) \\ &+ b_0 b_2 G^2(t_2) + b_1 b_2 G(t_1)G^2(t_2) + b_2^2 G^2(t_1)G^2(t_2) \end{aligned} \tag{3.19}$$

Taking the expectation of equation 3.19 and combining it with Eqn 3.7, a polynomial equation describing the relationship between R_X and R_G is obtained,

$$R_X(\tau) \simeq b_0^2 + 2b_0 b_2 \sigma_G^2 + b_2^2 \sigma_G^4 + b_1^2 R_G(\tau) + 2b_2^2 R_G^2(\tau) \tag{3.20}$$

The positive root of the quadratic equation yields $R_G(\tau)$,

$$R_G(\tau) \simeq \frac{-b_1^2 + \sqrt{b_1^4 - 8b_2^2 c}}{4b_2^2} \tag{3.21}$$

where $c = b_0^2 + 2b_0 b_2 \sigma_G^2 + b_2^2 \sigma_G^4 - R_X(\tau)$.

The above approach to estimate R_G gives the desired characteristics of R_X after the transformation. A vector Markov process describing crack growth then can be constructed, as described in the next section.

3.1.2 Construction of crack growth diffusion processes

The mathematical description of a vector diffusion process is in the form of stochastic Ito differential equations, which are basically a set of linear first-order equations with

white noise as input. As noted previously, a diffusion process can be constructed from a linear differential equation with a white noise input.

From the Fourier transform theorem, it is known that an arbitrary Gaussian stationary random process with rational power spectral density (PSD) can be obtained as the output of a linear filter with white noise as the input (Lin, 1967). Moreover, a linear filter of higher order can always be transformed into a first-order system. As a consequence, an arbitrary stationary Gaussian process with a rational PSD is a component of a multi-dimensional diffusion Markov process governed by a set of linear first-order stochastic equations. This can be demonstrated by the following examples.

Example 1:

Suppose that

$$S_X(\omega) = \frac{\sigma^2\alpha}{\pi(\omega^2+\alpha^2)} \tag{3.22}$$

This (two-sided) PSD corresponds to a differential equation,

$$dX/dt + \alpha X(t) = \sigma\sqrt{2\alpha}\xi(t) \tag{3.23}$$

where $\xi(t)$ is white noise with two sided PSD equal to $\frac{1}{2\pi}$. To see this, note that the sample power spectral density function of $X(t)$ is,

$$S_X = \lim_{T\to\infty} \frac{1}{2\pi T}\mathcal{F}(X)\mathcal{F}^*(X) \tag{3.24}$$

where Fourier transform $\mathcal{F}(X) = \lim_{T\to\infty}\int_{-T}^{T} e^{-i\omega t}X(t)dt$, and $\mathcal{F}^*(X)$ is the complex conjugate of $\mathcal{F}(X)$. Performing Fourier transforms of both sides of Eqn 3.23, we have

$$\mathcal{F}(X) = H(\omega)\mathcal{F}(\xi) \tag{3.25}$$

where

$$H(\omega) = \frac{\sigma\sqrt{2\alpha}}{i\omega+\alpha} \tag{3.26}$$

Thus,

$$S_X = |H(\omega)|^2 S_\xi \tag{3.27}$$

Eqn 3.23 is of the Ito form; thus $X(t)$ is a diffusion process with drift and diffusion term αX and $2\sigma^2\alpha$. By taking the derivative of S_X with respect to ω and setting the

derivative equal to zero, it is found that the maximum value of S_X occurs at $\omega = 0$. Integrating S_X yields the standard deviation of X, σ.

Example 2:

The linear filter corresponding to the two-sided PSD

$$S_X(\omega) = \frac{2\sigma^2\alpha}{\pi} \frac{\gamma^2}{(\omega^2 - \gamma^2)^2 + 4\alpha^2\omega^2} \tag{3.28}$$

is,

$$d^2X/dt^2 + 2\alpha dX/dt + \gamma^2 X = 2\sigma\gamma\sqrt{\alpha}\xi(t) \tag{3.29}$$

Setting $X = X_1$, this equation can be re-written as,

$$\begin{cases} dX_1/dt = & X_2 \\ dX_2/dt = & -\gamma^2 X_1 - 2\alpha X_2 + 2\sigma\gamma\sqrt{\alpha}\xi(t) \end{cases} \tag{3.30}$$

Eqn 3.30 is of the Ito form, and $[X_1, X_2]^T$ is a vector Markov diffusion process with drift term

$$\mathbf{M} = [X_2, -\gamma^2 X_1 - 2\alpha X_2]^T \tag{3.31}$$

and diffusion term

$$\mathbf{\Gamma} = \begin{bmatrix} 0 & 0 \\ 0 & 4\sigma^2\alpha\gamma^2 \end{bmatrix} \tag{3.32}$$

If $\alpha << \gamma$, the maximum value of S_X occurs at $\omega \simeq \gamma$. Integrating S_X over the domain $(-\infty, \infty)$ with respect to ω yields σ^2, that is, the variance of X.

The above illustrations show that once the spectral density function of $G(t)$ is available in a rational form, a diffusion process can be easily constructed. The power spectral density S_G can be obtained from its correlation function R_G by the Fourier integral,

$$S_G(\omega) = \lim_{T\to\infty} \frac{1}{2\pi} \int_{-T}^{T} e^{iv\omega} R_G(v) dv \tag{3.33}$$

$$= \lim_{T\to\infty} \frac{1}{\pi} \int_{0}^{T} cosv\omega R_G(v) dv \tag{3.34}$$

This integral can be carried out either theoretically or numerically. If $S_G(\omega)$ is not rational in form, an approximation is required.

Selection of basic rational functions and the parameters of each function to approximate an existing PSD for $G(t)$ should be determined by factors of interest such as the area and peaks of the power spectral density function; the former represents the variance and the latter reveals the dominant frequencies of $G(t)$.

If the power spectral density function is a function with one dominant mode within the non-negative frequency domain, the rational power spectral density functions expressed in Eqn 3.22, with its peak occurring at 0, and Eqn 3.28, with its peak at γ, often are sufficient. If a more complicated power spectral density function with several contributing modes is involved, one rational function may not provide good description. In this case, the multi-mode power spectral density, S_G, can be envisioned as the summation of several single mode power spectral density functions, S_{G_i},

$$S_G = \sum_{i=1}^{n} S_{G_i} \tag{3.35}$$

This corresponds to modeling the process as the summation of several independent Gaussian processes G_i,

$$G(t) = \sum_{i=1}^{n} G_i(t) \tag{3.36}$$

in which the cross power spectral density between G_i and G_j, $i \neq j$, is zero. The variance of G is equal to the summation of the variances of G_i, $i = 1, ..., n$. By approximating S_{G_i} with a rational function, such as Eqn 3.22 or 3.28, G_i can be interpreted as the output of a linear filter with a white noise input ξ_i. The approach is illustrated as follows.

Suppose that the two-sided power spectral density of $G(t)$ has n modes within the non-negative frequency domain, one occurring at $\omega = 0$ while the others are at non-zero frequencies, as shown in Figure 3.1. The variance and dominant frequencies are of interest. Eqn 3.22 and Eqn 3.28 are taken as the basic rational functions. The former is used to characterize the zero mode, with coefficients (σ_1, α_1) to be determined; the latter characterizes the non-zero modes, with γ_i equal to the frequency at the i^{th} mode, and (σ_i, α_i) to be determined for $i = 2, ..., n$. Taking the local minimum points between adjacent modes of S_G as the demarcation points, the power spectral density of G can be divided into n segments. If the area of S_{G_i} under the non-negative domain of ω is set to be the area under i_{th} segment of S_G, the summation of the variance of G_i is equal to the area under the PSD curve of $G(t)$, implying that the variance of $G(t)$ is satisfied.

Now there are n unknown variables, α_i, left, with n conditions: the values of local

maximum of $S_G(\omega_j)$, $j = 1, ..., n$. If we define the function f as,

$$f(\omega; \alpha_1, ..., \alpha_n) = \sum_{i=1}^{n} S_{G_i} \tag{3.37}$$

in which

$$S_{G_1}(\omega) = \frac{\sigma_1^2 \alpha_1}{\pi(\omega^2 + \alpha_1^2)} \tag{3.38}$$

$$S_{G_i}(\omega) = \frac{2\sigma_i^2 \alpha_i}{\pi} \frac{\gamma_i^2}{(\omega^2 - \gamma_i^2)^2 + 4\alpha_i^2 \omega^2}, \qquad i = 2, ..., n \tag{3.39}$$

the n unknown variables, α_i, can be obtained from n nonlinear equations,

$$S_G(\omega_j) = f(\omega_j; \alpha_1, ..., \alpha_n), \qquad i = 1, ..., n \tag{3.40}$$

where $\omega_1 = 0$ and $\omega_j = \gamma_j$, $j = 2, ..., n$. The solution of the above equations can be obtained by successive substitution. Assume initial values α_{i_0} for α_i, $i = 2, ..., n$, and then solve for α_1 from

$$S_G(\omega_1) = f(\omega_1; \alpha_1, \alpha_{2_0}, ..., \alpha_{n_0}) \tag{3.41}$$

Set the solution as α_{1_0}, and solve for α_2 from

$$S_G(\omega_2) = f(\omega_2; \alpha_{1_0}, \alpha_2, \alpha_{3_0}, ..., \alpha_{n_0}) \tag{3.42}$$

Set this solution as α_{2_0}, solve for α_3, and so on, repeating this process until α_i converges to α_{i_0}. Convergence of the successive substitution method is guaranteed if the initial value is close to the solution; this condition is usually satisfied if the initial value of α_i is selected as the solution of the equations,

$$S_G(\omega_1 = 0) = S_{G_1}(0; \alpha_1) \tag{3.43}$$

$$S_G(\omega_i = \gamma_i) = S_{G_i}(\gamma_i; \alpha_i) \qquad i = 2, ..., n \tag{3.44}$$

That is, each time we estimate α_{i_0}, we assume that there is only one mode for S_G; this assumption is relaxed later by the successive substitution.

Finally, we have the set of stochastic differential equations,

$$dA/dt = Q(A)F^{-1}(\Phi(G_1 + ... + G_n) \tag{3.45}$$

$$dG_1/dt = -\alpha G_1 + \sqrt{2\alpha_1}\sigma_1 \xi_1(t) \tag{3.46}$$

$$dG_i/dt = G_{i2} \tag{3.47}$$

$$dG_{i2}/dt = -\gamma_i^2 G_i - 2\alpha_i G_{i2} + 2\sigma_i \gamma_i \sqrt{\alpha_i}\xi(t) \tag{3.48}$$

Eqn 3.45-3.48 can be interpreted in the form of Ito stochastic differential equations. As a consequence, the $2n \times 1$ vector $[A, G_1, G_2, G_{22}, ...G_n, G_{n2}]^T$ is a diffusion process, with drift vector

$$\mathbf{M} = [m_1, m_2, m_3, m_4, ..., m_{2n-1}, m_{2n}]^T \tag{3.49}$$

where

$$\begin{aligned} m_1 &= Q(A)F^{-1}(\Phi(G_1 + G_2 + ... + G_n)) && (3.50)\\ m_2 &= -\alpha G_1 && (3.51)\\ m_3 &= G_{22} && (3.52)\\ m_4 &= -\gamma_2^2 G_2 - 2\alpha_2 G_{22} && (3.53)\\ m_{2n-1} &= G_{n2} && (3.54)\\ m_{2n} &= -\gamma_n^2 G_n - 2\alpha_n G_{n2} && (3.55) \end{aligned}$$

and diffusion matrix

$$\mathbf{\Gamma(t)} = \begin{bmatrix} 0 & & & & ... & 0 \\ 0 & 2\sigma_1^2\alpha_1 & 0 & & ... & 0 \\ 0 & 0 & 0 & 0 & ... & 0 \\ 0 & 0 & 0 & 4\sigma_2^2\alpha_2\gamma_2^2 & ... & 0 \\ ... & & & & & \\ 0 & & ... & & 0 & 0 \\ 0 & & ... & & 0 & 4\sigma_n^2\alpha_n\gamma_n^2 \end{bmatrix} \tag{3.56}$$

In general, the statistical characteristics of the fatigue crack growth law with respect to different marginal distributions and correlation structures of the noise term can be modeled as an autonomous $(m+1)$-dimensional vector Ito equation,

$$d\mathbf{X}(t) = \mathbf{M}(\mathbf{X}) + \mathbf{\Gamma} d\mathbf{W}(t) \tag{3.57}$$

where $\mathbf{X} = [A, G_1, ..., G_m]^T$, $\mathbf{M}(\mathbf{X})$ is a $(m+1) \times 1$ vector which does not explicitly include t, $\mathbf{\Gamma}$ is a $(n+1) \times (n+1)$ constant matrix with all the off-diagonal elements equal to zero, and $\mathbf{W}$ is a vector Wiener process. As a result, $\mathbf{X}$ is a homogeneous Markov process, that is, its transition probability density $f(t, \mathbf{x}|s, \mathbf{x_0})$ depends only on the elapsed time $\tau = t - s$ rather than on the specific values of s and t. In this case, we express it as $f(\tau, \mathbf{x}|\mathbf{x_0})$, and without loss of generality, take $s = 0$. The solution of Eqn 3.57 will be discussed in the subsequent section.

3.1.3 Analysis of vector diffusion processes

A solution to an Ito differential equation provides a probabilistic description of the properties of the process satisfying the equation. An exact and closed form solution

is not possible in most practical situations. Most often, approximate solutions are represented by analytical formulas or simulation schemes.

Analytical approaches

Suppose $f(t, \mathbf{x}|\mathbf{x}_0)$ is the transition probability density function of the vector diffusion process $\mathbf{X} = [A, G_1, ..., G_n]^T$, with drift vector $M(\mathbf{x})$ and diffusion matrix $\mathbf{\Gamma}$. Theoretical solutions to the Ito equations are usually accomplished by either the Kolmogorov forward (Fokker-Planck-Kolmogorov) equation (Arnold, 1974),

$$\frac{\partial f}{\partial t} + \sum_{i=1}^{n} \frac{\partial (m_i(\mathbf{x}) f)}{\partial x_i} - \frac{1}{2} \sum_{i=1}^{n} \sum_{j=1}^{n} \frac{\partial^2 (b_{ij} f)}{\partial x_i \partial x_j} = 0 \tag{3.58}$$

or backward equation,

$$-\frac{\partial f}{\partial t} + \sum_{i=1}^{n} m_i(\mathbf{x}_0) \frac{\partial f}{x_{i_0}} + \frac{1}{2} \sum_{i=1}^{n} \sum_{j=1}^{n} b_{ij} \frac{\partial^2 f}{\partial x_{i_0} x_{j_0}} = 0 \tag{3.59}$$

provided that all the derivatives exist. The coefficients $b_{ij} = (\mathbf{\Gamma}\mathbf{\Gamma}^T)_{ij}$, and for the diffusion term of crack growth, the off-diagonal elements are zero if $i \neq j$.

Integrating both sides of the Kolmogorov forward equation with respect to $\mathbf{x}_0$ in its entire domain, it can be seen that the joint probability density function of $\mathbf{X}$, $f(a, g_1, ..., g_n)$, also satisfies Eqn 3.58. The probability distribution function of crack size $P_A(A(t) < a_c)$ can be obtained by integrating $f(a, g_1, ..., g_n)$ for a from 0 to a_c and for g_i, $i = 1, ..., n$, from $-\infty$ to ∞.

On the other hand, if both sides of the Kolmogorov backward equation are integrated with respect to a from 0 to a_c, and with respect to g_i, $i = 1, ..., n$, from $-\infty$ to ∞, we obtain the transition probability $P(A(t) < a_c|a_0, g_{1_0}, ..., g_{n_0})$ satisfying Eqn 3.59,

$$\frac{\partial P}{\partial t} = m_1(\mathbf{x}_0) \frac{\partial P}{\partial a_0} + \sum_{i=1}^{n} m_{i+1}(\mathbf{x}_0) \frac{\partial P}{\partial g_{i_0}} + \frac{1}{2} \sum_{i=1}^{n} b_{ii+1} \frac{\partial^2 P}{\partial g_{i_0}^2} \tag{3.60}$$

The probability distribution of the crack size $P_A = P_A(A(t) < a_c)$ can be obtained from the solution of Eqn 3.60 by the theorem of total probability,

$$P_A = \int_{-\infty}^{\infty} ... \int_{-\infty}^{\infty} \int_{0}^{a_c} P(A(t) < a_c|a_0, g_{1_0}, ..., g_{n_0}) f_0(a_0, g_{1_0}, ..., g_{n_0}) da_0 dg_{1_0} ... dg_{n_0} \tag{3.61}$$

where $f_0(a_0, g_{1_0}, ..., g_{n_0}) = f_{A_0} \phi_{G_{1_0}} ... \phi_{G_{n_0}}$, and ϕ is the normal density function. If the initial value of the crack size is deterministic, say $a_0 = c_0$, that is, f_{A_0} is a Dirac delta function, then $P_A = P(A(t) < a_c|a_0 = c_0)$.

It is usually difficult to get a closed-form solution to the Kolmogorov equations; instead, numerical tools must be employed. In this study, the finite difference method is used. The Kolmogorov forward equation involves a Dirac delta function in its initial condition when the initial crack size is deterministic. This might cause some difficulty in numerical discretization; thus, the Kolmogorov backward equation, rather than forward equation, is used to obtain the probability distribution of the crack size in this study.

It should be noted that the variables in Eqn 3.60 are $a_0, g_{1_0}, ..., g_{n_0}$, with boundary $[a_l, a_c]$ for a_0 and $(-\infty, \infty)$ for g_{i_0}, where a_l is the smallest possible initial crack size ($a_l = 0$ if no crack is present, and greater than zero if a flaw of unknown initial size is present), and a_c is the value of interest. As a result, the initial condition is,

$$P(a(0) < a_c | a_0, g_{1_0}, ..., g_{n_0}) = 1 \qquad \forall a_0, g_{i_0} \tag{3.62}$$

The number of boundary conditions (b.c.) with respect to each variable depends on the highest order of the derivatives of f with respect to that variable in Eqn 3.60. Therefore, we need one b.c. for a_0, and two for each g_{i_0}. If the initial crack size is a_c, the crack size at any given time, $t > 0$, must be no less than a_c because the crack is propagating. This implies that,

$$P(a(t) < a_c | a_c, g_{1_0}, ..., g_{n_0}) = 0 \qquad \forall g_{i_0}, t > 0 \tag{3.63}$$

The boundary condition with respect to g_{i_0} depends on the statistical characteristics of the noise term. For example, suppose that the sample space of the noise term is the positive real line; if $g_{i_0} \to \infty$, the noise term would become infinite according to monotonic property of the transformation function Eqn 3.2 between g and the noise term. As a result, the crack growth rate would be infinite at $t = 0$. Consequently, the crack size would approach infinity at any time $t > 0$, which implies that it is almost impossible for the crack size to be bounded,

$$P(a(t) < a_c | a_0, ..., \infty, ...) \simeq 0 \qquad \forall a_0, t > 0 \tag{3.64}$$

Similarly, if $g_{i_0} \to -\infty$, the noise and the crack growth rate would be zero at $t = 0$. If the noise is perfectly correlated, the crack remains in a dormant state at all times. Then we have

$$P(a(t) < a_c | a_0, ..., -\infty, ...) = 0 \qquad \forall a_0, t > 0 \tag{3.65}$$

Finally, if the noise is totally uncorrelated, the initial crack size does not affect the probability distribution of crack size at $t > 0$, meaning that,

$$\partial P(a(t) < a_c | a_0, ... - \infty ...) / \partial a_0 = 0 \qquad \forall a_0, t > 0 \tag{3.66}$$

Eqn 3.65 also implies Eqn 3.66, though not vice versa. If the correlation structure is somewhere in between these extremes, Eqn 3.66 can be adopted. Spencer and Sobczyk (1992) used Eqn 3.66 for all correlation structures.

With the initial and boundary conditions in hand, Eqn 3.60 can be solved by finite difference methods. As an example, consider a two-dimensional problem, in which time and space are divided into discrete uniform subinterval, as depicted in Figure 3.2. The partial derivatives of the parabolic equation are replaced by finite differences using the explicit method, which allows one to compute easily values of the function at time $t_i = \Delta t + t_{i-1}$ using the values at $t = t_{i-1}$. Using subscripts to denote position and superscript for time, we have,

$$\begin{aligned}\frac{P_{i,j}^{k+1} - P_{i,j}^{k}}{\Delta t} &= (m_1)_{i,j}\frac{P_{i+1,j}^{k} - P_{i,j}^{k}}{\Delta a} + (m_2)_{i,j}\frac{P_{i,j+1}^{k} - P_{i,j-1}^{k}}{2\Delta x} \\ &\quad + \frac{1}{2}b_{22}^2\frac{P_{i,j+1}^{k} - 2P_{i,j}^{k} + P_{i,j-1}^{k}}{\Delta x^2} \end{aligned} \tag{3.67}$$

If the relative size of the time and distance steps is not chosen properly, errors made at one stage of the calculations will be magnified as the computation is continued. To ensure stability and convergence in the numerical integration, $\frac{1}{2}b_{22}^2\Delta t/(\Delta x)^2$ must be less than or equal to 1/2 (Gerald and Wheatley, 1989).

Simulation approaches

An alternative solution to the Ito equations involves simulation, which generates a large number of different samples that can be used to estimate various statistical properties of the desired solution. This method is usually straightforward and is not unreasonably expensive with the use of modern computers. In this report, the Euler scheme is employed when simulation is used (Kloeden and Platen, 1992; Sobczyk, 1991). Suppose the initial value of Eqn 3.57 is $\mathbf{X}_0 = [a_0, g_{1_0}, ..., g_{n_0}]^T$, where g_{i_0} are normal variates following $N(0, \sigma_i)$. For a given discretization $0 = t_0 < t_1 < ... < t_K = T$ of the time interval $[0, T]$, the Euler scheme gives the recursive algorithm,

$$\mathbf{X}(t_{i+1}) = \mathbf{X}(t_i) + \mathbf{M}(\mathbf{X}(t_i))\Delta t + \mathbf{\Gamma}(\mathbf{W}(t_{i+1}) - \mathbf{W}(t_i)) \tag{3.68}$$

for $i = 1, ..., N-1$, with initial value $\mathbf{X}_0$. The j_{th} component of the independent vector increment $\mathbf{W}(t_{i+1}) - \mathbf{W}(t_i)$, $\Delta W_{ji} = W_j(t_{i+1}) - W_j(t_i)$ is a normal variate, with

$$E(\Delta W_{ji}) = 0 \tag{3.69}$$

$$Var(\Delta W_{ji}) = (t_{i+1} - t_i) \tag{3.70}$$

Using the Euler scheme, samples of the crack size within time interval $[0, T]$ can be obtained, and the probability distribution of the crack size can be estimated. The Euler scheme converges in the mean-square sense to $\mathbf{X}(t)$, as the time increment Δt approaches zero, and the mean-square error is $O(\Delta t)$. An appropriate Δt can be identified easily by trial and error, as illustrated subsequently.

3.2 Loading uncertainty

If the uncertainty in the load is taken into account, the crack growth rate law (without considering the model uncertainty, X) becomes,

$$dA/dt = \nu(t)Q(A, \Delta\sigma(t)) \tag{3.71}$$

where the the loading cyclic rate $\nu(t)$, and the stress ranges $\Delta\sigma(t)$ both are random processes. Depending on the nature of the service loading on the structure, the loading history may be provided either in the form of a stress range history or a stress history. The modeling approaches for these two forms of loading history are different.

If the marginal distribution $F(\bullet)$ and the correlation structure $R_{\Delta\sigma}$ of the stress range are given, the treatment of random loading in fatigue analysis is similar to what was described for the noise term of the crack growth law. The stress range is modeled as,

$$\Delta\sigma(t) = F^{-1}\Phi(G(t)) \tag{3.72}$$

where $G(t)$ is a Gaussian process with marginal distribution $\Phi(\bullet)$ and correlation function R_G, which is estimated by the polynomial approximation of the transformation function $F^{-1}\Phi$. The power spectral density function of G, S_G, is estimated in the form of a rational function, and serves as the basis for the construction of a linear filter. Finally, a vector Markov process is established to model crack growth.

If the data or structural analysis describes the stress history, however, a stress range model must be obtained from this stress history. Depending on the frequency content of the stress history, the stress process can be either narrow band or wide band. The stress range of a narrow band process can be modeled as a random variable, which is approximately twice the amplitude of the process if the mean stress is zero. The cyclic rate is approximately equal to the mean occurrence rate of peaks or zero upcrossing rate of the process. The distribution and mean occurrence rate of peaks are given in Chapter 2. For the special case when the process is stationary Gaussian, the range of a narrow band Gaussian process can be modeled as a Rayleigh random

variable and the cyclic rate is $\frac{\sigma_{\dot{X}}}{2\pi\sigma_X}$. For non-Gaussian process, it is difficult to obtain the distribution of peaks because the joint distribution of X, $\dot{X}$ and $\ddot{X}$ may not be available. An alternative way to approach the problem is to transform the process into a Gaussian process by Eqn 3.2. Since the transformation function is monotonic, the peaks of the two processes correspond to each other, and assuming the mean stress is zero, the stress ranges, which are approximately twice the peak stresses, are,

$$\Delta\sigma(t) \simeq 2F^{-1}\Phi(G_{max}) \tag{3.73}$$

where G_{max} is a Rayleigh random variable. The load cycling rate for a narrow band process is approximately the zero upcrossing rate of the process.

If the loading history is a wide band process, load cycles are indistinct and the above approaches do not apply. However, rainflow analysis, which has been widely applied in cycle counting for stress-life (e.g., Wirsching and Light, 1980) and strain-life approaches (e.g., Dowling, 1983) when loading sequence effects are neglected, can be used to define cycles in the time domain for crack propagation analysis. The justifications for this approach are: 1) each of the cycles identified by rainflow analysis of the loading history is a closed stress-strain hysteresis loop of the type obtained from constant amplitude tests, and these loops are the same for both total life and crack propagation analysis; and 2) the initiation phase in welded or riveted structures often is negligible, and therefore the propagation life is approximately equal to the total life. Since the rainflow analysis has been demonstrated experimentally to be a reliable approach to cycle counting for total life prediction, it should be applicable to the analysis of crack propagation in welded or riveted structures. Support for this judgment is provided by Suresh (1991). It should be noted that the effect of load sequencing, to the extent that it affects the fatigue behavior of the structure, cannot be reflected in the rainflow analysis because the order of the cycles is randomized. For most civil structures, this is not a significant consideration.

Crack growth can be modeled probabilistically using rainflow analysis and direct simulation:

1. Generate a discrete time series of stress σ, say M_T sets (t_i, σ_i), $i = 1, ..., M_T$, in time interval $[0, T]$, from the given power spectral density of stress. If the process is Gaussian, the random spectral amplitude approach (RSA) discussed in Chapter 2 is adopted. If the process is non-Gaussian and the marginal distribution function is known, the correlation structure of a corresponding Gaussian process can be determined by using the approach proposed in section 3.1.1. A Gaussian time series then can be generated from that correlation structure by the RSA method. A non-Gaussian sample can then be obtained by the transformation given in Eqn 3.2.

2. Conduct rainflow analysis of the time series of stress, and obtain the cycle number, n_r, and amplitudes of cycles $\Delta\sigma_i$, $i = 1, ..., n_r$ in $[0, T]$. The mean cyclic rate is estimated as $\nu = n_r/T$.

3. Using an Euler scheme, calculate the value of crack size recursively from,

$$a_{i+1} = a_i + \nu Q(a_i, \Delta\sigma_i)\Delta t; \qquad i = 1, ..., n_r \tag{3.74}$$

where Δt is assumed to be T/n_r. Thus $\nu\Delta t = 1$, and

$$a_{i+1} = a_i + Q(a_i, \Delta\sigma_i) \tag{3.75}$$

A sample function of crack size $a(t)$, from which size at any time can be determined, is obtained.

4. Repeat steps 1, 2, 3 n times, and get n samples of crack size at $t = T$, a_T^j, where the superscript j, $j = 1, ..., n$, represents the j^{th} sample.

5. Estimate the probability distribution of crack sizes at time $t = T$ by rank-ordering the values of a_T^j, and estimating the cumulative probability $F_k(a_T)$, as $k/(n+1)$, $k = 1, ..., n$.

This approach is very expensive since a large number of computations, including stress history simulation and rainflow analysis of a large sample size (say 10^5), is involved each time a sample of crack sizes at time $t = T$ is desired.

To reduce the expense of computation, a probabilistic model of stress range that is obtained from the rainflow analysis is developed instead. Conducting rainflow analysis does not preserve the correlation structure of the process as can be seen from Figure 3.3. Therefore, samples of the stress range obtained from the rainflow analysis can be envisioned as samples from a process which is uncorrelated with respect to time. The marginal distribution is estimated from a long history of stress under the assumption that the process is ergodic. The cyclic rate is available in the average sense for rainflow analysis, because the number of cycles is counted within a certain interval of time. If the stress is stationary, the variation of the total number of cycles within a long history (for a high-cycle fatigue problem) is small, as will be shown in the example in section 4.2. Accordingly, the cyclic rate can be modeled as a constant, which is equal to the mean occurrence rate of the peaks of the stress process.

The marginal distribution of the stress range process can be estimated by fitting the data with a known distribution, or by a numerical table generated from a sufficiently large sample. The former provides a closed-form model, and is often sufficient to depict the interval around the mean value; however, the description at the tail region,

which is important in reliability analysis, may be poor. The latter can characterize the behavior very well across almost the entire region of the random variable if the sample size is sufficiently large, even if no closed-form PDF is available. Since the analysis of crack growth is usually conducted by numerical methods, a closed-form model of the marginal distribution of the stress range is not essential, and the distribution can be modeled in a tabulated form. The approach is as follows:

1. Generate a long loading history, say $t = m \times T$, from a given power spectral density of the stress, where T is the time of interest for the crack growth analysis, and m is greater than or equal to 1, depending on the length of T.
2. Conduct a rainflow analysis to get the cycle number n_r and sequence of stress range amplitudes $\Delta\sigma_i$, $i = 1, ..., n_r$.
3. Estimate $\nu = n_r/(m \times T)$ and rank order $\Delta\sigma_i$ to estimate the cumulative probability of $\Delta\sigma$.

Crack growth can then be analyzed by transforming the problem into Ito equations and using the Euler scheme. Since the the stress range process is uncorrelated with respect to time, the scheme of the simulation is as follows, supposing that the crack size at $t = T$ is of interest;

1. Generate an uncorrelated sequence $\Delta\sigma_i$, i=1,...,$\lfloor \nu \times T \rfloor$, from the empirical distribution above;
2. Simulate a sample of crack size at time T, a_T, by the Euler scheme,

$$a_{i+1} = a_i + Q(a_i, \Delta\sigma_i) \qquad i = 1, ..., \lfloor \nu \times T \rfloor \tag{3.76}$$

3. Repeat steps 1 and 2 n times to get n samples of crack size at $t = T$, a_T^i, $i = 1, ..., n$
4. Estimate the probability distribution of a_T.

Computation time is reduced because the samples of stress ranges are generated from the empirical distribution obtained by analyzing one stress record instead of from a rainflow analysis for each sample. The time that is required to estimate the distribution of the stress range from one (ergodic) sample is relatively small. The error involved in this approximation and its computational efficiencies will be investigated in Chapter 4.

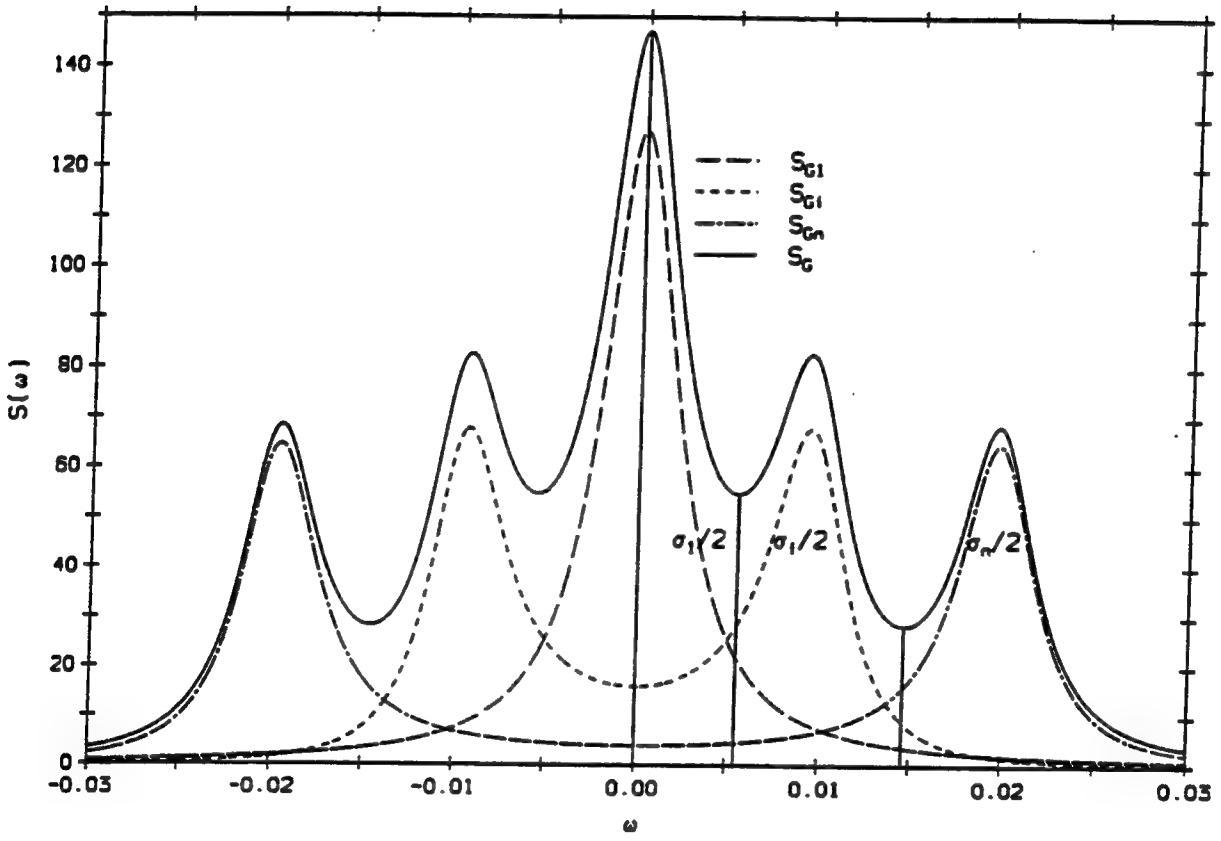

Figure 3.1: Composition of a PSD with several dominating frequencies

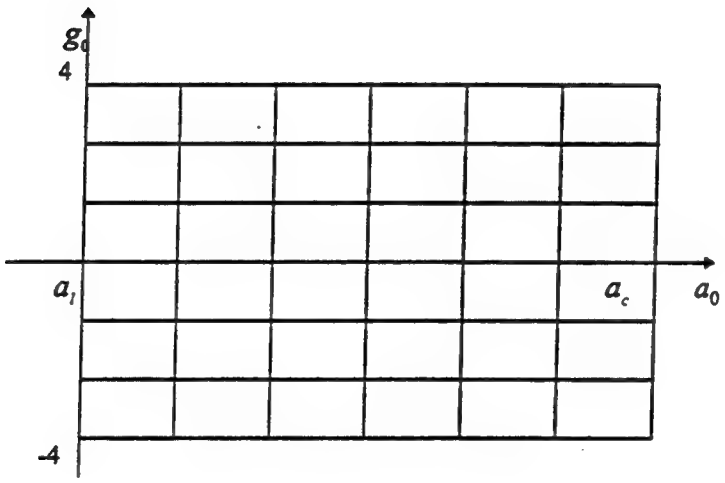

Figure 3.2: Finite difference mesh

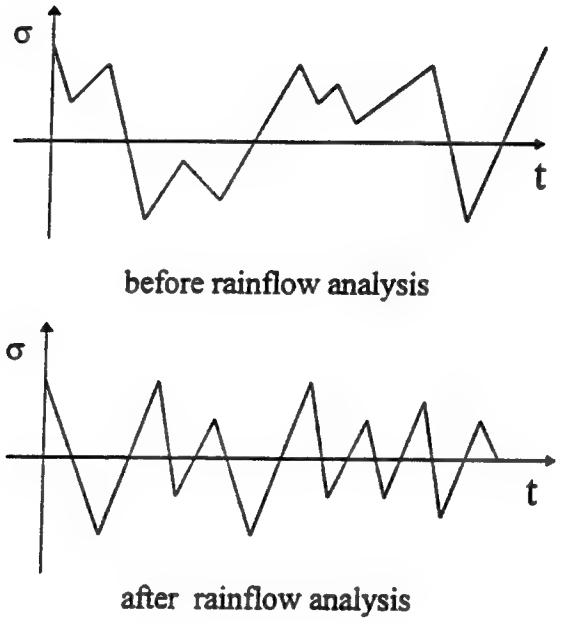

Figure 3.3: Stress histories before and after rainflow counting

Chapter 4

Fatigue Crack Growth Illustrations

In this chapter, the stochastic approaches to fatigue analysis developed in Chapter 3 are illustrated. Their validity is established and their advantages over existing methods of fatigue analysis are investigated. The sensitivity of stochastic crack growth due to different factors, such as the autocorrelation structure of the model noise term and the variance and bandwidth of the loading, is examined in detail.

4.1 Statistical evaluation of the crack growth rate model

In this section, the treatment of the noise term that models inherent randomness in the crack growth rate is illustrated. The effects of the marginal distribution and correlation structure of the noise on crack propagation are examined. The loading is deterministic and is assumed to result in constant amplitude stresses; this assumption is relaxed in section 4.2.

The stochastic crack growth rate is modeled as,

$$dA/dt = QA^b X(t) \tag{4.1}$$

in which $X(t)$ is the random noise term. This law is similar to that in Lin and Yang (1985), who applied their method to the analysis of the crack propagation of 7475-T7351 aluminum fastener specimens subjected to an aircraft load spectrum. The

parameters Q and b are constants. The noise $X(t)$ is assumed to be a stationary process with mean μ and autocorrelation function,

$$R_X(\tau) = \begin{cases} \mu_X^2 + 2\beta(1 - |\tau|/\Delta); & |\tau| \leq \Delta \\ 0; & \text{otherwise} \end{cases} \tag{4.2}$$

The initial crack size is 0.004 in (0.1 mm). The correlation time Δ is assumed to be 8000 hr, the mean μ_X is 1.0206, and the variance σ_X^2 is 2β, with β equal 0.021643. Parameters b and Q are 0.9297 and 1.1051×10^{-4}, respectively. The complementary cumulative distribution function (CCDF) at 8000 hr estimated by Lin and Yang is plotted arithmetically and on lognormal probability paper, respectively, with the solid line in Figure 4.1 and 4.2.

When the approach described in section 3.1 is applied to the same problem, assumed that the noise of $\log dA/dt$ versus $\log \Delta K$ is normal with mean equal to zero and variance equal to σ_1^2, the noise term of the crack growth rate model is modeled as,

$$X(t) = 10^{\sigma_1 G(t)} \tag{4.3}$$

The marginal distribution of $G(t)$ in Eqn 4.3 is standard normal. The relationship between $V_X = \sigma_X/\mu_X$ and σ_1 is (Ang and Tang, 1975; Benjamin and Cornell, 1970)

$$V_X^2 = \exp(\sigma_1 ln10)^2 - 1 \tag{4.4}$$

In order to estimate the autocorrelation function of $G(t)$, Eqn 4.3 is approximated by a quadratic equation as explained in Chapter 3,

$$X \simeq b_0 + b_1 G + b_2 G^2 \tag{4.5}$$

in which the coefficients b_i are determined by least-squares regression analysis. Experimental runs are conducted with experimental points G_i evenly distributed over domain $(-4, 4)$ at intervals of 0.5. The responses X_i corresponding to G_i are computed from Eqn 4.3. By minimizing the mean-squared error, we find that $b_0 = 0.9981$, $b_1 = 0.2169$ and $b_2 = 0.0214$. The results of this approximation are presented in Figure 4.3, where it can be seen that Eqn 4.5 is a good fit to Eqn 4.3. The integral of the mean-square error over the domain $(-4, 4)$ is 1.643×10^{-3}.

The relationship between the autocorrelation function of $G(t)$ and $X(t)$, derived from Eqn 4.5, is (cf Chapter 3),

$$R_X \simeq b_0^2 + 2b_0 b_2 \sigma_G^2 + b_2^2 \sigma_G^4 + b_1^2 R_{G_1 G_2} + 2b_2^2 R_{G_1 G_2}^2 \tag{4.6}$$

or,

$$R_G(\tau) \simeq \frac{-b_1^2 + \sqrt{b_1^4 - 8b_2^2 c}}{4b_2^2} \tag{4.7}$$

The R_G thus determined is plotted in Figure 4.4 and has a triangular shape. This is not surprising if we examine Eqn 4.6 closely. The ratio b_2/b_1 is less than 0.1, its square is smaller than 0.01, and the contribution of the last term, i.e., the nonlinear contribution, is relatively small. Accordingly, R_G is approximately linear in R_X, the shape of which is a triangle superimposed on a rectangle. The first three terms of Eqn 4.6 are constants, which represent the constant component induced from μ_X. As a result, the shape of R_X has a triangular form.

The two-sided power spectral density function of $G(t)$ is obtained by the integral,

$$\begin{aligned} S_G(\omega) &= \frac{1}{\pi}\int_0^\infty \cos\tau\omega R_G(\tau)d\tau & (4.8)\\ &= \frac{1}{\pi}\int_0^\Delta \cos\tau\omega(1-\tau/\Delta)d\tau & (4.9)\\ &= \frac{1-\cos\Delta\omega}{\pi\Delta\omega^2} & (4.10)\\ &= \frac{\Delta/2}{\pi(\omega\Delta/2)^2}\sin^2(\omega\Delta/2) & (4.11) \end{aligned}$$

$S_G(\omega)$ is plotted with the solid line in Figure 4.5. The dominant frequency is zero, at which $S_G(0) = \Delta/2\pi$.

In order to construct a Markov diffusion process model for crack growth analysis, $S_G(\omega)$ is replaced by a rational function, as discussed in Chapter 3. There is only one dominant frequency centered at zero; accordingly, the function,

$$\hat{S}_G = \frac{\sigma_G^2\alpha}{\pi(\omega^2+\alpha^2)} \tag{4.12}$$

which corresponds to the first-order linear filter,

$$dG/dt = -\alpha G + \sqrt{2\alpha}\xi(t) \tag{4.13}$$

is judged to be sufficient when only the standard deviation and dominant frequency are the factors of interest. The constant σ_G is the standard deviation of G and α is determined by,

$$S_G(0) = \Delta/(2\pi) = \frac{\sigma_G^2}{\pi\alpha} \tag{4.14}$$

As a result, σ_G equals 1 and α equals 2.5×10^{-4}. Eqn 4.12 is plotted with the dashed line in Figure 4.5 for comparison with Eqn 4.11.

Approximating Eqn 4.11 with Eqn 4.12 implies that R_G is now approximated by an exponential function,

$$R_G = \exp(-\alpha|\tau|) \tag{4.15}$$

To examine the error regarding the correlation function of the noise term X due to the above numerical approximation, the estimate of R_X obtained by substituting Eqn 4.15 into Eqn 4.6 is plotted with the dashed line in Figure 4.6 for comparison with the true R_X. It can be seen that the maximum absolute value of the relative error for $R_X(\tau)$ is less than 1%.

Based on Eqns 4.13 and 4.3, the fatigue crack growth now is formulated as a two-dimensional vector Markov diffusion process,

$$dA/dt = QA^b 10^{\sigma_1 G(t)} \tag{4.16}$$

$$dG/dt = -\alpha G + \sqrt{2\alpha}\xi(t) \tag{4.17}$$

with drift term,

$$\mathbf{M} = [m_1, m_2]^T = [QA^b 10^{\sigma_1 G}, -\alpha G]^T \tag{4.18}$$

and diffusion term,

$$\Gamma = \begin{bmatrix} 0 & 0 \\ 0 & 2\alpha \end{bmatrix} \tag{4.19}$$

with initial condition $[a_0, g_0]$, where a_0 = 0.004in (0.1mm) and g_0 is a standard normal variate. Due to the complexity of the drift components, a closed-form solution to Eqns 4.16 and 4.17 is not possible. As discussed in Chapter 3, there are two approaches to obtain an approximate solution: the Euler scheme or the numerical solution to the Kolmogorov backward equation. The Euler simulation-based scheme is straightforward, and its accuracy depends on the time step dt. The solution obtained from this approach for dt = 1.0 hr is plotted with the solid curve on lognormal probability paper in Figure 4.7. To check whether the time step is small enough, a smaller value dt = 0.01 hr is assumed, and the solution is plotted with the dashed curve in Figure 4.7. The result is close to that obtained using dt = 1.0 hr, which implies that dt = 1.0 hr is sufficient. The CPU time required is about 80 sec when dt = 1.0 hr and the sample size of crack length at T = 8000 hr equals 2000.

The Kolmogrov backward equation for the crack growth process is,

$$-\frac{\partial f}{\partial t} + m_1(a_0, g_0)\frac{\partial f}{a_0} + m_2(a_0, g_0)\frac{\partial f}{g_0} + \alpha\frac{\partial^2 f}{\partial g_0^2} = 0 \tag{4.20}$$

Integrating both sides of the equation with respect to a from 0 to a_c, and with respect to g, from $-\infty$ to ∞, the transition probability $P(A(t) \leq a_c|a_0, g_0)$ satisfies,

$$\frac{\partial P}{\partial t} = m_1(a_0, g_0)\frac{\partial P}{\partial a_0} + m_2(a_0, g_0)\frac{\partial P}{g_0} + \alpha\frac{\partial^2 P}{\partial g_0^2} \tag{4.21}$$

with initial condition,

$$P(A(0) \leq a_c|a_0, g_0) = 1 \qquad \forall a_0 in [a_l, a_c] \tag{4.22}$$

and boundary conditions,

$$P(A(t) \leq a_c|a_c, g_0) = 0 \qquad \forall g_0 \tag{4.23}$$

$$P(A(t) \leq a_c|a_0, \infty) = 0 \qquad \forall a_0 \tag{4.24}$$

$$\partial P(A(t) \leq a_c|a_0, -\infty)/\partial g_0 = 0 \qquad \forall a_0 \tag{4.25}$$

where a_l, the lower bound of the variable a_0, is 0.004 in (0.1mm).

The explicit finite difference scheme discussed in Chapter 3 is used to solve Eqns 4.21-4.25. The infinite domain of G is approximated by $(-4, 4)$, the intervals of a_0 and g_0 are 3.0×10^{-4} and 4.0×10^{-2}, respectively, and the interval of Δt is less than $\Delta x^2/(4\alpha^2)$ to ensure the stability of the solution $P(A(t) \leq a_c|a_0, g_0)$.

Since the initial crack size is a single value, a_l, we have,

$$P(A(t) \leq a_c) = \int_{-\infty}^{\infty} P(A(t) \leq a_c|a_0 = a_l, g_0)\phi(g_0)dg_0 \tag{4.26}$$

The probability of crack exceedance $P(A(t) > a_c)$ at $T = 8000$ hr is plotted with the dot-dashed curve in Figure 4.8 for comparison with the Euler scheme solution. Figure 4.8 shows that there are some differences between the solutions. As the mesh of the finite difference method becomes finer (interval of crack size da_0 is reduced to 1.5×10^{-4}), the difference between the solutions becomes smaller. However, the computation time required for the explicit finite difference method is expensive, with 6 hr for the original mesh and 1 day for the refined mesh, while the CPU time required for the Euler scheme is only 80 sec. Therefore, unless the problem is simple and a closed-form solution can be obtained from the Kolmogorov equation, the Euler scheme is preferable. In the following, solutions to the Ito equations all are obtained by the Euler scheme.

For comparison with the result obtained by Lin and Yang (1985), the solution from the proposed Euler scheme with $dt = 1$ hr is plotted with a dashed curve in

Figures 4.1 and 4.2. Over the central region of the CCDF (95% interval of the crack size), both results are close. However, it can be seen that there is some deviation between the two solutions at the extremes of the probability distribution. There are two possible sources for the difference. One is the numerical error of the proposed approach, arising from the approximation of R_X and solution of Eqn 4.21. The second is the assumption made by Lin and Yang (1985): "the correlation time of the noise term is short compared with the characteristic time of $a(t)$". Note that in this example, the correlation time was equal to the total time of interest for crack growth (8000 hr).

To investigate whether the latter is indeed the main source of the difference, another numerical experiment was conducted in which it was assumed that the correlation time is much shorter, say, 80 hr, which is 1% of the total time of interest for crack growth; while all other parameters remain the same. The difference between the estimated R_X and the true R_X, plotted in Figure 4.9, is similar to that of the previous example when Δ is reduced. Both solutions for CCDF of crack size at $T = 8000$ hr are plotted on lognormal paper in Figure 4.10. It is seen that even at the extremes of the probability distribution, the results are quite close to each other when $\Delta = 80$ hr. These imply that the main source of the difference between the results in the previous example is not the numerical error of the proposed method, but the assumption regarding the length of the correlation time with respect to characteristic time of $a(t)$. When Δ/T is small, this assumption is valid and both approaches lead to similar results. When the correlation time increases, this assumption may no longer be valid; however, the proposed method can be still applied since it involves no assumption regarding correlation time. To further confirm the agreement of both approaches when Δ/T gets smaller, we increase the time of interest to $T = 12,000$ hr, while the correlation length is assumed to be 8000 and 80 hr, respectively. The CDFs are plotted on lognormal paper in Figure 4.11, and it is seen that the conclusion holds when T increases.

The mean and variance of the crack size both increase when time is increased. The coefficient of variation of the crack size (c.o.v.(a)) when $\Delta = 80$ hr and 8000 hr is calculated and plotted versus time with the solid line in Figure 4.12. The value of c.o.v.(a_t) increases as time increases. The mean and variance of the time required for the crack size to reach a given size also increase with respect to the crack size. However, as can be seen in Figure 4.13, the value of c.o.v.(t_a) decreases as the crack size increases in the short crack length region, and approaches a constant as the crack size gets longer. This trend is consistent with other experimental and theoretical studies of the statistical nature of fatigue crack propagation in 2024-T3 aluminum alloy (Virkler et al (1979); Ortiz and Kiremidjian (1986)). The correlation length Δ of the noise term also affects the values of c.o.v.(a_t) and c.o.v.(t_a), as can be seen

by comparing the results in Figures 4.12 and 4.13 for different values of Δ. The shorter correlation length leads to smaller values of c.o.v. in both cases. In other words, uncorrelated noise results in the smallest dispersion in the crack size at a certain time and in the time to reach a crack size. Therefore, the stochastic model $dA/dN = C(\Delta K)^m X$, in which X is treated as a random variable rather than a random process, would overestimate the scatter in crack size at a given time in the service life. However, at a given time, the CCDF of crack size not only depends on the scatter, but also on the mean of the crack size, which has only a slight increase when the noise becomes more correlated as can be seen in Figure 4.14. As a result, whether taking X as a random variable is a more conservative approach when estimating the failure probability depends on the critical flaw size.

Lin and Yang's approach only takes into account the first two moments of $X(t)$. In other words, as long as the autocorrelation function of the noise is the same, their model yields the same probability distribution of crack size, regardless of the marginal distribution of $X(t)$. In order to examine the effect of the marginal distribution of $X(t)$ on the CDF of $a(t)$, the lognormal distribution of $X(t)$ is replaced by a uniform distribution; the target mean and autocorrelation function remain the same. In this case,

$$X = (b-a)\Phi(G) + a \tag{4.27}$$

where

$$a = \mu_X - \sqrt{3}\sigma_X \tag{4.28}$$

and

$$b = \mu_X + \sqrt{3}\sigma_X \tag{4.29}$$

It was found that $a = 0.6602$ and $b = 1.3810$ by substituting the values of μ_X and σ_X into Eqns 4.28 and 4.29.

Due to the behavior of the uniform distribution, a quadratic polynomial is not sufficient to approximate Eqn 4.27. Instead, a cubic polynomial is employed,

$$X = b_0 + b_1 G + b_2 G^2 + b_3 G^3 \tag{4.30}$$

with coefficients, $b_0 = 1.0206$, $b_1 = 0.2352$, $b_2 = 0.0$ and $b_3 = -0.0134$ obtained by least-squares regression analysis, as discussed before. The correlation function of R_G must satisfy,

$$R_G^3 + pR_G + q = 0 \tag{4.31}$$

where

$$p = (b_1^2 + 6b_3b_1 + 9b_3^2)/(6b_3^2) \qquad (4.32)$$
$$q = (b_0^2 - R_X)/(6b_3^2)$$

There are two imaginary roots and one real root. The real root is,

$$R_G = A^{1/3} + B^{1/3} \qquad (4.33)$$

where

$$A = -0.5q + \sqrt{p^3/27 + q^2/4} \qquad (4.34)$$
$$B = -0.5q - \sqrt{p^3/27 + q^2/4}$$

This R_G is plotted in Figure 4.15. The reason for the linearity in R_G can be seen by examining Eqn 4.31 and the values of b_3 and b_1, which implies that the linear terms dominate the function of R_G. Accordingly, a linear filter described by Eqn 4.13 is employed to construct an auxiliary Markov process for crack growth. This implies that R_G is approximated by the exponential function Eqn 4.15. The estimated values of R_X, based on the the estimated values R_G, and Eqn 4.31 are compared with the true R_X in Figure 4.16. The relative error is less than 1%.

Based on Eqn 4.27 and Eqn 4.13, the probability distribution of crack size is obtained by the Euler scheme discussed in Chapter 3, and the result is plotted with the dash-dotted line in Figure 4.17 for $T = 8000$ hr and $\Delta = 8000$ hr. The CCDF becomes asymptotic at its extremes because the domain of the noise term is limited for an uniform distribution. Note that there can be a considerable difference in the probability distribution of crack size, depending on the assumptions made regarding the marginal distribution of the noise term when Δ is comparable to T. However, the difference decreases when Δ becomes smaller, say $\Delta = 1\%T$; this can be explained by the central limit theorem.

The positive crack growth rate requires $X(t)$ to be positive. As a result, the marginal distribution of $X(t)$ is generally non-Gaussian. However, when the standard deviation of X is small, the probability that X is negative is small (in the above example, the mean of X is 1.0206, and the standard deviation is 0.208; thus, the probability that $X < 0$ is less than 10^{-6} if X is normal) Therefore, assuming the marginal distribution function of X to be normal. may not lead to misleading results (say, negative values of crack size), particularly if Δt is small, can be seen from Figure 4.17.

4.2 Loading uncertainty

In this section, the contribution of the uncertainty in the stress process to the probability distribution of the crack size is assessed. The noise is suppressed, and all material parameters are assumed to be deterministic. Results obtained from the proposed approach are compared with those obtained (at considerable expense) from direct simulation. The effect of the bandwidth of the stress history on the crack growth also is investigated.

The crack growth rate is assumed to be described by,

$$dA/dt = \nu C(Y\sqrt{\pi A}\Delta\sigma)^m \tag{4.35}$$

Crack growth parameters are $Y = 1.12$, $C = 0.66 \times 10^{-8}$ and $m = 2.25$ and the initial crack size is $a_0 = 0.3$ in (7.6 mm). These data are obtained from the study of deterministic edge crack growth in an infinite-width plate fabricated from A514 steel by Barsom and Rolfe (1987). The yield stress is 100ksi (689 MPa). The stress $\sigma(t)$ is assumed to be a Gaussian process with constant one-sided power spectral density $S(\omega) = 60/\pi$ ksi^2-hr/rad within a limited bandwidth $(0, 4\pi)$, which is selected such that the root-mean-mth-power of the stress range, $\sqrt[m]{\sum \Delta\sigma_i^m/m}$, is approximately 36 ksi (248 MPa). Stress histories are simulated from the RSA method with the given power spectral density as discussed in Chapter 2; stress ranges are obtained by rainflow analysis.

Since the stress is Gaussian, according to Chapter 2, the mean occurrence rates of zero upcrossing, ν_0^+, and peaks, ν_p^+, are $\frac{1}{2\sqrt{3}\pi}\sqrt{\frac{\omega^3|_0^{4\pi}}{\omega|_0^{4\pi}}} \simeq 1.155$ cycle/(time unit) and $\frac{\sqrt{3}}{2\sqrt{5}\pi}\sqrt{\frac{\omega^5|_0^{4\pi}}{\omega^3|_0^{4\pi}}} \simeq 1.549$ cycle/(time unit). Examining the 100 samples of cycle number obtained from 100 stress histories by rainflow analysis, it is found that the average cyclic rate is around 1.51 cycle/hr, which is close to ν_p^+. The coefficient of variation of the number of cycles in 12,500 hr is only 0.24%. Thus, the cyclic rate, which equals the total number of cycles divided by total time, can be modeled as a deterministic value ν_p^+.

The cumulative distribution function of the crack size at $T = 12,500$ hr obtained from direct simulation using the (nearly) exact approach discussed in Chapter 3 is plotted with the dashed line in Figure 4.18 and on lognormal probability paper in Figure 4.19. The simulation is expensive, with CPU time on a Digital Alpha Station 4000 equal to approximately 4 days (if no Fast Fourier Transform (FFT) algorithm is used), or 30 min (if FFT is used), for 100 samples of crack size at $T = 12,500$hr.

The approximate method described in Chapter 3 bases the analysis of crack growth

on the average cyclic rate and distribution of stress ranges obtained from one long stress history. The total time of the stress history is selected to be twice the time of interest for crack growth (25,000 hr). Rain flow analysis of this one stress history yields an average cyclic rate of the stress range of 1.51 cycle/hr, and an empirical distribution of the stress range. The stress range then is modeled as an uncorrelated process with this empirical marginal distribution. The probability distribution of the crack size at $T = 12,500$ hr is computed by the Euler scheme and is plotted with the solid line in Figure 4.18 and on lognormal probability paper in Figure 4.19 for comparison with the exact solution. The solutions from the two different approaches are close, with around 1% relative difference between the crack size corresponding to 0.99 cumulative probability (the upper limit of the probability that the 100 direct simulation samples can estimate). However, the CPU time of the proposed method is reduced. Around 3 hr (without FFT), or less than 1 min (with FFT), is spent for rain-flow analysis to obtain an empirical distribution of stress ranges, which can be used for different fatigue studies as long as the statistics of the stress remain unchanged. Subsequently, only 2-3 min is required to determine the CDF of crack sizes. Accordingly, the proposed approach is more efficient for dealing with fatigue analysis involving wide band load processes.

To examine the effect of the bandwidth (index of wide or narrow band), area (variance of the stress process) and shape of the PSD of a stress process on the parameters of the stress range and the probability distribution of the crack size, four stress processes, the PSDs of which are illustrated in Figure 4.20, are considered. The first PSD is $60/\pi$ ksi^2-hr/rad, $0 < \omega < 4\pi$, the second is $120/\pi$ ksi^2-hr/rad, $\pi < \omega < 3\pi$, the third is $\frac{60}{\pi^2}\omega$ if $0 < \omega < 2\pi$ and $\frac{240}{\pi} - \frac{60}{\pi^2}\omega$ if $2\pi < \omega < 4\pi$, and the fourth is $60/\pi$ ksi^2-hr/rad, $\pi < \omega < 3\pi$. The first three have the same area, but different bandwidth or shape. The fourth has the same shape and bandwidth as the second one, but different area. The theoretical values of ν_p^+, estimated ν_p^+, ${}^m\sqrt{\sum \Delta\sigma_i^m/m}$, $\mu_{\Delta\sigma}$, and $c.o.v.(\Delta\sigma)$ based on rainflow analysis are summarized in Table 4.1. For the first three cases, which have the same area of PSD (variance in stress), the second has the narrowest bandwidth, the highest ${}^m\sqrt{\sum \Delta\sigma_i^m/m}$, lowest $c.o.v.(\Delta\sigma)$, and lowest ν_p; the parameters for the third are in the middle, but are closer to those of the second. All parameters for the fourth are the lowest. The CDFs of crack size at $T = 12,500$ hr are shown for all four in Figure 4.21. The CDFs for the second and third cases are very close, the mean values being approximately 1.86 in (47.2 mm). The mean value for the first case is 1.79 in (45.5 mm). The dispersion for the first three cases are close, while the fourth has the smallest mean (0.66 in or 16.8 mm), and dispersion.

4.3 Sensitivity study

Linear regression analysis of the logarithm of crack growth rates, $\log dA/dt$, on the logarithm of stress intensity factors, $\log \Delta K$ yields only the mean value of $\log dA/dt$ (or the median of dA/dt). The relationship between the mean of normal and lognormal variables (Ang and Tang, 1975) implies that even though the mean of the noise in $\log dA/dt$ is zero, it is greater than unity for dA/dt. Thus, deterministic models of crack growth rate based on parameters obtained from the regression analysis can result in an unconservative estimate of crack size following a period of stable crack growth due to service loading. Stochastic models take into account the noise and thus compensate for this underestimation. This is illustrated in the following.

Assume that the logarithm of the noise, $log_{10}X$ is modeled by two extreme cases: as an uncorrelated Gaussian process or as a Gaussian random variable, with zero mean and standard deviation $\sigma_1 = 0.087635$ in both cases. The stochastic crack growth model is

$$da/dt = \nu C(Y\sqrt{\pi a}\Delta\sigma)^m 10^{0.087635G} \tag{4.36}$$

where the marginal distribution function of $G(t)$ is standard normal, $\Delta\sigma = 36.1$ ksi (249 MPa) and $\nu = 1.51$ cycle/hr, (the values of root-mean-mth-power of the stress range and average cyclic rate of a stress process with $S_{\Delta\sigma}(\omega) = 60/\pi$, $0 < \omega \leq 4\pi$, as determined in the preceding section). The other parameters remains the same as in Section 4.2. The deterministic crack size at $T = 12,500$ hr and its probability distributions under these two extreme assumptions regarding the stochastic nature of the noise are compared in Figures 4.22 and 4.23. The deterministic value is approximately 96% of the median value obtained from the uncorrelated noise model and 99% of the median value from the random variable model. The variance of the crack size is very small when $X(t)$ is uncorrelated, because each sample of $A(t)$ is the summation of uncorrelated variables over a long time. When $X(t)$ is perfectly correlated, the variance of the crack size becomes large because X is the same within a crack growth path, but different between different crack growth paths. Almost all crack sizes would be larger than that determined from deterministic analysis if noise is an uncorrelated process; if the noise is modeled as a random variable, about 50% of the crack sizes would be larger.

To investigate the combined effect of both model noise, X(t), and loading uncertainty on crack growth, the CDFs of crack growth at $T = 12,500$ hr are plotted in Figure 4.24 for three cases. The first describes the effect of the loading uncertainty, with the stress power spectral density $S_{\Delta\sigma} = 60/\pi$ within $0 < \omega < 4\pi$ when noise is not included. The second depicts the effect of the model noise $X(t)$, in which

$log_{10}X(t)$ is an uncorrelated normal process, with zero mean and standard deviation 0.087635; the stress range is deterministic with value equal to the root-mean-mth-power value of the stress range history in the first case. The third characterizes the combined effect of both sources of uncertainty. The CDF of crack size shifts to the right when the model noise is taken into account, but the variance in the loading dominates the variance of the crack growth in this example.

However, when the model noise is highly correlated, critical factors for the variance in crack size change as illustrated in Figure 4.25, where four cases are presented with the loading characterized by the same $S_{\Delta\sigma}(\omega)$ as before. One case represents uncertainty only due to loading. The remaining cases represent combinations of both loading and noises with different correlation functions, the first for the case when noise term is uncorrelated with respect to time, the second for the case when noise is a random variable, and the third for the case when noise is in between these extremes modeled by $R_G = \exp(-\alpha|\tau|)$, where $G = \frac{\log_{10} X}{\sigma_X}$ and $\alpha = 2.5 \times 10^{-4}$. The noise dominates the variance of crack size when $X(t)$ is highly correlated. The correlation length of $X(t)$ is related to the value of α. When α gets smaller and smaller, $G(t)$ converges to a random variable, while when α gets larger and larger, $G(t)$ becomes uncorrelated. Thus, an accurate measurement of α is required in order to have a good prediction of the CDF of crack size. Experimental data (similar to the repeated trials by Virkler et al (1979)) for crack growth histories under different conditions must provide the basis for statistical analysis of the correlation structure of $X(t)$.

The uncertainty of the fatigue exponent m has not been considered in the above. The value of m can vary for different materials, components and environments. Thus it can be modeled as a random variable. To assess whether uncertainty in m plays an important role in crack growth, a uniform distribution is assumed for m with mean equal to 2.25 and c.o.v. equal to 0.01, 0.03, 0.05, respectively. In each case, the noise, X, is assumed to be either perfectly correlated or uncorrelated with respect to time. The variance of X and the values of other parameters in the crack growth law are assumed to be the same as before. The effects of m on the c.o.v. of time to reach various crack sizes are illustrated in Figure 4.26. When the c.o.v. of m is small (≤ 0.01), the uncertainty in m plays an important role if X is uncorrelated, but is negligible if X is perfectly correlated. In other words, the contribution of the uncertainty of m and X to the uncertainty in the time required to reach a given crack size depends on the correlation structure of X for small values of c.o.v. of m. As the c.o.v. of m gets larger, the uncertainty in m dominates the uncertainty in the time required to reach a given crack size, and the correlation structure of X becomes less important.

Type	ν_p	$\hat{\nu}_p$	$\sqrt[m]{\sum \Delta\sigma_i^m/m}(ksi)$	$\mu_{\Delta\sigma}(ksi)$	$c.o.v.(\Delta\sigma)$
1	1.55	1.51	36.1	27.9	0.73
2	1.18	1.17	40.8	33.3	0.64
3	1.33	1.30	38.9	30.8	0.69
4	1.18	1.17	28.8	23.5	0.64

Table 4.1: Stress history parameters with respect to different PSDs

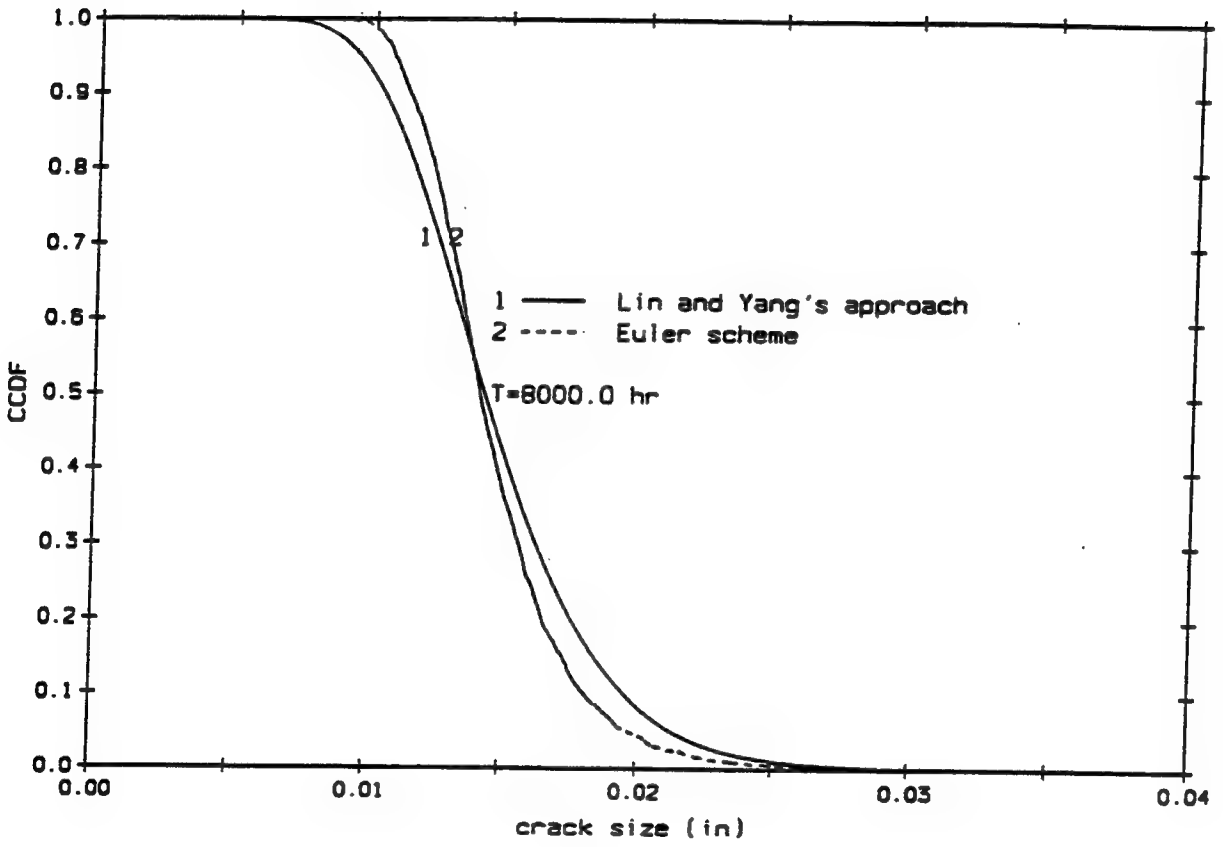

Figure 4.1: CCDF of crack size

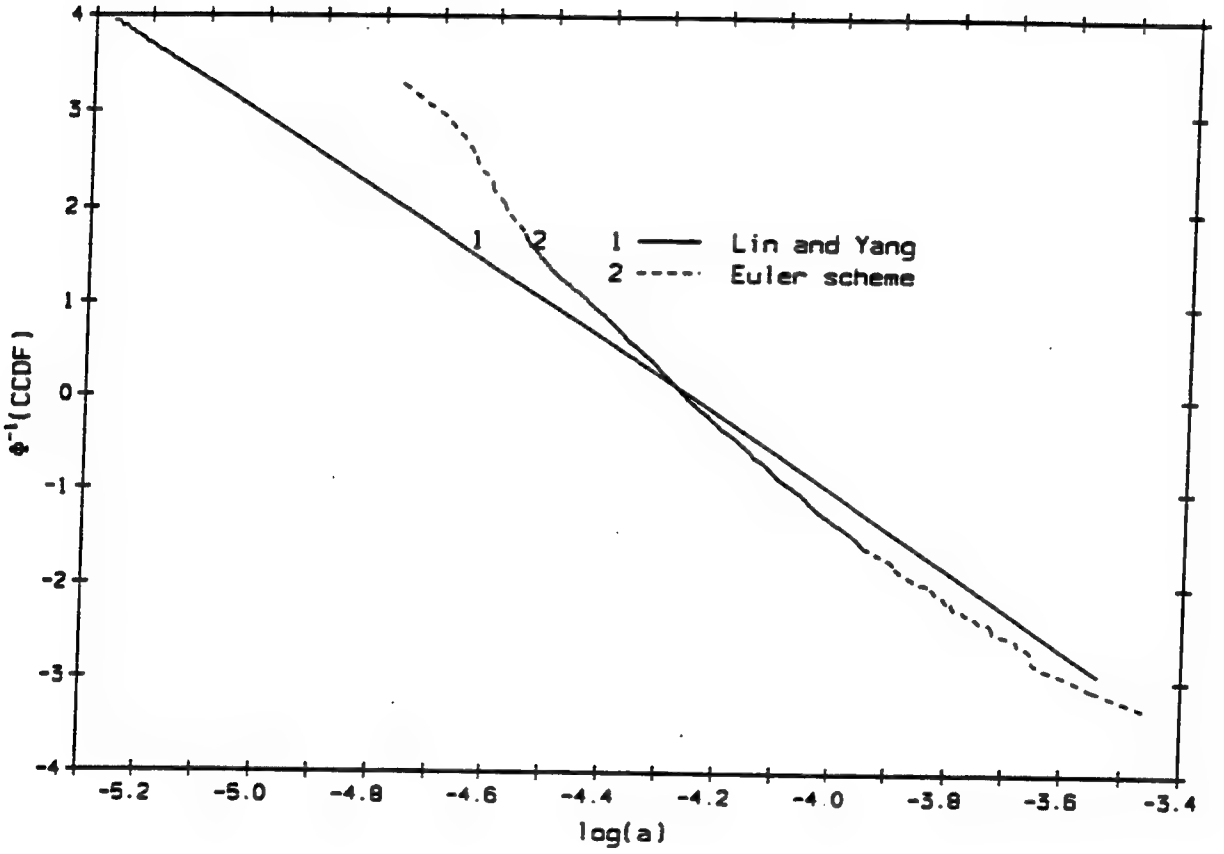

Figure 4.2: CCDF of crack size on lognormal paper

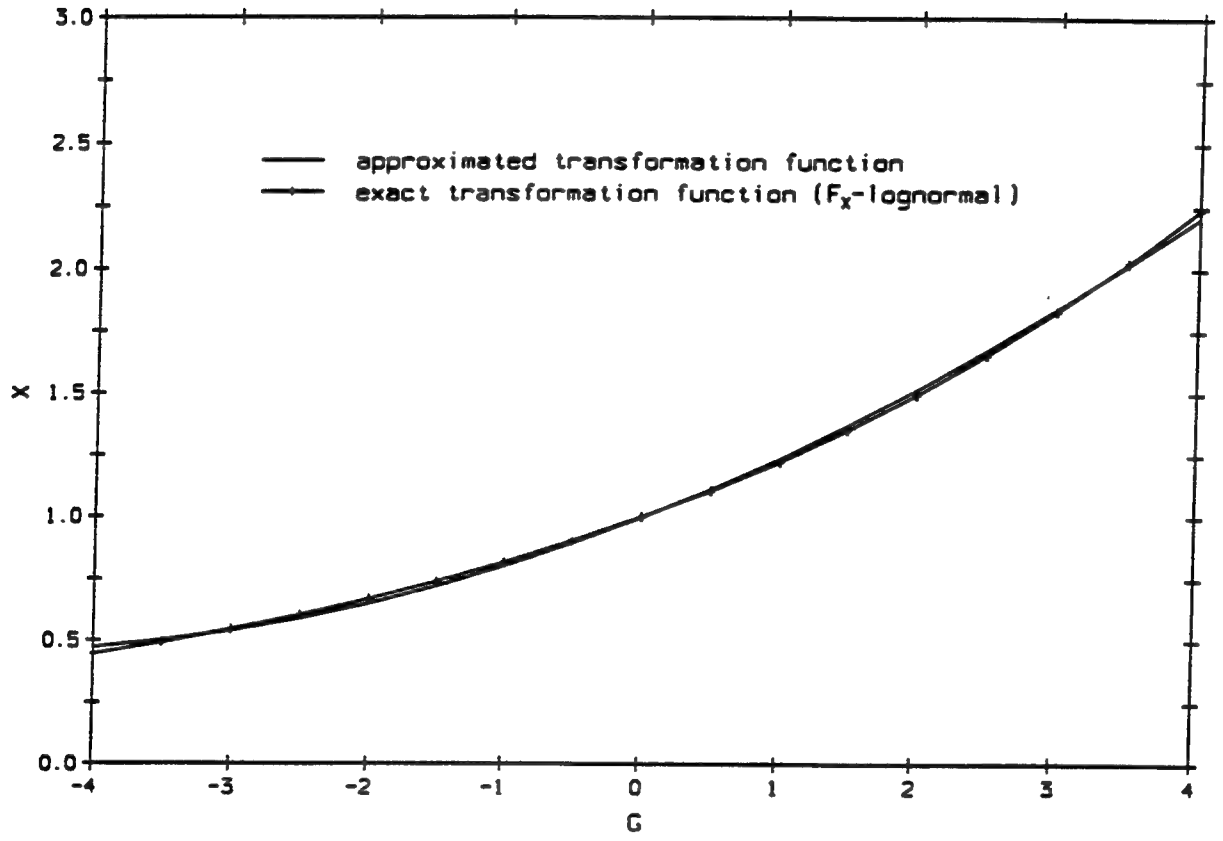

Figure 4.3: Approximation of the transformation from non-gaussian to gaussian space

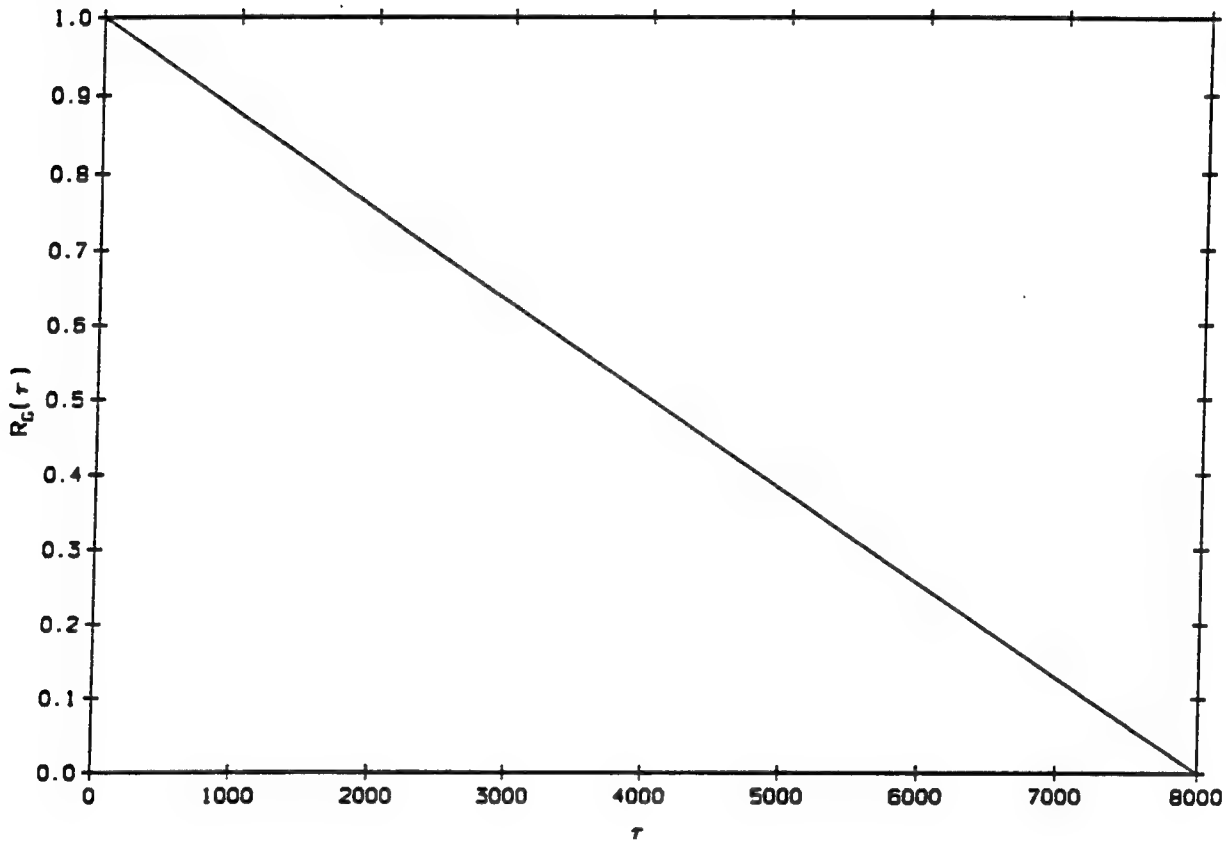

Figure 4.4: The estimated autocorrelation function of G(t)

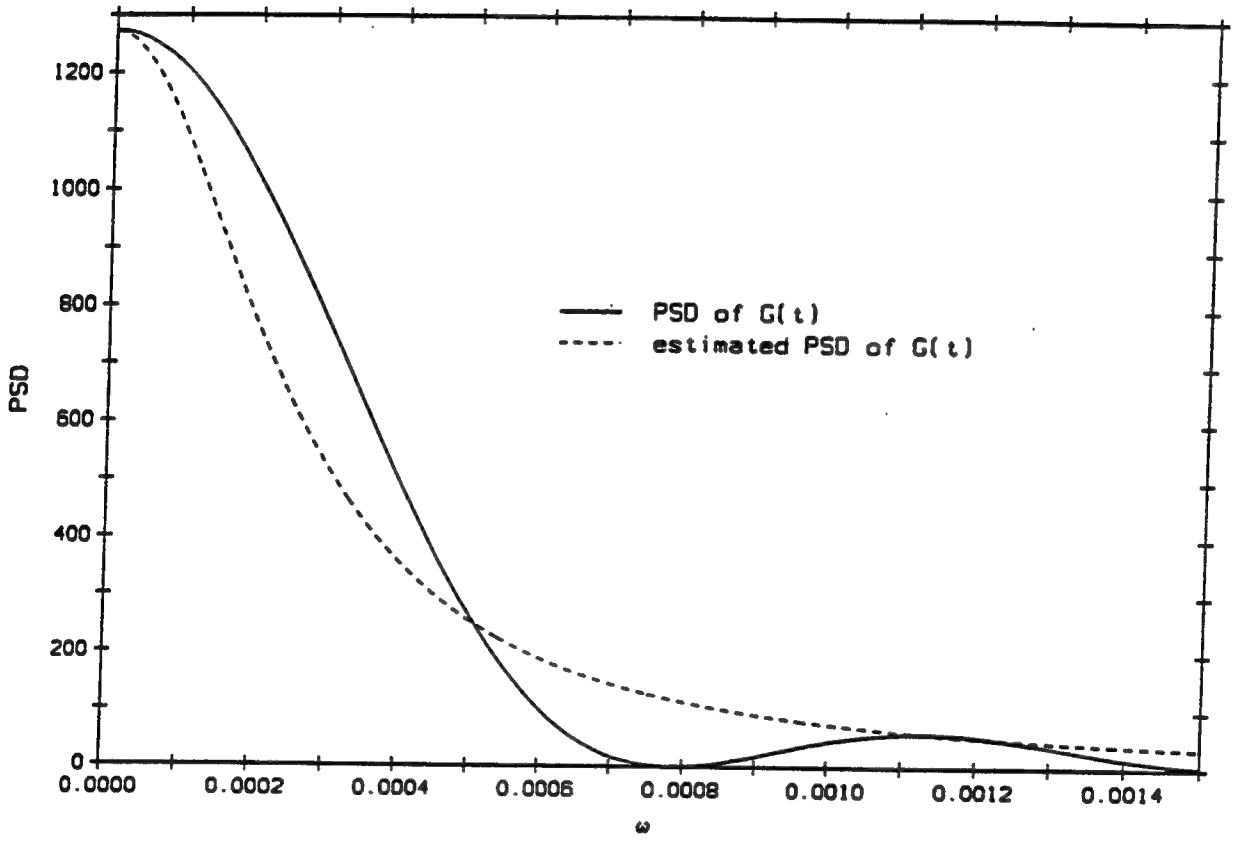

Figure 4.5: The power spectral density (two-sided) of G(t)

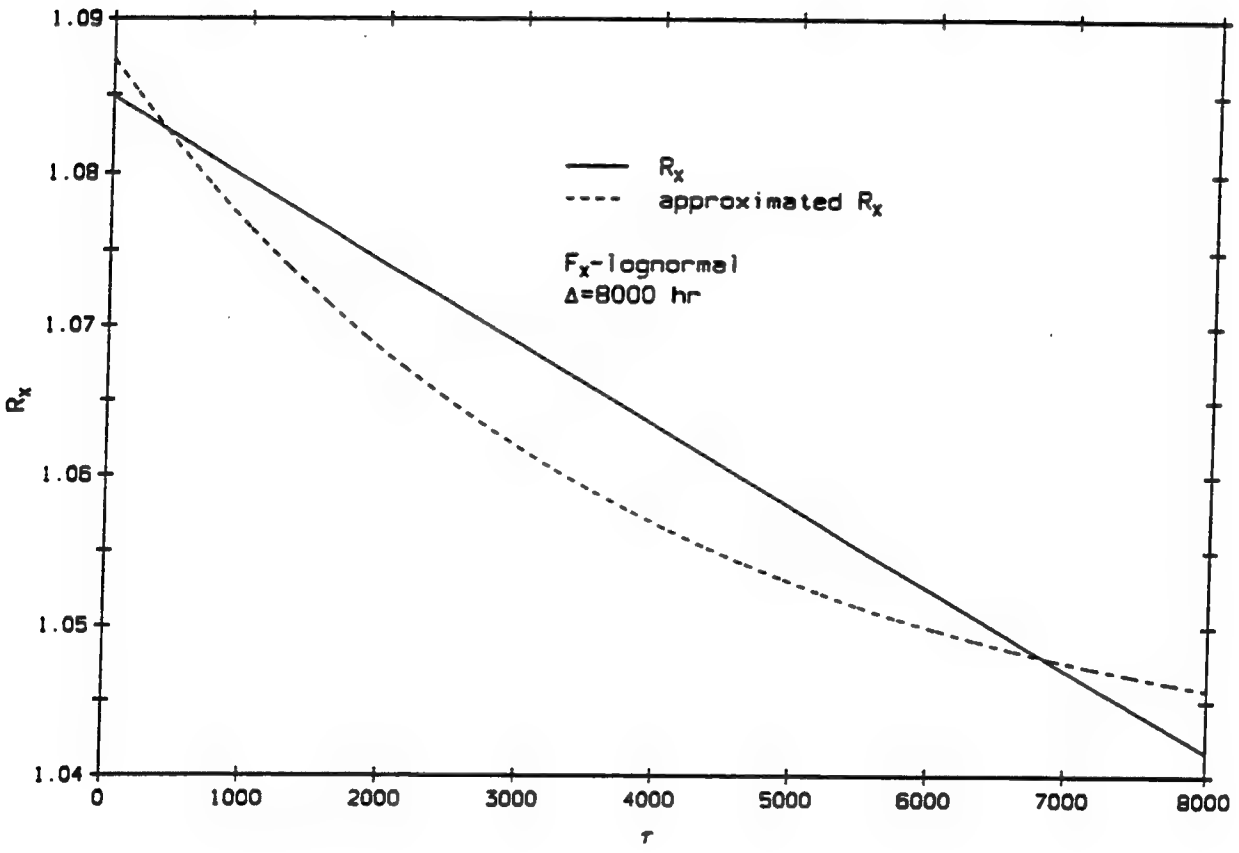

Figure 4.6: The autocorrelation function of X when $\Delta = 8000$ hr

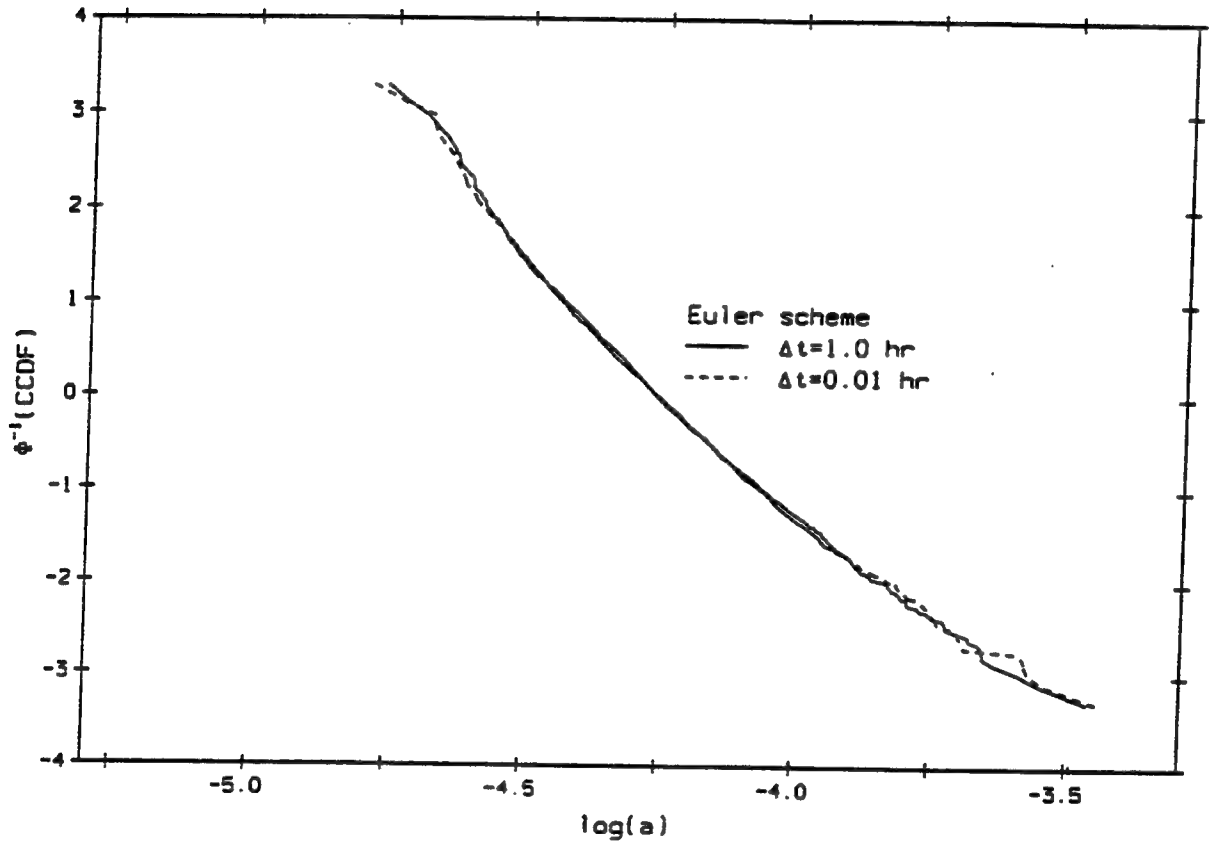

Figure 4.7: CCDF of crack size using Euler scheme with different time increments

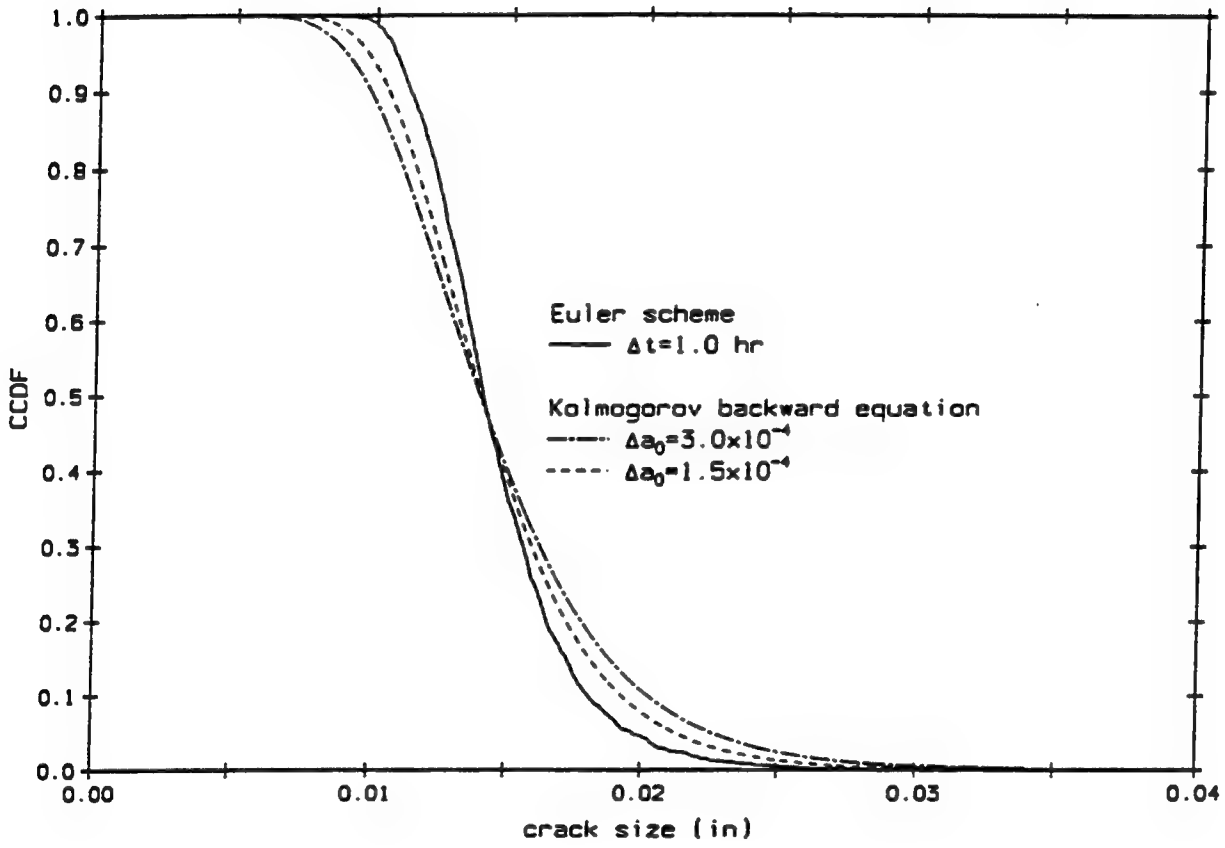

Figure 4.8: CCDF of crack size using different numerical schemes

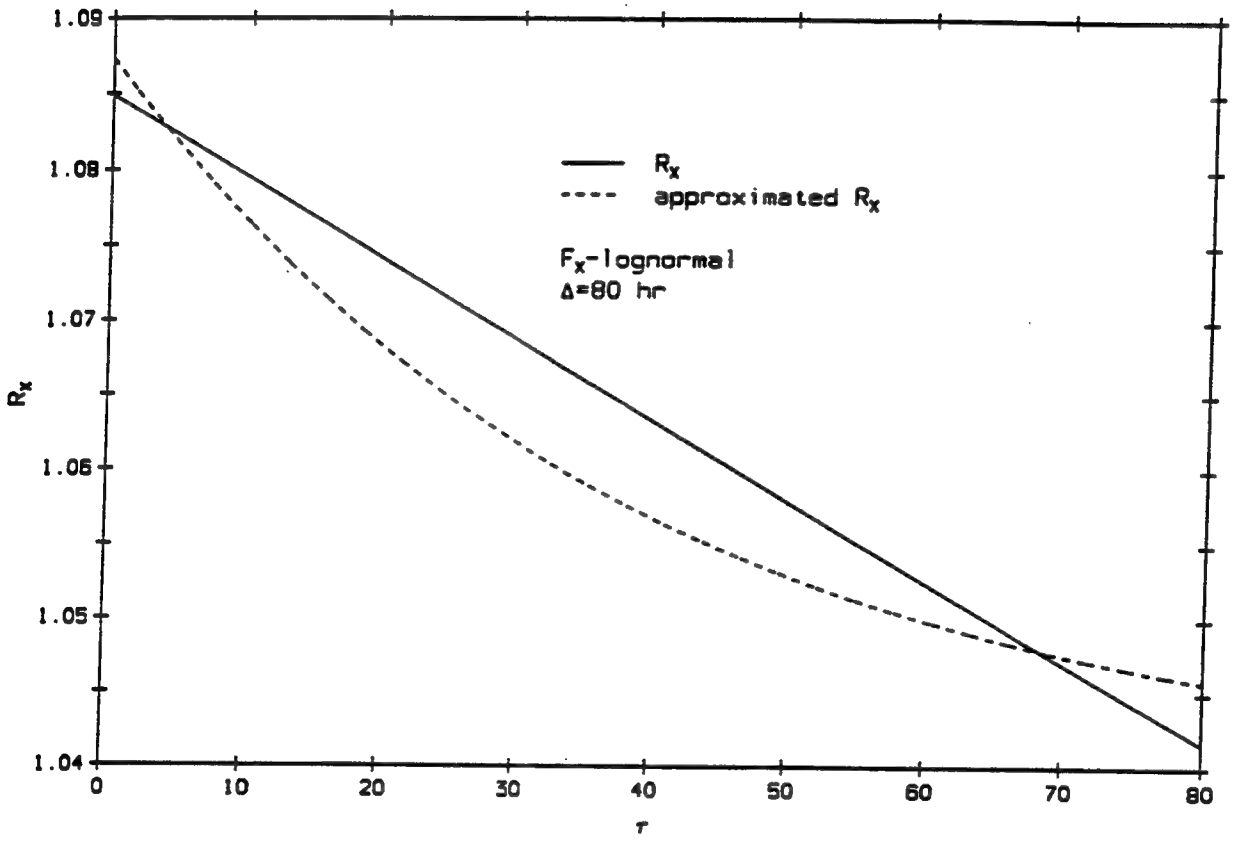

Figure 4.9: The autocorrelation function of X when $\Delta = 80$ hr

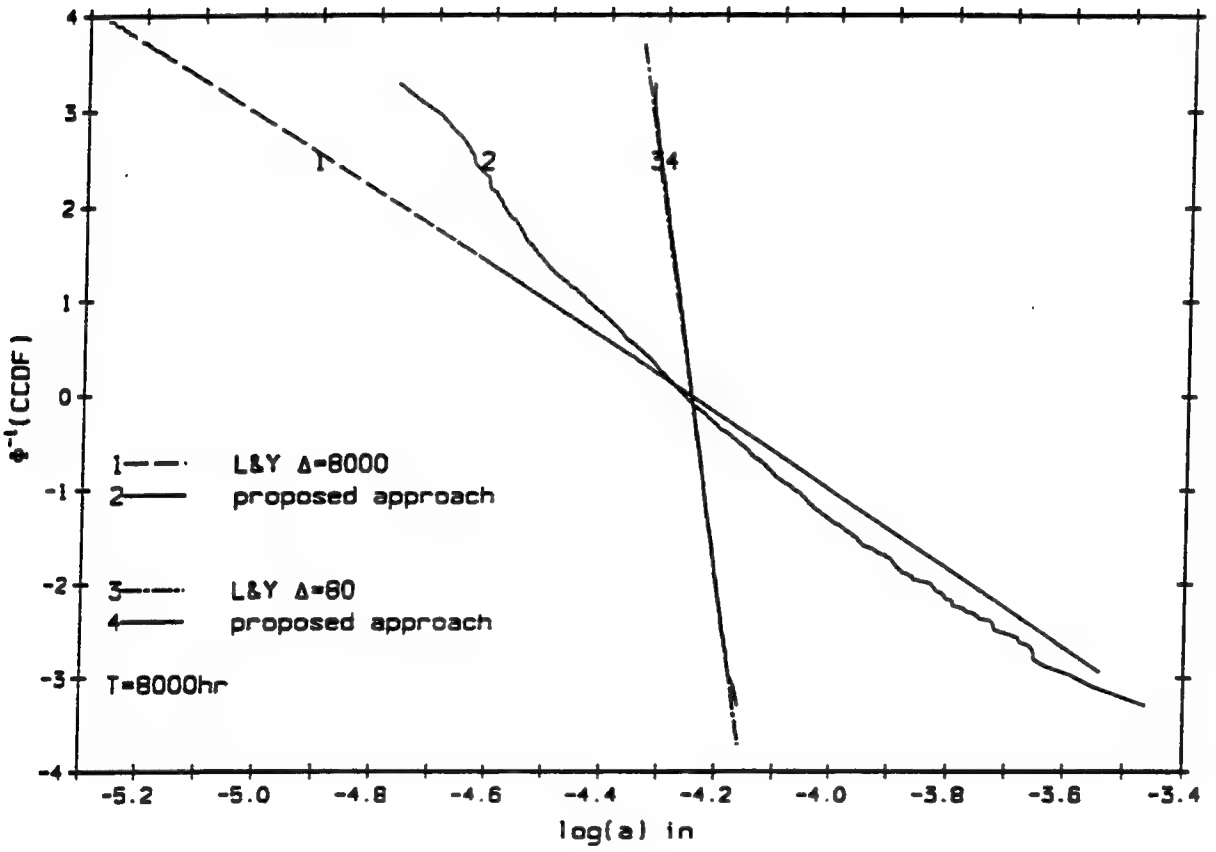

Figure 4.10: CCDF of crack size due to model uncertainty (T=8000hr)

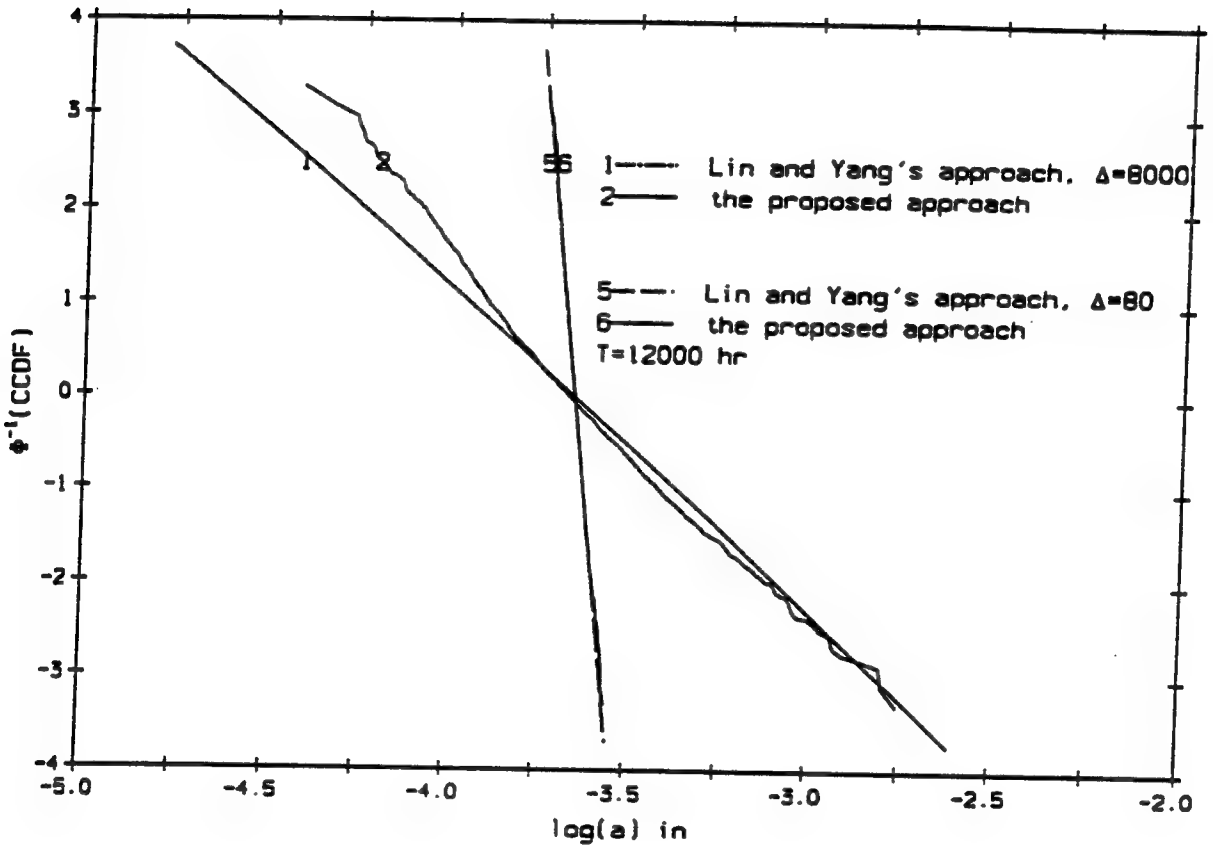

Figure 4.11: CCDF of crack size due to model uncertainty (T=12000hr)

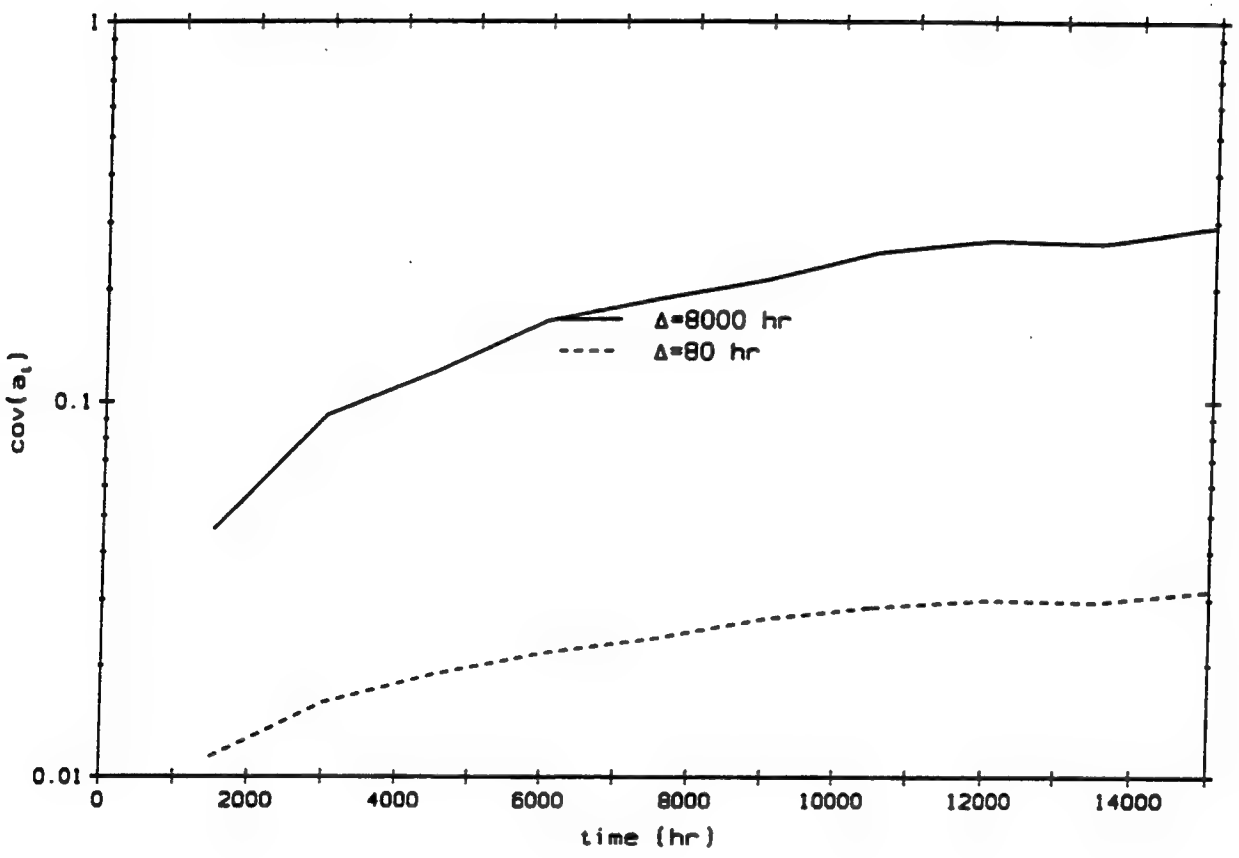

Figure 4.12: C.o.v of crack size versus time

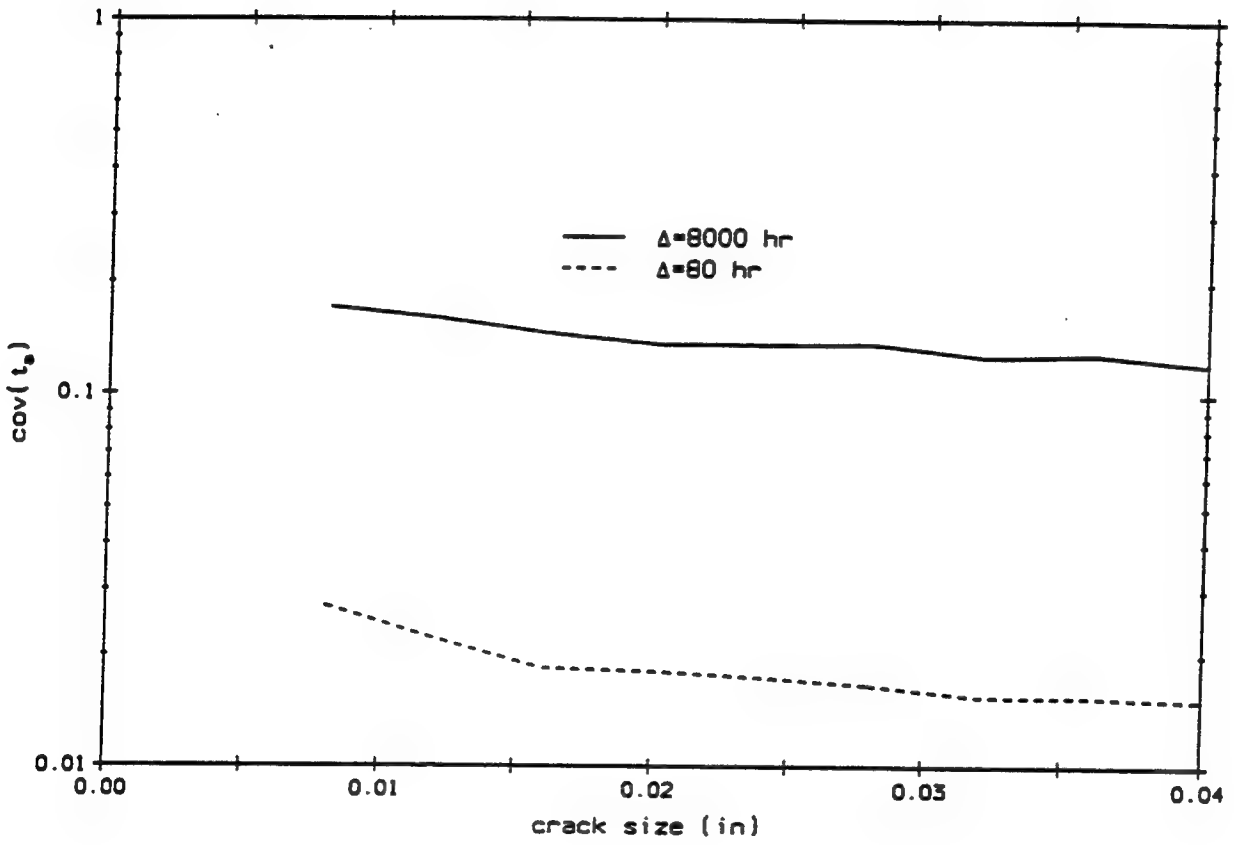

Figure 4.13: C.o.v of time versus crack size

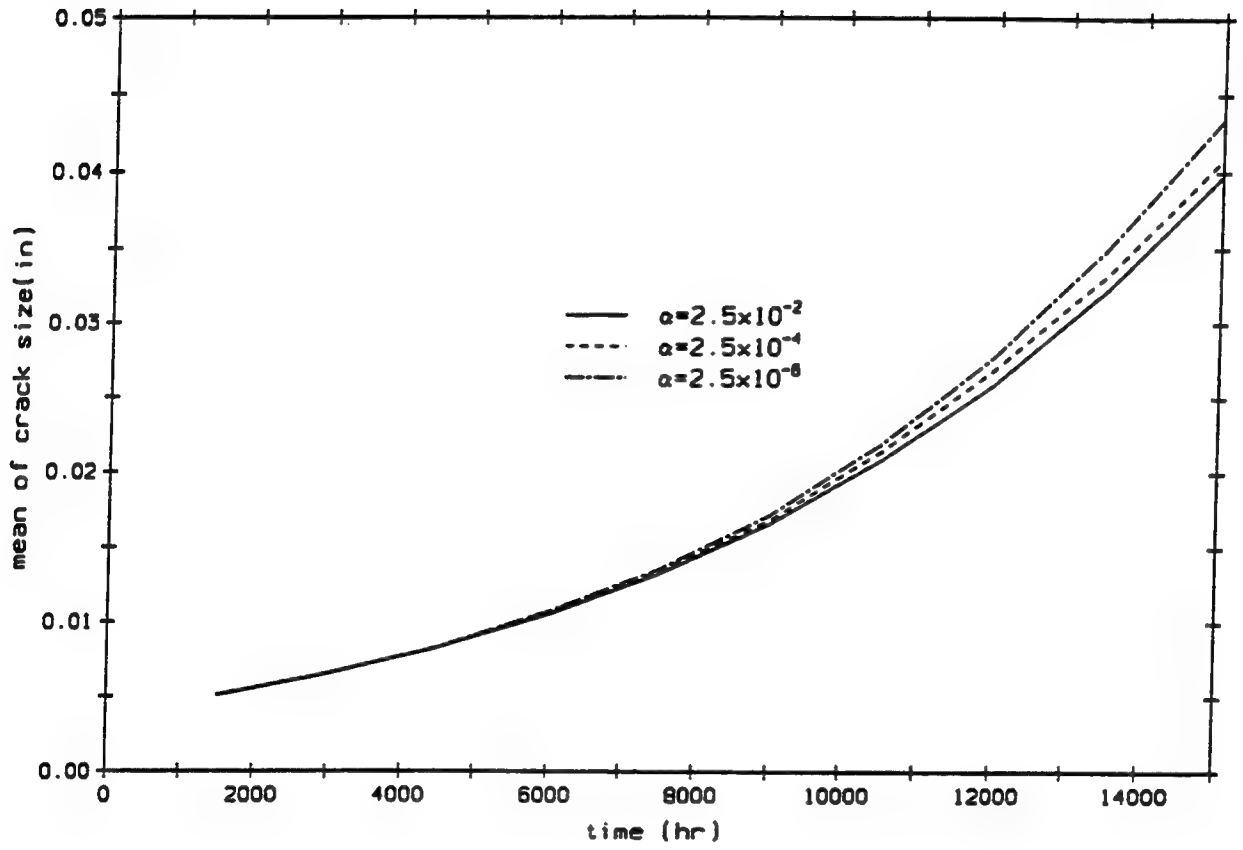

Figure 4.14: Mean of crack size versus time

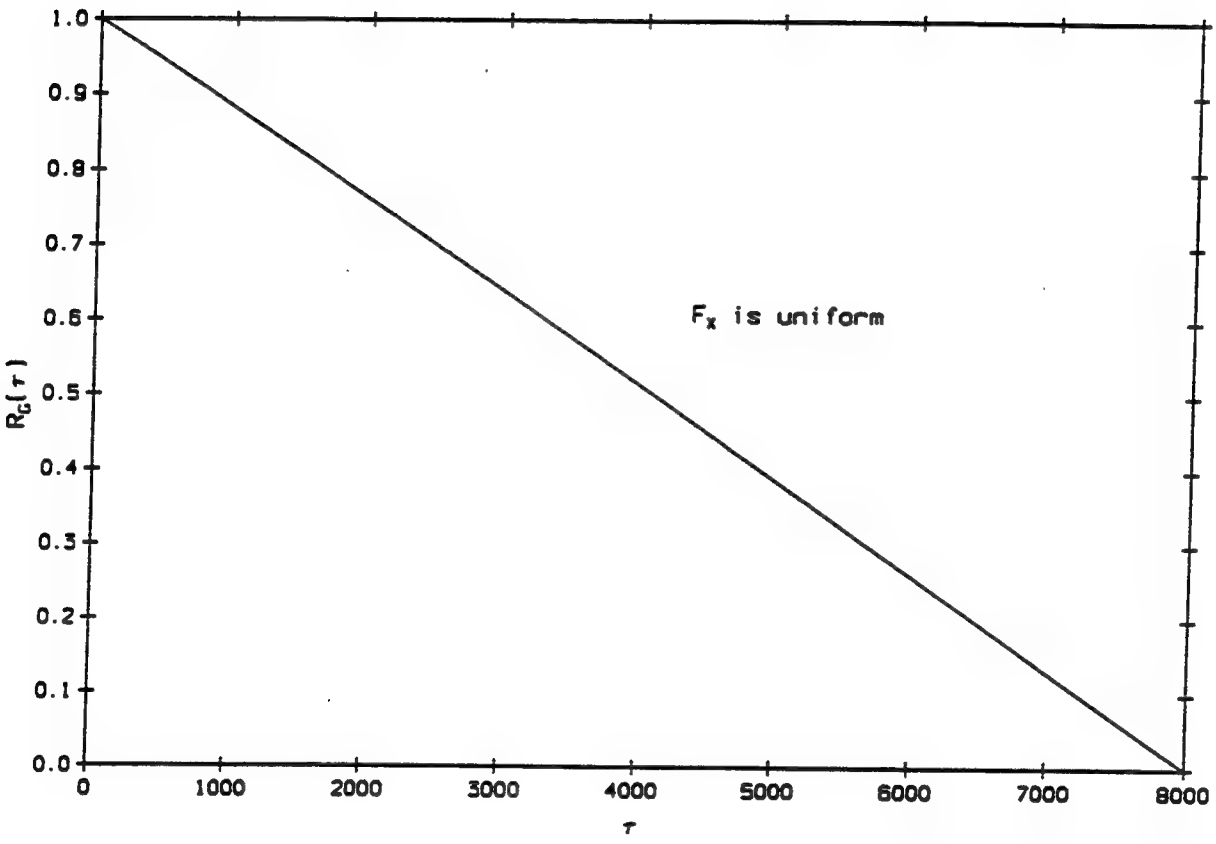

Figure 4.15: Correlation function of G

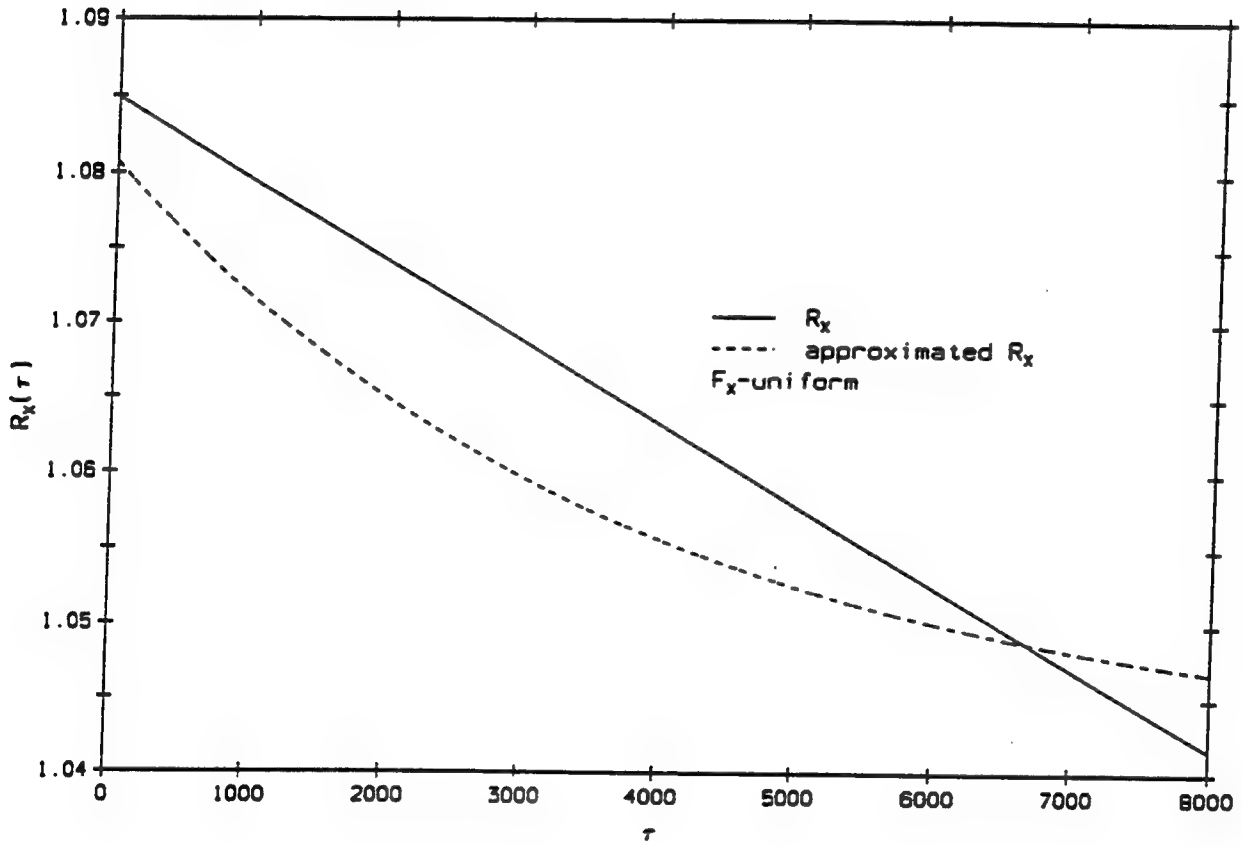

Figure 4.16: Correlation function of X

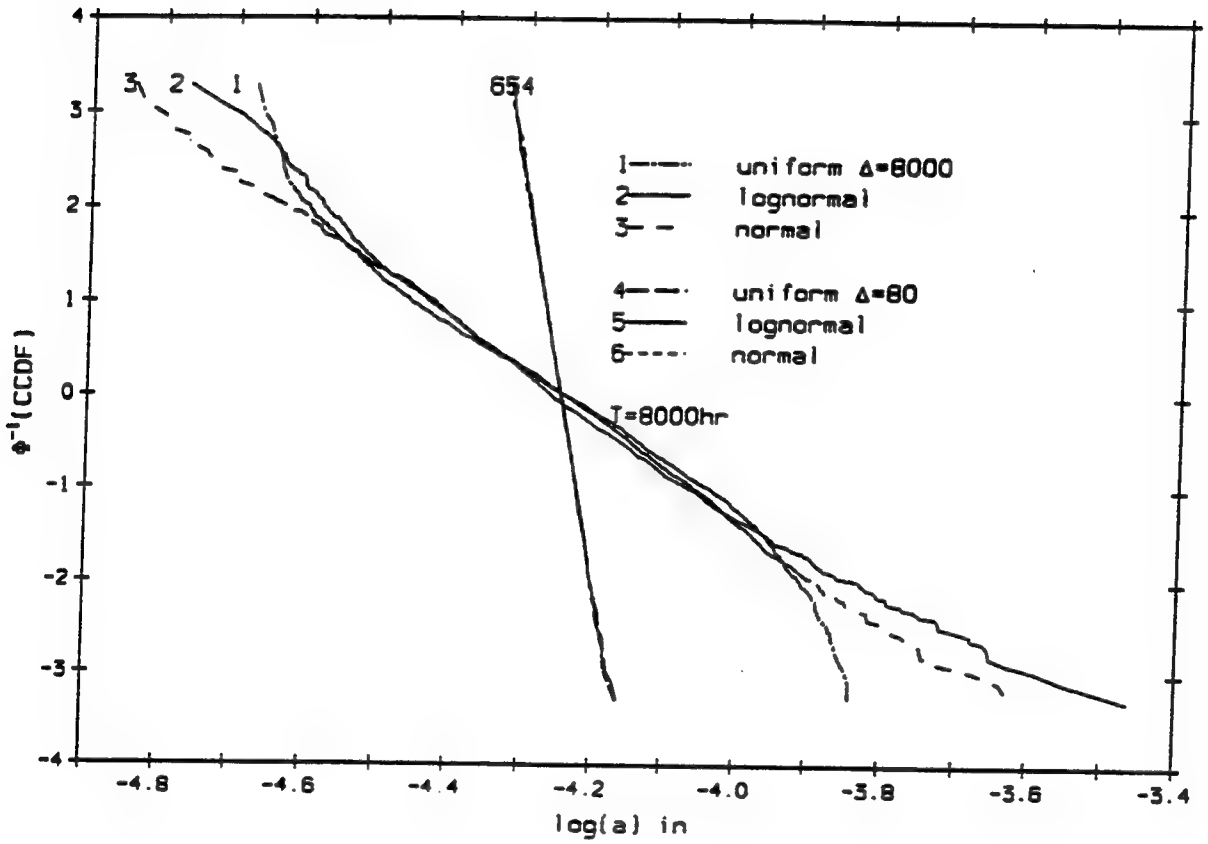

Figure 4.17: CCDF of crack size due to different distribution of model uncertainty

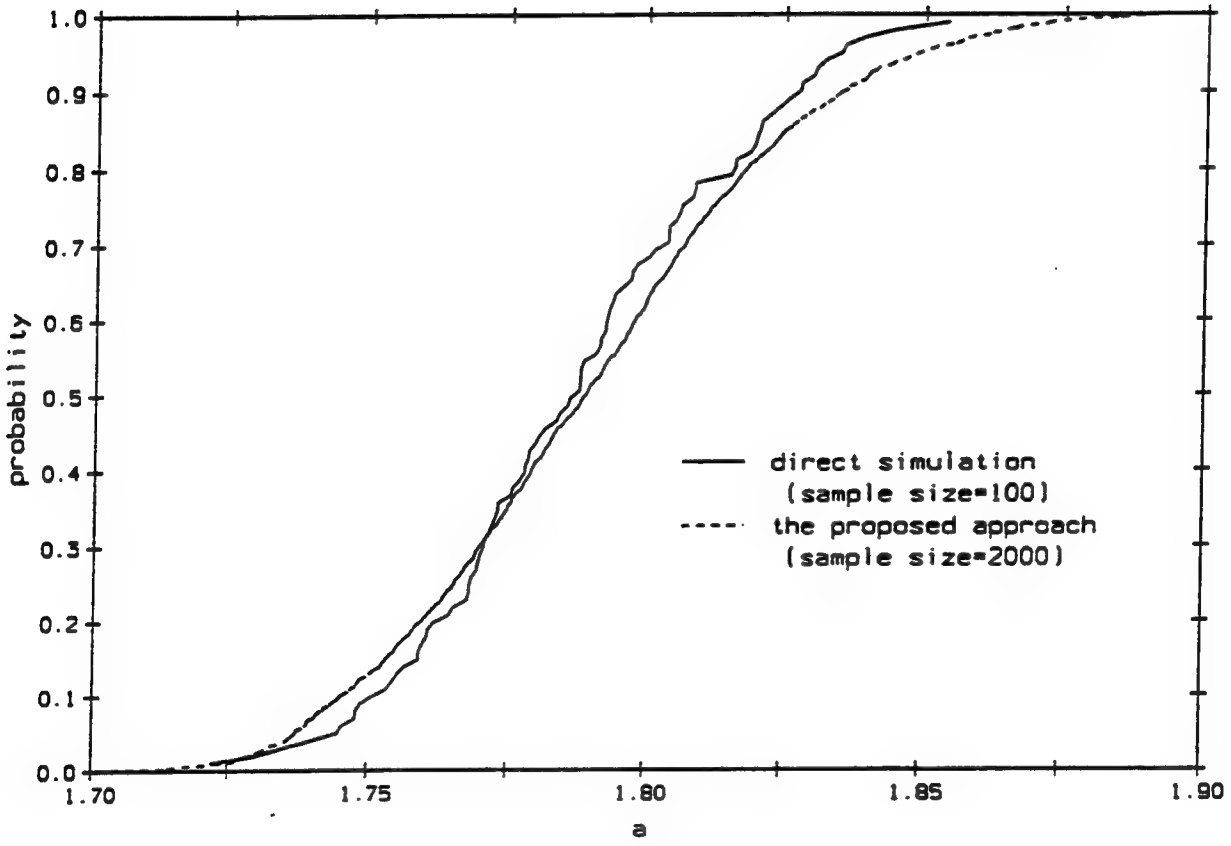

Figure 4.18: CDF of crack size due to random loading

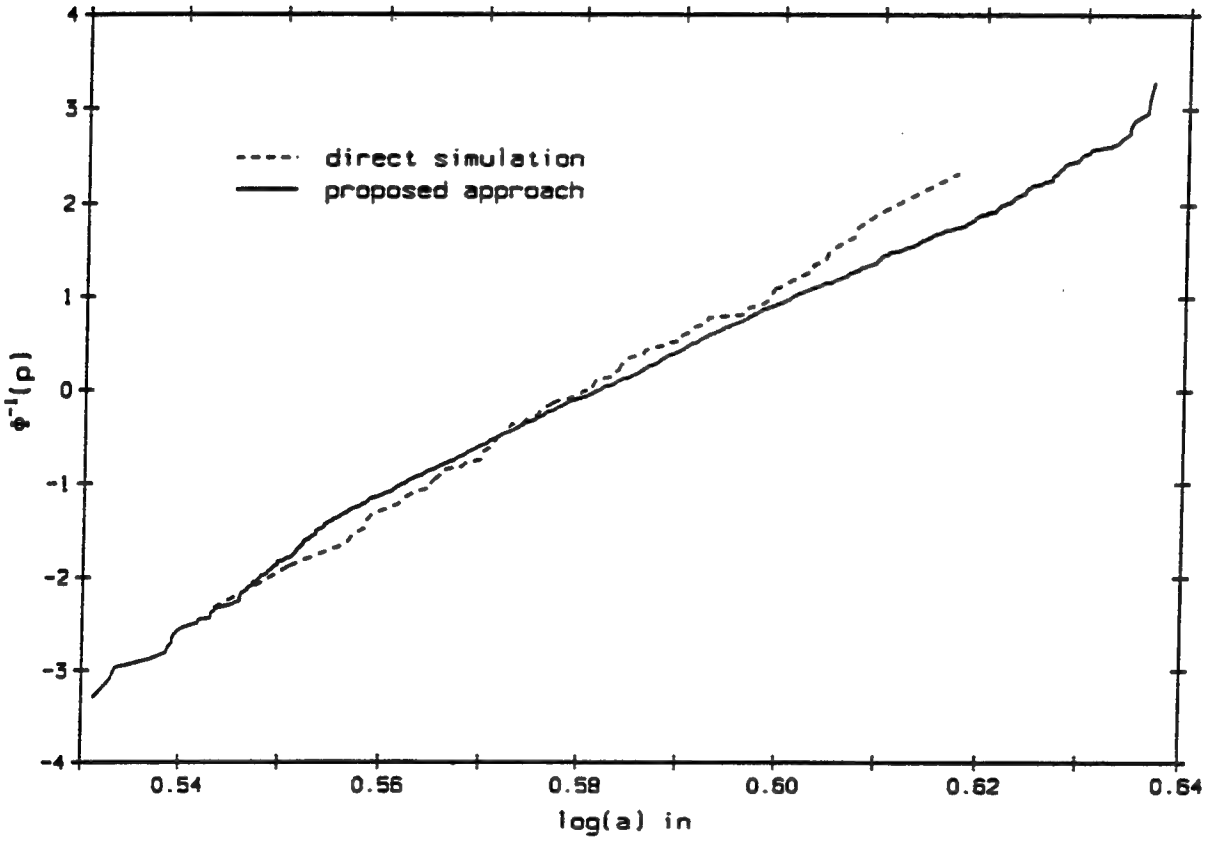

Figure 4.19: CDF of crack size due to random loading (lognormal)

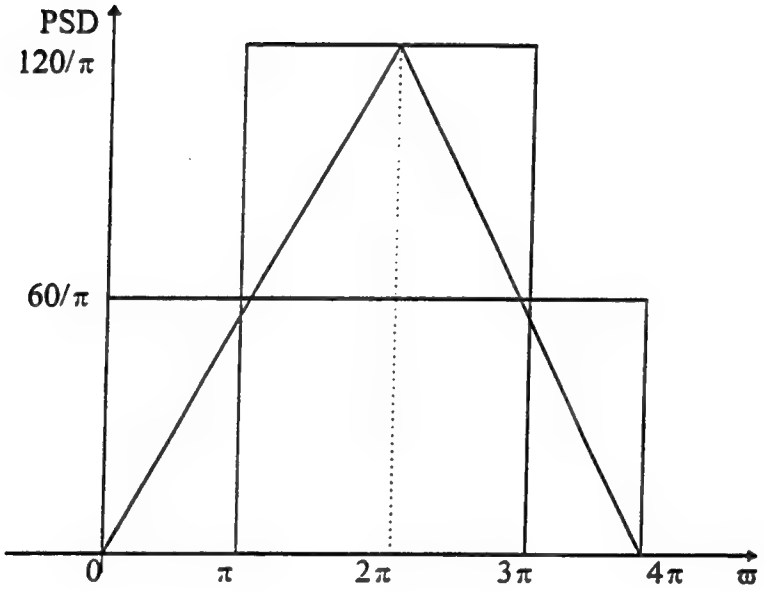

Figure 4.20: PSDs of stress processes

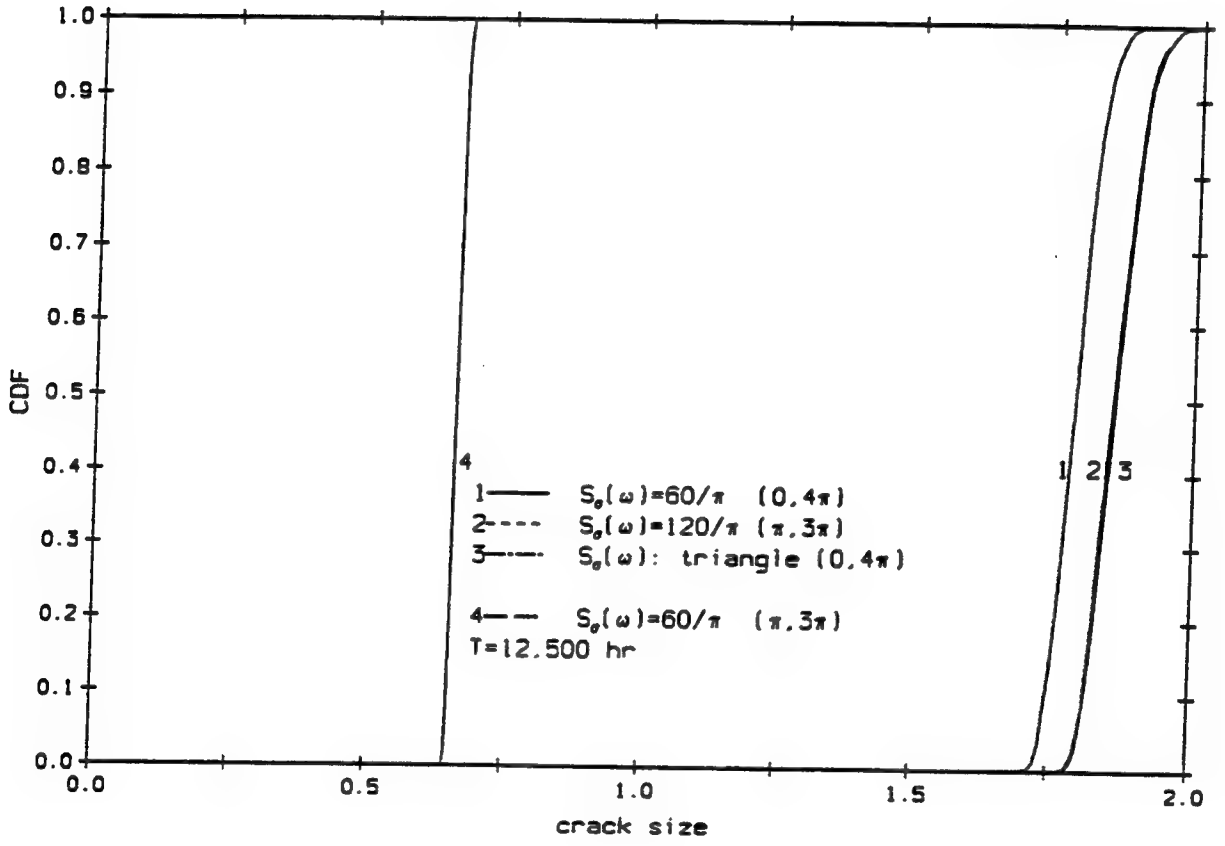

Figure 4.21: CDF of crack size due to different PSDs

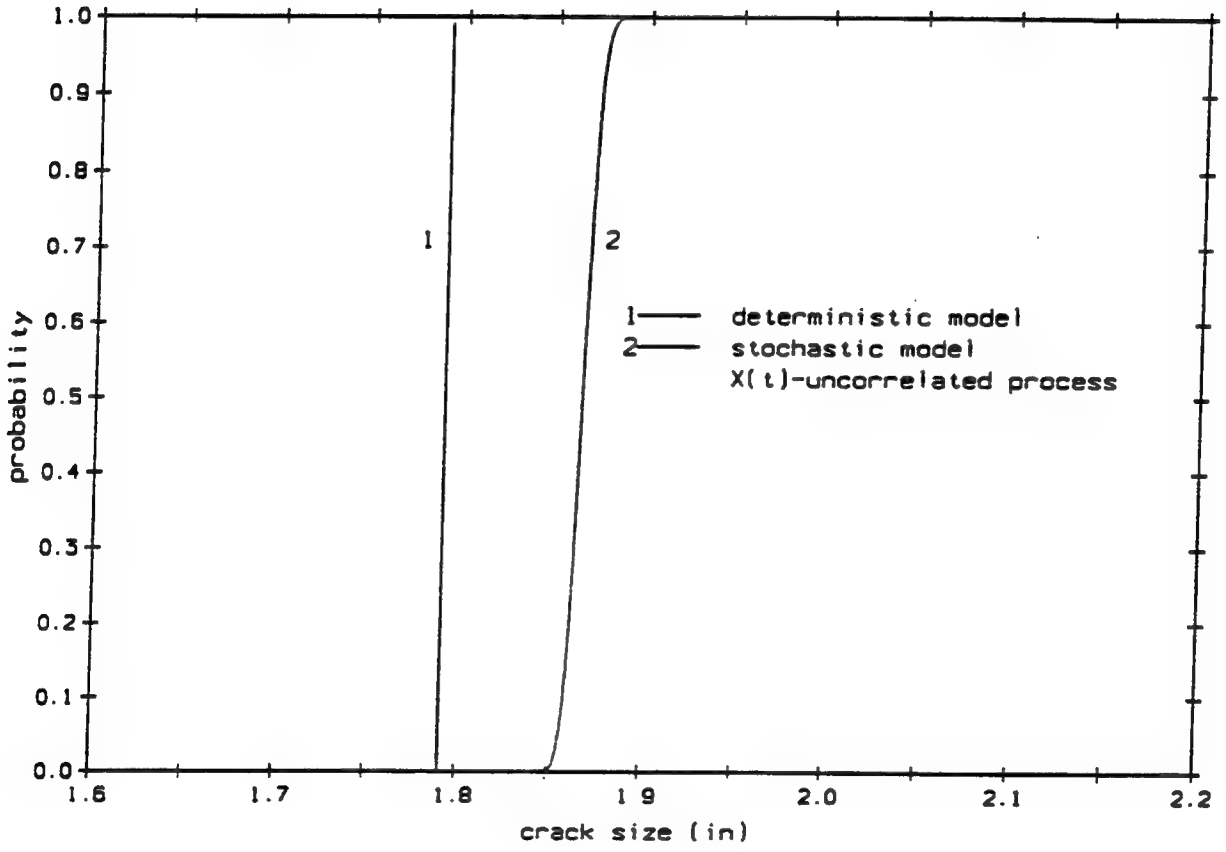

Figure 4.22: Deterministic versus stochastic crack size under constant amplitude loading (X(t) uncorrelated)

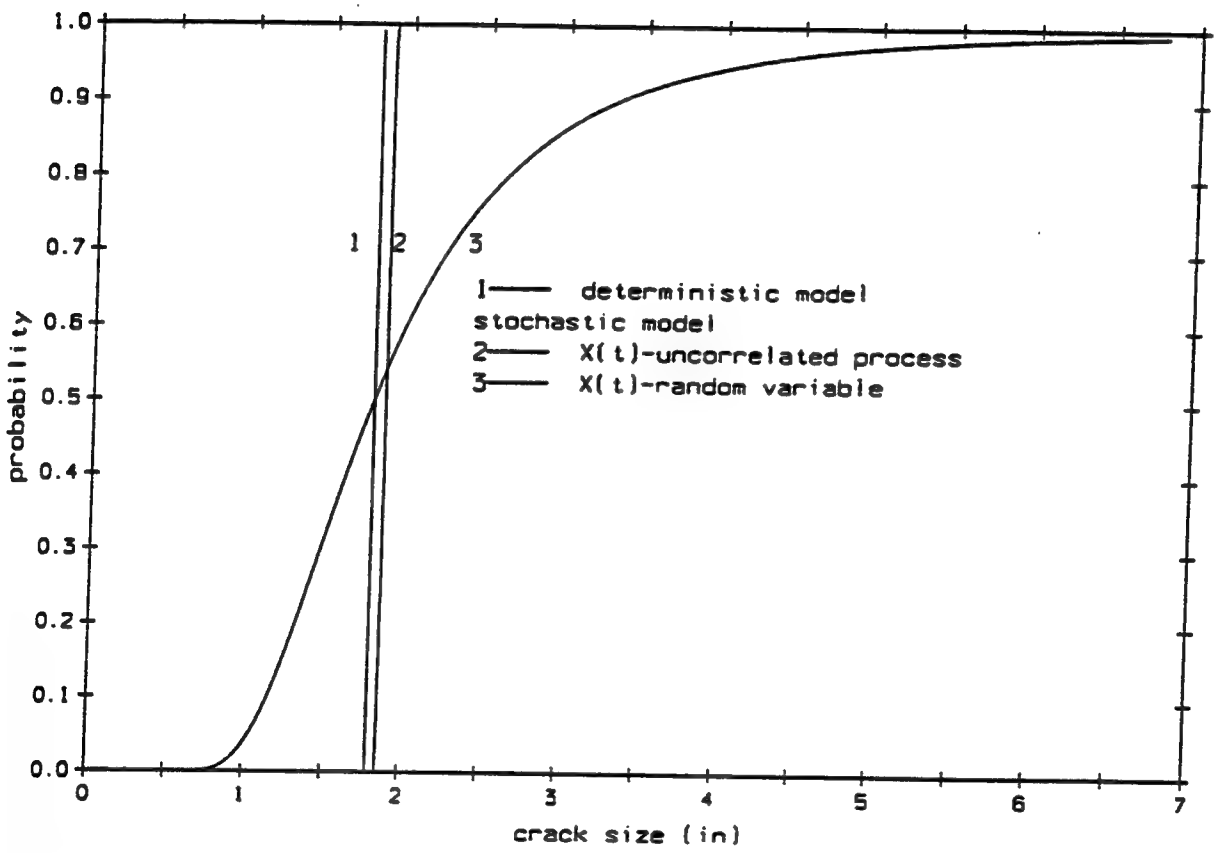

Figure 4.23: Deterministic versus stochastic crack size under constant amplitude loading

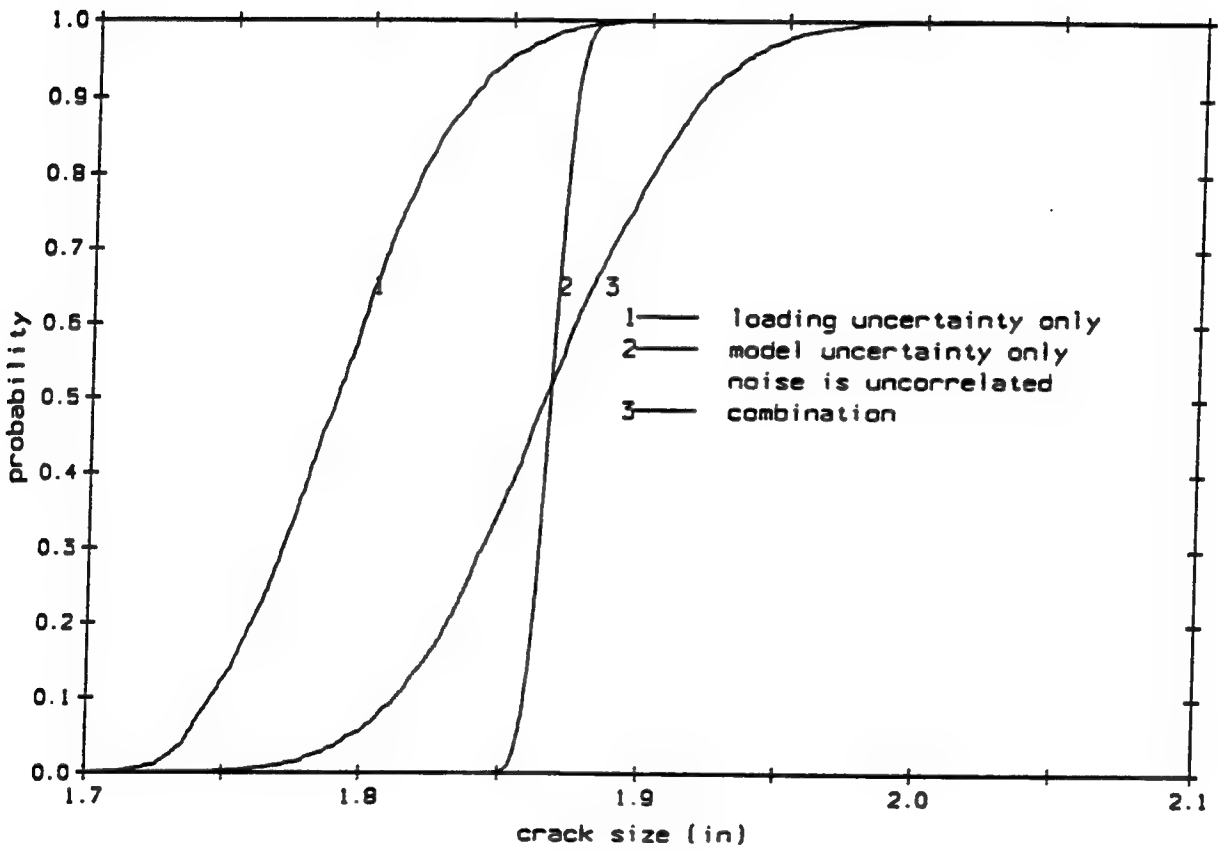

Figure 4.24: Effect of loading and model uncertainty

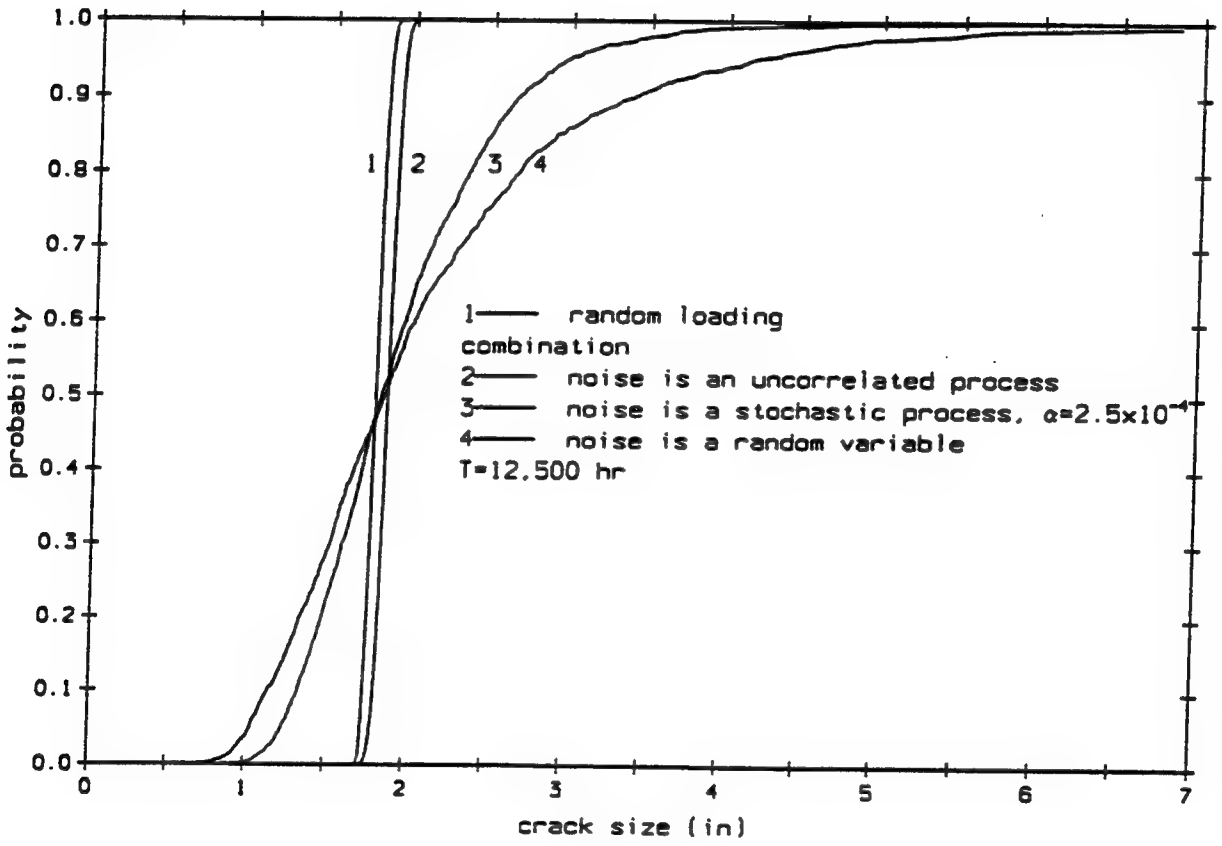

Figure 4.25: Sensitivity of crack size to correlation in noise

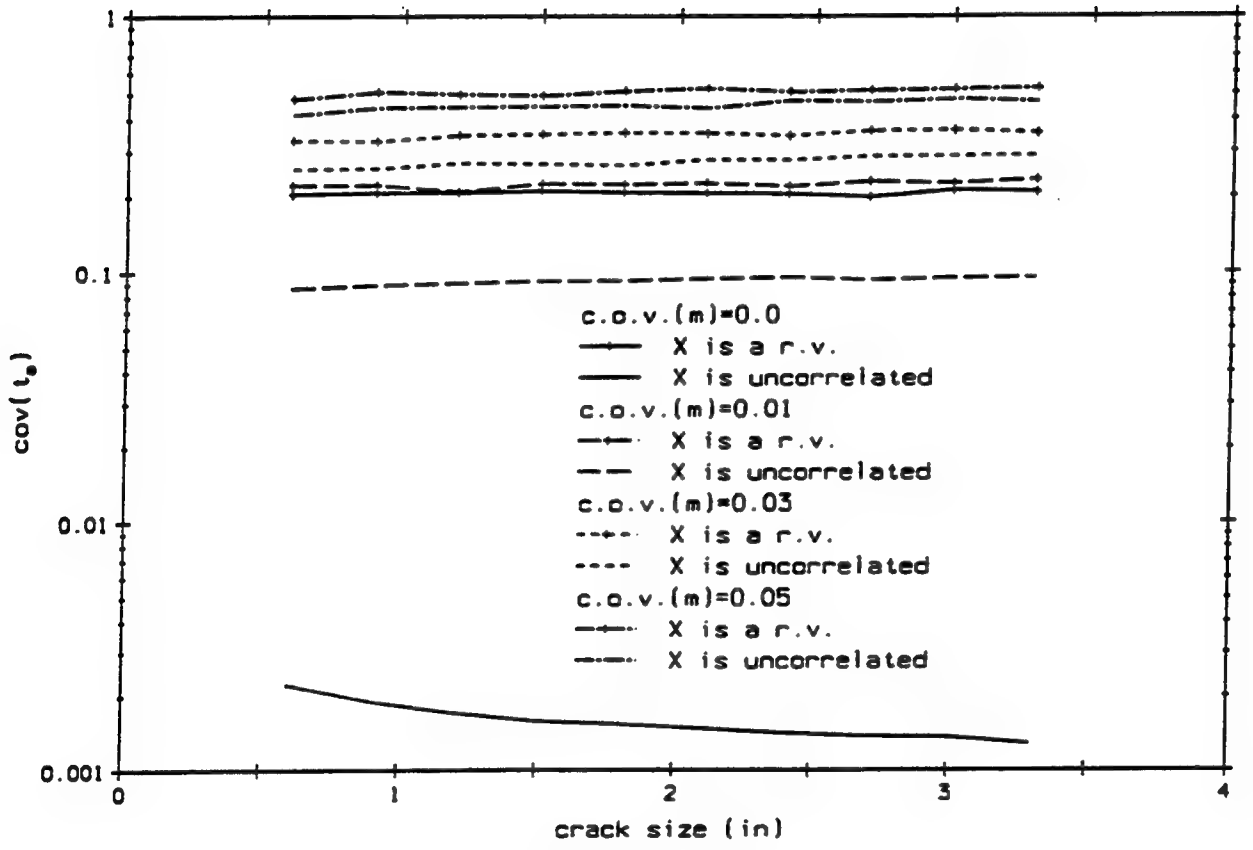

Figure 4.26: Sensitivity of crack size to m

Chapter 5

Fatigue Crack Growth Analysis of the Emsworth Miter Gate

The inland waterway system in the United States plays a significant role in the transportation of agricultural and industrial products. Among the most important components of navigation infrastructure on these waterways are steel miter gates installed at locks and dams. Many of these gates were constructed more than fifty years ago and during their service lives have been subjected continuously to various loadings and environmental effects, such as cyclic hydrostatic loadings, vessel impact, and alternate wetting and drying. Deterioration of steel gates during service has occurred from fatigue or corrosion-fatigue (U.S. Army Corps of Engineers, 1993). Failure consequences for such facilities are costly and their repair and maintenance is expensive and potentially disruptive to transportation on the waterway. Rational policies for condition assessment and maintenance actions are required from both safety and economic perspectives.

The methods presented in Chapters 3 and 4 provide tools for time-dependent reliability assessment and service life prediction of aging structures in the presence of uncertainties due to construction conditions, service load and environmental factors. As a demonstration of the use of these tools, the reliability analysis with respect to crack growth in a miter gate at the Emsworth Lock on the Ohio River is presented in this chapter.

5.1 Emsworth miter gate description

The Emsworth Lock and Dam is located on the Ohio River about 6 miles downriver from Pittsburgh, Pennsylvania. The main lock chamber is 110 ft by 600 ft (34m × 183m). The original steel miter gates were designed in 1920 and were replaced in 1979 after suffering significant fatigue and corrosion damage during their service life (Ellingwood, Zheng and Bhattacharya, 1996). The availability of the records of the service history of these gates provides a good opportunity to validate the time-dependent reliability analysis methods for condition assessment and life prediction of such structures.

Both the original gate and its replacement gate are vertically framed steel structures, as illustrated in Figure 5.1. They are similar structurally, except in the position of the vertical girders and the configuration of the diagonal bracing. For the original gate, a vertical beam, indicated in Figure 5.1 as Beam No. 7, was placed at the midspan of this gate; in the replacement gate, a stronger vertical girder was used in this position. Each gate leaf is framed by two large horizontal girders at the top and bottom that span approximately 61.5 ft (18.7 m) from the quoin to the miter, and by vertical beams spaced at 58 in (1.47 m) that are laterally braced. The height of the gate from the sill to top girder is approximately 26.5 ft (8.1 m). Diagonal bracing is provided for torsional stiffness and dimensional stability. The upstream face of the gate leaf is covered by skin plates, which provide water-retention and resistance to lateral-torsional buckling of the beams.

Typical cross sections of the top girder and Vertical Beam No. 7 of the original gate are illustrated in Figure 5.2 (Ellingwood, Zheng and Bhattacharya, 1996). Both components were designed as flexural members, with flange consisting of two angles that are riveted to the web plate. A portion of the plate is included in the compression (upstream) flanges of the vertical beam. The effective width of this compression flange is determined from the local plate stability requirements in the AISC Specification (1989).

The original gate was fabricated with ASTM A7 steel, with a specified yield strength F_y =33 ksi (228 MPa). The replacement gate was constructed with ASTM A36 steel, with specified yield strength F_y = 36 ksi (248 MPa).

5.2 Service load analysis

The cyclic loads used for the fatigue damage analysis in this study are the hydrostatic loads resulting from normal operation of the lock. Extreme service loads, such as impact by barges and debris, are not considered because not enough data is available. A typical load profile on a miter gate is illustrated in Figure 5.3 (Ellingwood, Zheng and Bhattacharya, 1996). The magnitude and fluctuation of the hydrostatic load depend on both upper pool and lower pool elevations. The upper pool is maintained at a nearly constant level by the dam, but the lower pool level fluctuates according to the flow conditions in the river.

Histories of daily pool elevations on the gate and computed stress amplitudes associated with different locations on the top girder and Vertical Beam No. 7 were provided courtesy of Black and Veatch Engineers. Their stress analysis was based on the assumption of elastic structural behavior. The top girder was analyzed as a three-hinge arch, with forces induced from the reactions of the vertical beams. The vertical beams were analyzed as simply supported, with nonuniform distributed load resulting from the hydrostatic loadings. The validity of this approach to structural analysis reportedly was established by a finite element analysis of the gate leaf for selected upper and lower pool elevations.

Each time history includes 5502 data, spanning from Jan 1, 1980 to June 30, 1995. The pool elevations and thus the stress amplitudes were not necessarily the daily maxima/minima; rather, they represented the values at some arbitrary time during the day at which the measurement was taken. An average of about 10 days' data were missing each year. When the data provided were subjected to a preliminary screening prior to analysis, two incorrect readings were identified, in which the lower pool reported was below the sill. These were replaced by the average of readings on preceding and following days. The corrected stress amplitude data are the basis of the subsequent fatigue reliability analysis.

The maximum tension stress in Beam No 7 occurred in the downstream flange about 10 ft (3m) above the sill. The daily mean was 15,250 psi (105 MPa) (within the elastic range), standard deviation was 903 psi (6 MPa), skewness coefficient was -5.3 and kurtosis coefficient was 52.4. The maximum stress for the top girder occurred at its intersection with Vertical Beam No. 7; the mean was 687 psi (4.7 MPa) and the standard deviation was 32 psi (0.2 MPa). Thus the more highly stressed Vertical Beam No. 7 is more critical as far as fatigue damage is concerned. Accordingly, the fatigue reliability analysis is performed on the Vertical Beam No 7.

The PSD of the pool elevations and stress ranges were calculated and are plotted

in Figures 5.4 and 5.5. These PSDs are related clearly, since the stresses were computed from the pool elevations by elastic analysis. The dominant frequency of 0.0177 rad/day is equivalent to a cyclic period of 355 days, which is the annual number of recorded data, and reflects the yearly seasonal fluctuations in river level.

The 5502 data only provide daily stress amplitudes. To evaluate fatigue behavior, the elapsed number of cycles is also needed. Therefore, a complete cyclic stress history must be constructed from the daily stress amplitude data. Due to the operating characteristics of the waterway, the variation in the pool levels during one day is very small. Accordingly, it can be assumed that the amplitudes of the cyclic stresses during each day remains constant, but that the amplitudes vary randomly from day to day. The average number of cycles per day is obtained by dividing the number of cycles per month by the number of days within that month; the average yearly and monthly cycles were determined from the data provided by the US Army Corps of Engineers Ohio River District, as summarized in Figures 5.6 and Figure 5.7, respectively (Ellingwood, Zheng and Bhattacharya, 1996). The ten missing days of data each year are assumed to occur the last 5 days of December and first 5 days of January, corresponding to the holiday season. The mean number of load cycles per day at the Emsworth Lock is approximately 12. The linearity in the yearly data prior to 1940 seems questionable; however, it had only a minor impact on reliability of the gate since the dispersion in other parameters, such as environmental effects, are more significant.

The analysis of cyclic stresses described in Chapter 3 is facilitated if the distribution of stress ranges can be fitted by a known theoretical distribution. Apart from the four moments, the lower and upper limits of the loading corresponding to the limits of the upper and lower pool levels should be matched. Several distributions, including the Beta and Pearson families of distribution, (Elderton and Johnson, 1969) were tried; however, none of these distributions fitted the data particularly well, especially with regard to the skewness and kurtosis. Therefore, the fatigue analysis was conducted by utilizing an empirical distribution constructed directly from the stress data provided by Black and Veatch Engineers. The empirical PDF of this stress range, $\Delta\sigma$, based on the reconstructed data, is shown in Figure 5.8. The value of stress range is bounded, which is consistent with the limited height of pool elevation. The most likely values of $\Delta\sigma$ range from 12 ksi (83 MPa) to 16 ksi (110 Mpa). Stress ranges below 6 ksi (41 MPa) are unlikely to occur.

5.3 Stochastic crack growth model

Characterization of uncertainty in stochastic crack growth has two components: loading uncertainty and randomness in the crack growth. Both sources of uncertainty must be considered. The loading data are provided in terms of stress range rather than stress, which is different from the examples in Chapter 4. Accordingly, rainflow analysis is not required, and a stochastic model of the stress range process can be developed directly from the data on miter gate operating loads.

In order to analyze fatigue crack growth as a Markov diffusion process, the stress range $\Delta\sigma$ is transformed into a Gaussian process, $G_1(t)$, by the transformation function,

$$\Delta\sigma = F^{-1}\Phi(G_1) \tag{5.1}$$

where $F(\bullet)$ is the empirical CDF of $\Delta\sigma$ (the empirical PDF corresponding to this empirical CDF is shown in Figure 5.8), and $\Phi(\bullet)$ is the standard normal distribution function of $G_1(t)$. The autocorrelation function and power spectral density of the stress range process can be determined from Eqn 5.1. Based on the reconstructed stress history, a time series $G_1(t)$ is produced, and the two-sided power spectral density of $G_1(t)$ is obtained by Fourier transformation of the time series. The value of $S_{G_1}(\omega)$ when $\omega > 0$ is plotted with the dashed line in Figure 5.9. There are several peaks in this PSD, but only one of them, with magnitude equal to 124.0 ksi^2–day/rad, is significant. The other peaks are relatively small. The process $G_1(t)$ is narrow band. The dominant frequency of 0.0177 rad/day is equivalent to a cyclic period of 355 days. This matches the annual number of daily pool level records per year in the original sample. The contribution of $S_{G_1}(\omega)$ at the frequency related to the average daily cycle number, 12, is very small and is not plotted in Figure 5.9.

In order to facilitate the analysis, the power spectral density of $G_1(t)$ was fitted by a rational function. Since there is only one major peak, which is centered at a non-zero frequency, the function,

$$S_{G_1} = \frac{2\alpha\sigma^2\gamma^2}{\pi} \frac{1}{(\omega^2 - \gamma^2)^2 + (2\alpha\omega)^2} \tag{5.2}$$

which corresponds to the second order linear filter,

$$d^2G_1/dt^2 = -2\alpha dG_1/dt - \gamma^2 G_1 + 2\gamma\sqrt{\alpha}\xi(t) \tag{5.3}$$

is sufficient to describe the standard deviation and dominant frequency of interest. Parameter σ is the standard deviation of G_1, γ is equal to the dominant frequency,

α is determined by the peak value of the power spectral density. Therefore, $\sigma = 1$, $\gamma = 0.0177$ and $\alpha = 1/(2\pi S_{G_1}(\gamma)) = 0.00128$. The PSD approximated by Eqn 5.2 is plotted for comparison with the empirical PSD determined from the data with a solid line in Figure 5.9. The mean and c.o.v. of $\Delta\sigma$ estimated from the approximated PSD of G_1 and Eqn 5.1 are 15.3 ksi (106 MPa) and 0.052, which are close to the values, 15.3 ksi and 0.057, estimated from the empirical CDF (cf Figure 5.8).

By characterizing $G_1(t)$ as the output of the second-order linear filter in Eqn 5.3, a three-dimensional Markov vector process can be constructed to depict the crack growth due to random loadings,

$$dA/dt = \nu C(Y\sqrt{\pi A}F^{-1}(\Phi(G_1)))^m \quad (5.4)$$

$$dG_1/dt = G_2 \quad (5.5)$$

$$dG_2/dt = -\gamma^2 G_1 - 2\alpha G_2 + 2\gamma\sqrt{\alpha}\xi_2(t) \quad (5.6)$$

Apart from loadings, propagation of a fatigue crack also depends on factors such as material properties, structural details and environmental effects. The mean effect of these factors on the logarithm of the crack growth rate is reflected by parameters m and log C in Eqn 5.4, and the dispersion is reflected by the noise term X.

The tension flange of Vertical Beam No. 7 has stress raisers due to the presence of the rivets connecting the angles to the webs and uneven corrosion from the aggressive environmental effects due to cycles of alternate wetting and drying. Taking into account these stress raisers, Vertical Beam No. 7 is believed to be comparable to AASHTO (1989) Fatigue Categories D or E (Ellingwood, Zheng, Bhattacharya, 1996; U.S. Army Corps of Engineers, 1992). The AASHTO fatigue data provide information on total life, described in terms of S-N curves for different riveted, bolted and welded structural details, but crack growth rate data for theses fatigue categories could not be located. Thus, to illustrate the proposed method, the parameters of the crack growth rate law are determined from the S-N curves for Categories D and E by assuming that the fatigue lives predicted by both models are identical. The justification for this assumption is that small cracks are inherent in most gate structural components as a result of the fabrication process. As a result, the crack initiation phase is negligible.

The S-N relationship for steel is,

$$\Delta\sigma^m N = C_s \quad (5.7)$$

where $C_s = 10^{9.275}$, and $m = 3.105$ for a Category E detail and $C_s = 10^{9.6648}$, and $m = 2.988$ for a Category D detail (Barsom and Rolfe, 1987).

The deterministic crack growth model is (Eqns 2.20 and 2.21),

$$da/dN = C(Y\sqrt{\pi a}\Delta\sigma)^m \quad (5.8)$$

Assume that Y is a constant, say 1.12, the approximate value for edge cracks when the crack size is not larger than half of the element thickness. Separating a and N and integrating both sides of Eqn 5.8, we have,

$$\Delta\sigma^m N = \frac{a_{cr}^{1-m/2} - a_0^{1-m/2}}{(1-m/2)C(Y\sqrt{\pi})^m} \tag{5.9}$$

in which a_0 is the initial crack size (assumed here to be deterministic) and a_{cr} is the critical crack size. Combining Eqn 5.7 with Eqn 5.9, and assuming $C_0 = C(Y\sqrt{\pi})^m$, we have

$$C_0 = \frac{a_{cr}^{1-m/2} - a_0^{1-m/2}}{(1-m/2)C_s} \tag{5.10}$$

Suppose that a_0 is 0.05 in (1.3mm) and a_{cr} is 3/16 in (4.8mm), which is half the thickness of the flange of the beam. The value of a_0 is near the threshold of detection of several NDE techniques, as will be shown in Chapter 6. When the crack size exceeds half the element thickness, crack growth accelerates rapidly, and there is a considerable decrease in the section modulus, which results in a significant decrease of the element flexural resistance. Eqn 5.10 yields different values of C_0 for different Categories.

To account for the uncertainty in crack growth due to environmental and material variability, assume that the noise for the linear regression equation, expressing $log da/dN$ versus $log\Delta K$, is normal, $\mathcal{N}(0, \sigma_3)$. The noise term for crack growth rate is modeled as,

$$X = 10^{\sigma_3 G_3(t)} \tag{5.11}$$

Since data are unavailable to describe the correlation function of $G_3(t)$, an exponential form is assumed for illustrative purposes,

$$R_{G_3} = \sigma_3 \exp(-\alpha_3|\tau|) \tag{5.12}$$

The standard deviation of the crack growth rate data of carbon steel base plate in a benign environment is approximately 0.1 (Barsom and Rolfe, 1987). Since the gates are subject to a corrosive environment, this standard deviation would be larger; here, σ_3 is assumed to be 0.2. Different values of the correlation factor α_3 are assumed to assess its effect on the probability distribution of crack size. The stochastic fatigue crack growth taking into account the randomness in environmental and material behavior is,

$$dA/dt = \nu C_0(\sqrt{A}\Delta\sigma)^m 10^{\sigma_3 G_3(t)} \tag{5.13}$$

$$dG_3/dt = -\alpha_3 G_3 + \sqrt{2\alpha_3}\xi_3(t) \tag{5.14}$$

Combining Eqns 5.13, 5.14, 5.4, 5.5 and 5.6, we obtain a four-dimensional Markov vector process $\mathbf{Y} = [A, G_1, G_2, G_3]^T$, defined by the stochastic differential equation,

$$d\mathbf{Y}/dt = \mathbf{M} + \mathbf{\Gamma}\xi(t) \tag{5.15}$$

with drift term,

$$\mathbf{M} = [\nu C_0(\sqrt{A}\Delta\sigma)^m 10^{\sigma_3 G_3(t)}, G_2, -\gamma^2 G_1 - 2\alpha G_2, -\alpha_3 G_3]^T \tag{5.16}$$

diffusion term,

$$\mathbf{\Gamma} = \begin{bmatrix} 0 & 0 & 0 & 0 \\ 0 & 0 & 0 & 0 \\ 0 & 0 & 4\gamma^2\alpha & 0 \\ 0 & 0 & 0 & 2\alpha_3 \end{bmatrix} \tag{5.17}$$

and white noise vector,

$$\xi(t) = [0, 0, \xi_2(t), \xi_3(t)]^T \tag{5.18}$$

Solutions to this equation are obtained from the Euler scheme, as discussed in Chapter 3. The CDF of the crack size during the service life of the gate is analyzed in the subsequent section.

5.4 Fatigue reliability analysis of miter gates

The deterioration of the miter gates is most commonly associated with damage due to corrosion, fatigue and fracture (U.S. Army Corps of Engineers, 1993). General corrosion involves a uniform section loss over the entire exposed surface. The section loss aggregates the fatigue/fracture damage processes, and catastrophic failure may result. During the service life of the original Emsworth miter gate, it was noted that due to corrosion-fatigue damage, four vertical beams developed fractures in the downstream flanges under normal loading before the gate was replaced in 1979 (U.S. Army Corps of Engineers, 1992).

The interaction of corrosion and fatigue/fracture damage processes are non-linear and cannot be analyzed by linear superposition (Barsom and Rolfe, 1987). The section loss, L, due to general corrosion is described by

$$L(t) = C_1(t - t_0)^{c_2} \tag{5.19}$$

where $C_1 \simeq 140$, $c_2 \simeq 0.67$ and t_0 =corrosion induction period for the environment of the Emsworth Lock (Ellingwood, Zheng and Bhattacharya). The constants are obtained from experiments, and are defined so that L is in units of μm when t is in years. The section loss decreases the section modulus, thereby increasing the maximum tension stress and stress range in the beam. This increase in the stress range is amplified by the power m when crack propagation occurs. The corrosion-fatigue damage is modeled by,

$$dA/dt = \nu(t)C(Y\sqrt{\pi A}R(t)\Delta\sigma(t))^m X(t) \tag{5.20}$$

where $\Delta\sigma(t)$ and $X(t)$ are random stress processes as described in the preceding sections. The correlation factor α_3 of the noise $X(t)$ was assumed to be 2.5×10^{-6}, which represents the situation in which the noise is highly correlated with respect to time. The cyclic rate ν is modeled as a deterministic value before 1940 and a uniform random variable after 1940. The ratio of the original elastic section modulus to the degraded section modulus with respect to time, $R(t)$, is modeled as $C_R B(t)$, where $B(t)$[1] is the mean value of $R(t)$, and C_R is assumed to be a uniform random variable with unit mean and $c.o.v = 0.2$.

The CDFs of the crack size due to corrosion-fatigue for Vertical Beam No. 7 modeled as a Category E detail at T =20, 40 and 60 years are plotted on Figure 5.10. The curves shift to the right and the probability that $a \geq a_{cr}$ increases when the time increases. Defining $p_f = P(a \geq a_{cr})$, the failure probability with respect to time is plotted with the solid line in Figure 5.11. The failure probability at $T = 60$ years is around 0.47, which is consistent with the observed gate performance.

To examine the effects of the parameters of X on corrosion-fatigue damage, the standard deviation, σ_3, was changed from 0.2 to 0.1 and the failure probability, p_f, is replotted in Figure 5.11. The effect of σ_3 is not significant and becomes negligible when the time increases. Next, the correlation parameter, α_3, was increased to 2.5×10^{-2}, corresponding to weakly correlated noise. As shown in Figure 5.11, differences in p_f due to α_3 are more significant than those due to σ_3. Weakly correlated crack growth noise results in lower values of p_f when $p_f \leq 0.12$, but higher values of p_f when $p_f \geq 0.12$ due to the interaction of the mean and dispersion discussed in section 4.1. In reality, small values of p_f are of most concern. While an assumption that the noise is uncorrelated causes p_f to be slightly underestimated, replacing the noise with a random variable with the same variance yields a pessimistic estimate of the reliability of the structure, and might lead to unnecessary repair and costly maintenance actions. Further experiments are required to determine the characteristics of the correlation structure of the noise term and to ensure an accurate life prediction.

[1] $B(t)$ is provided courtesy of Dr. Baidurya Bhattacharya, graduate of The Johns Hopkins University

To study the effect of the randomness in the corrosion process, $R(t)$ is modeled as a deterministic function, as in an earlier study (Ellingwood, Zheng and Bhattacharya, 1996). The failure probability is shown in Figure 5.11, indicating a significant role in the randomness of the corrosion process. The randomness in the corrosion should be considered in reliability-based condition assessment and in scheduling maintenance and repair prior to failure. Failure probabilities with and without the corrosion effect are calculated and plotted in Figure 5.12. To separate the effects of randomness and mean in the corrosion, only mean corrosion is considered. The failure probabilities are very sensitive to the presence of corrosion, plausible variations leading to an order of magnitude difference in failure probability for a service period of 60 years. It is also interesting to note that the probability is very close to that found in the earlier study based on a total life analysis (S-N curve) using Miner's rule for variable amplitude fatigue (Ellingwood, Zheng and Bhattacharya, 1996) in Figure 5.12. The close agreement is due to the small variance in the cyclic stresses.

The effect of change in structural detail is examined by recomputing the failure probability assuming that vertical Beam No. 7 can be modeled as a Category D detail. It was found that $p_f = 1.5 \times 10^{-3}$ at $t = 60$ years and zero when $t < 60$ years. This is of the same order as those found in an earlier study based on a total life analysis, which indicated that $p_f = 2.1 \times 10^{-3}$ at 60 years, and around zero, otherwise (Ellingwood, Zheng and Bhattacharya, 1996). The failure probability is much lower compared with that for the Category E detail. It seems possible that gate performance in service might be improved by detailing its connections in a manner that would reduce the stress raisers that result from current design and fabrication practice.

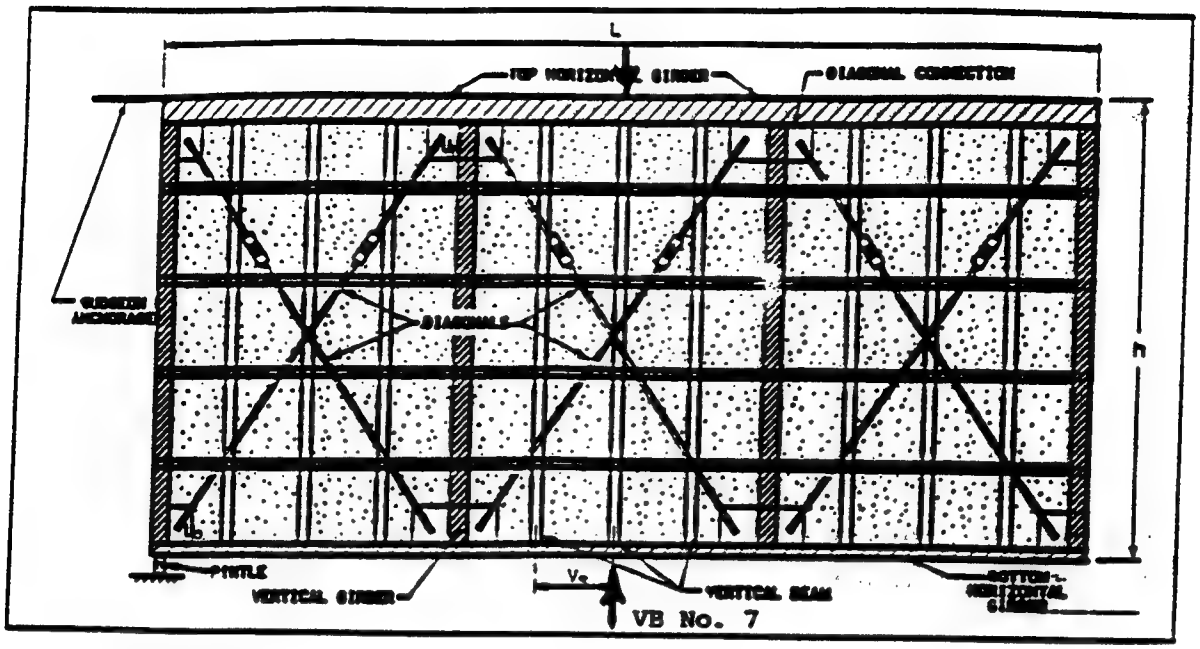

Original miter gate at Emsworth

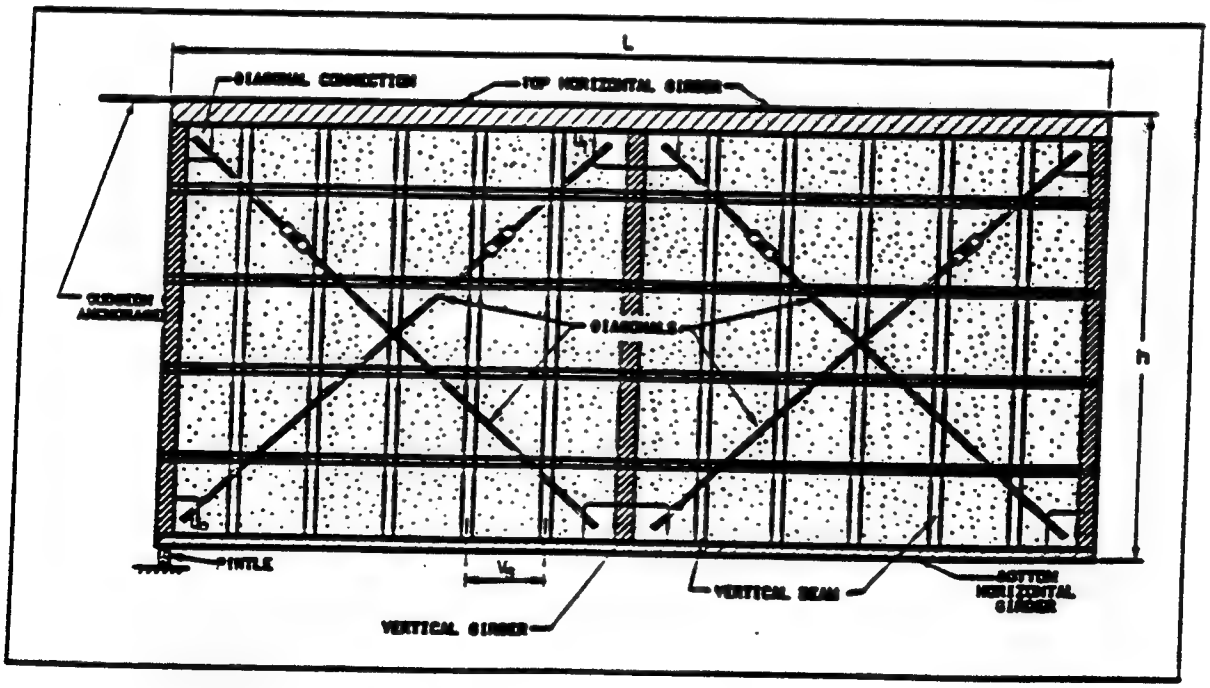

Replacement miter gate at Emsworth

Figure 5.1: Schematic of original and replacement miter gates-Emsworth Lock (Ellingwood, Zheng and Bhattacharya, 1996)

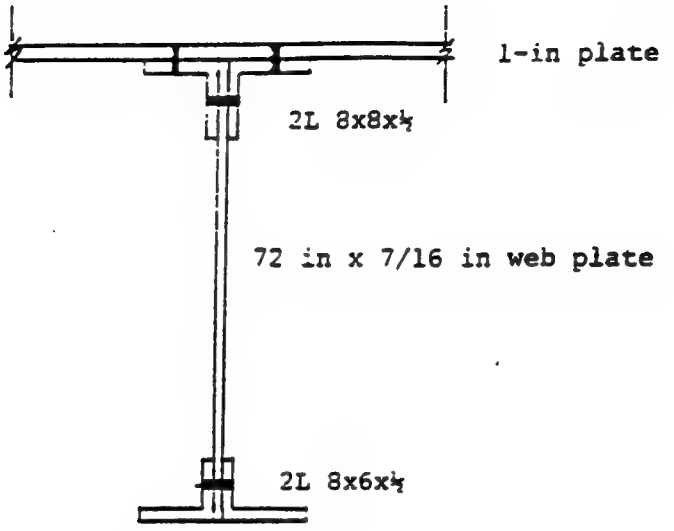

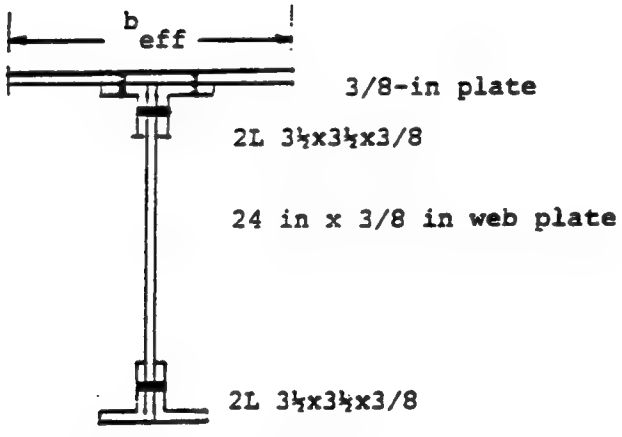

Figure 5.2: Cross section of top girder and vertical beam from Emsworth Lock (Ellingwood, Zheng and Bhattacharya, 1996)

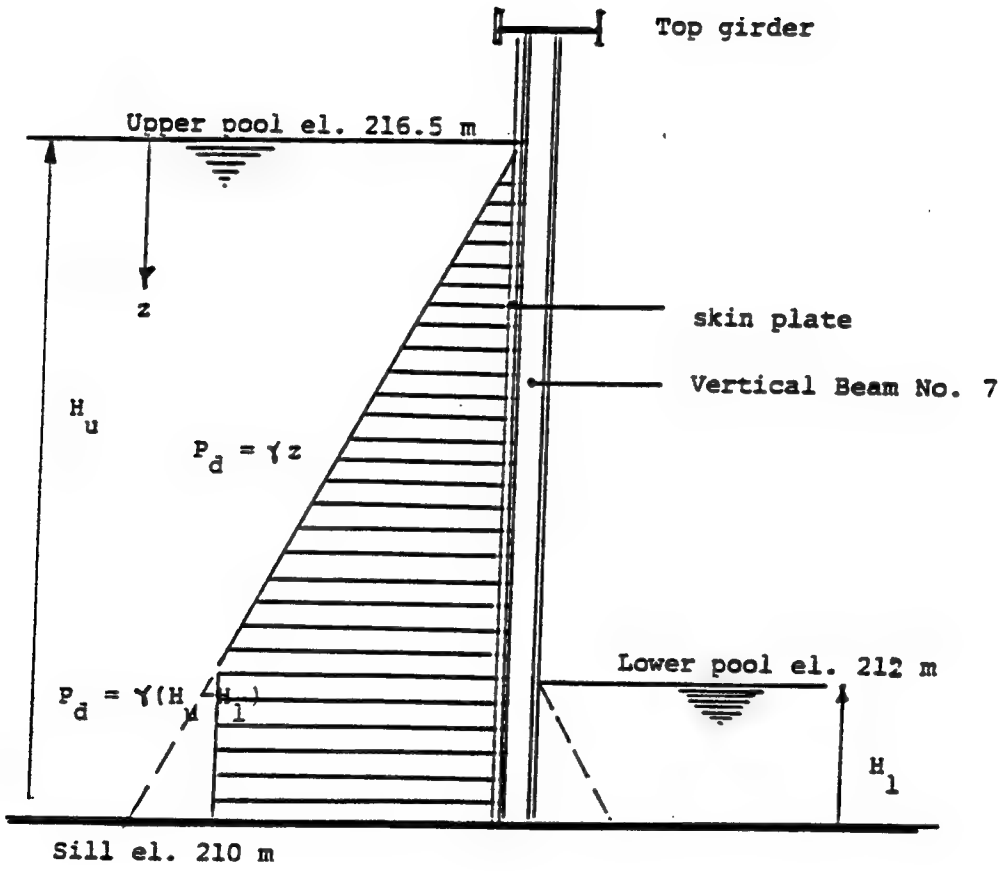

Figure 5.3: Hydrostatic load acting on gate (Ellingwood, Zheng and Bhattacharya, 1996)

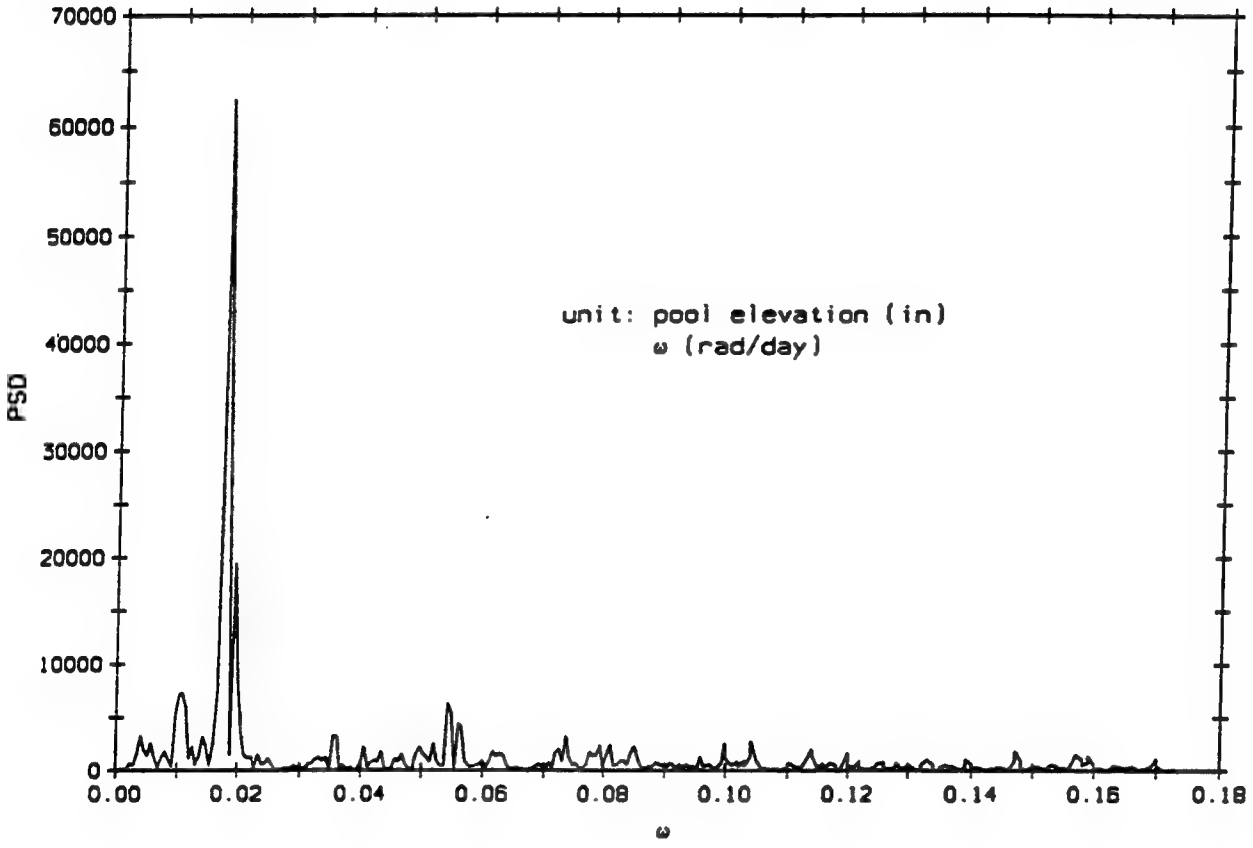

Figure 5.4: PSD of the pool elevation

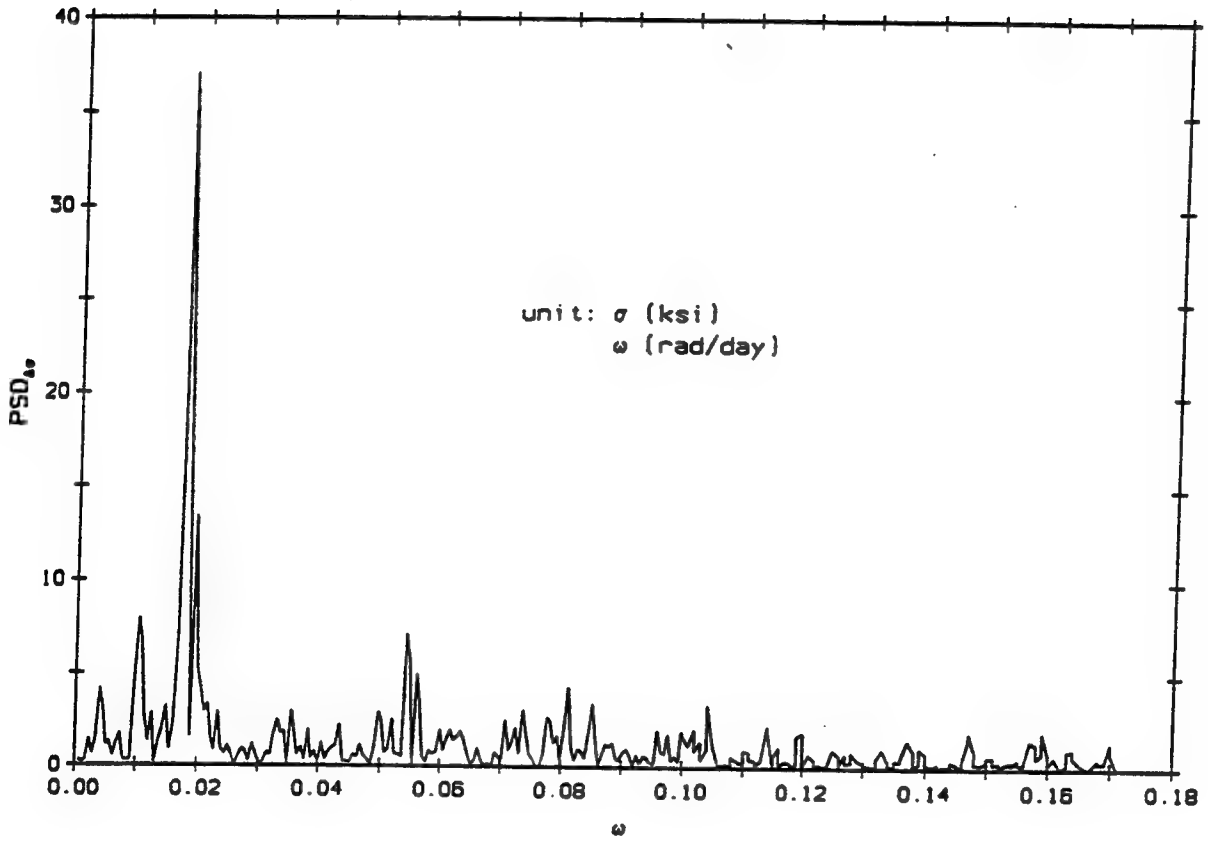

Figure 5.5: PSD of the stress range

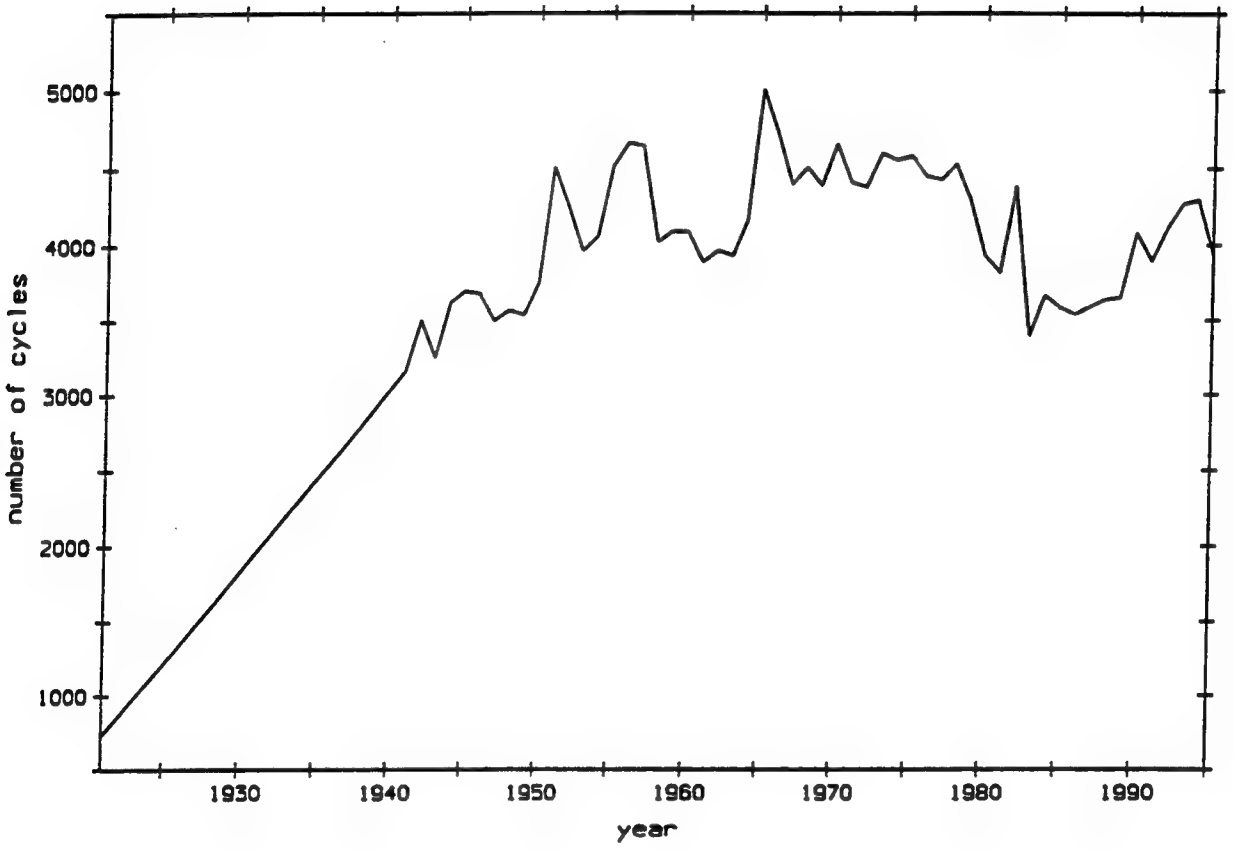

Figure 5.6: Yearly hydrostatic cycles for Emsworth Lock

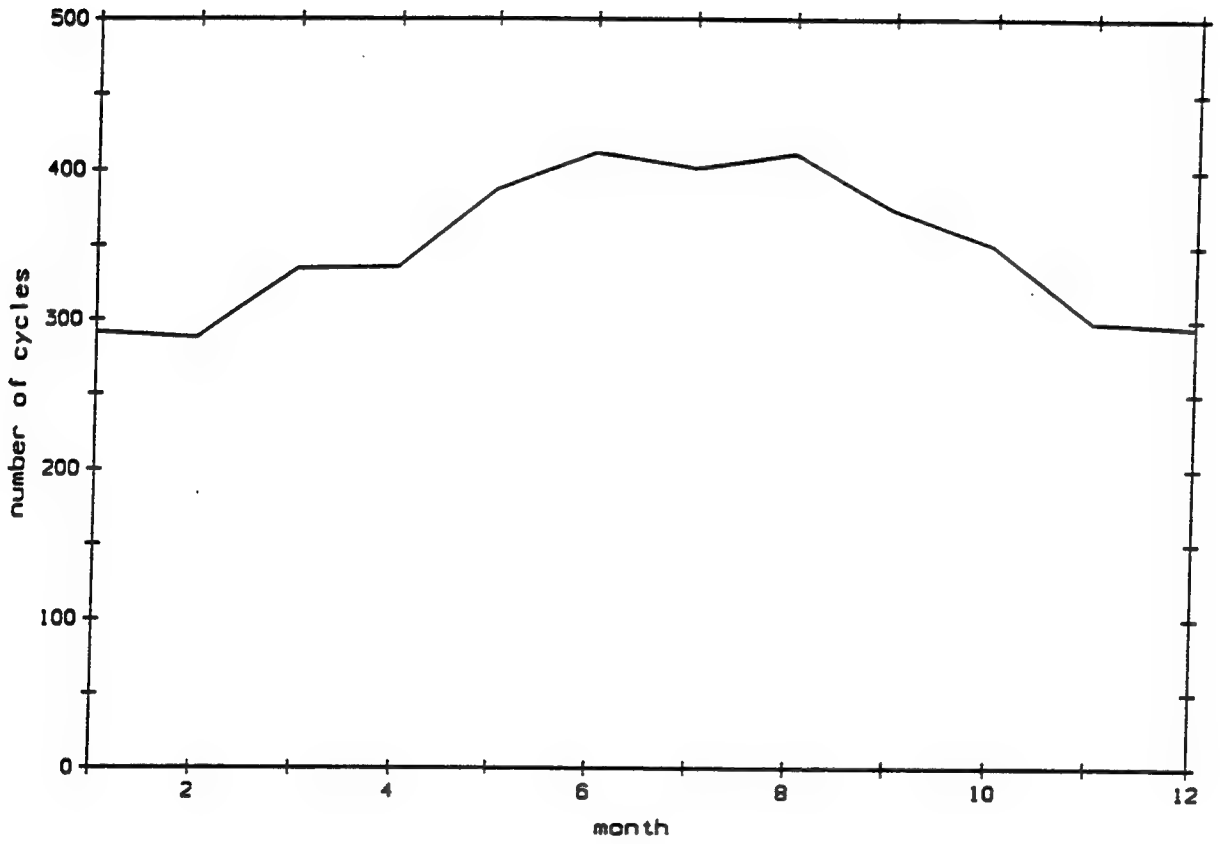

Figure 5.7: Monthly hydrostatic cycles for Emsworth Lock from 1956 to 1995

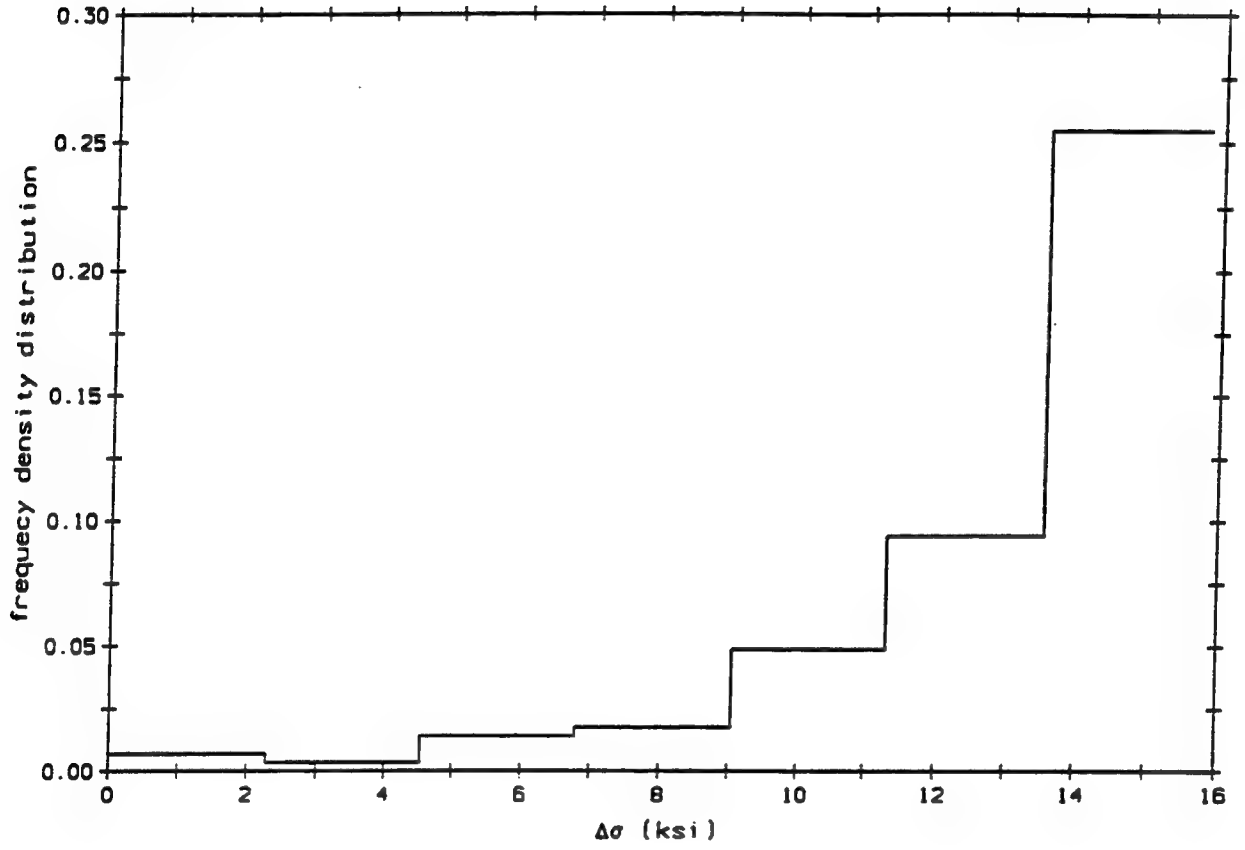

Figure 5.8: Frequency density distribution of the stress range

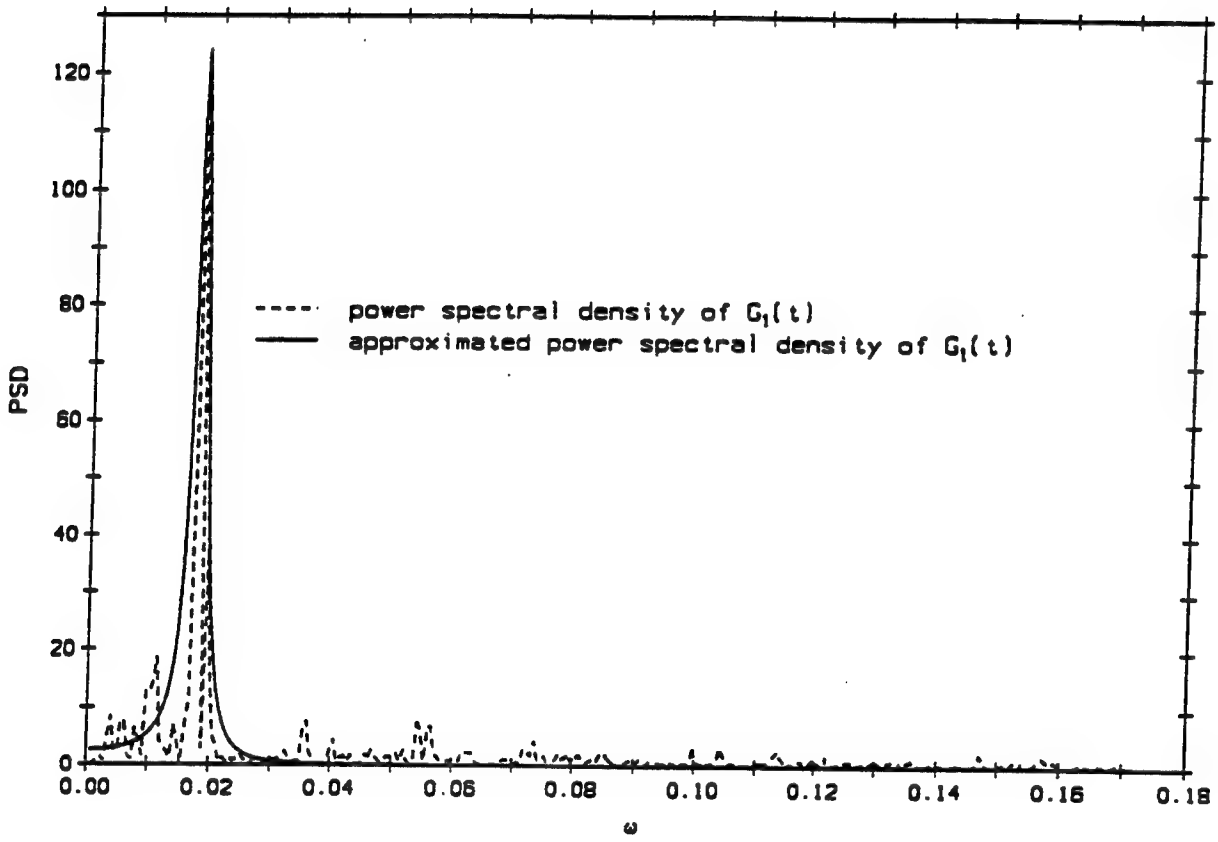

Figure 5.9: PSD of $G_1(t)$

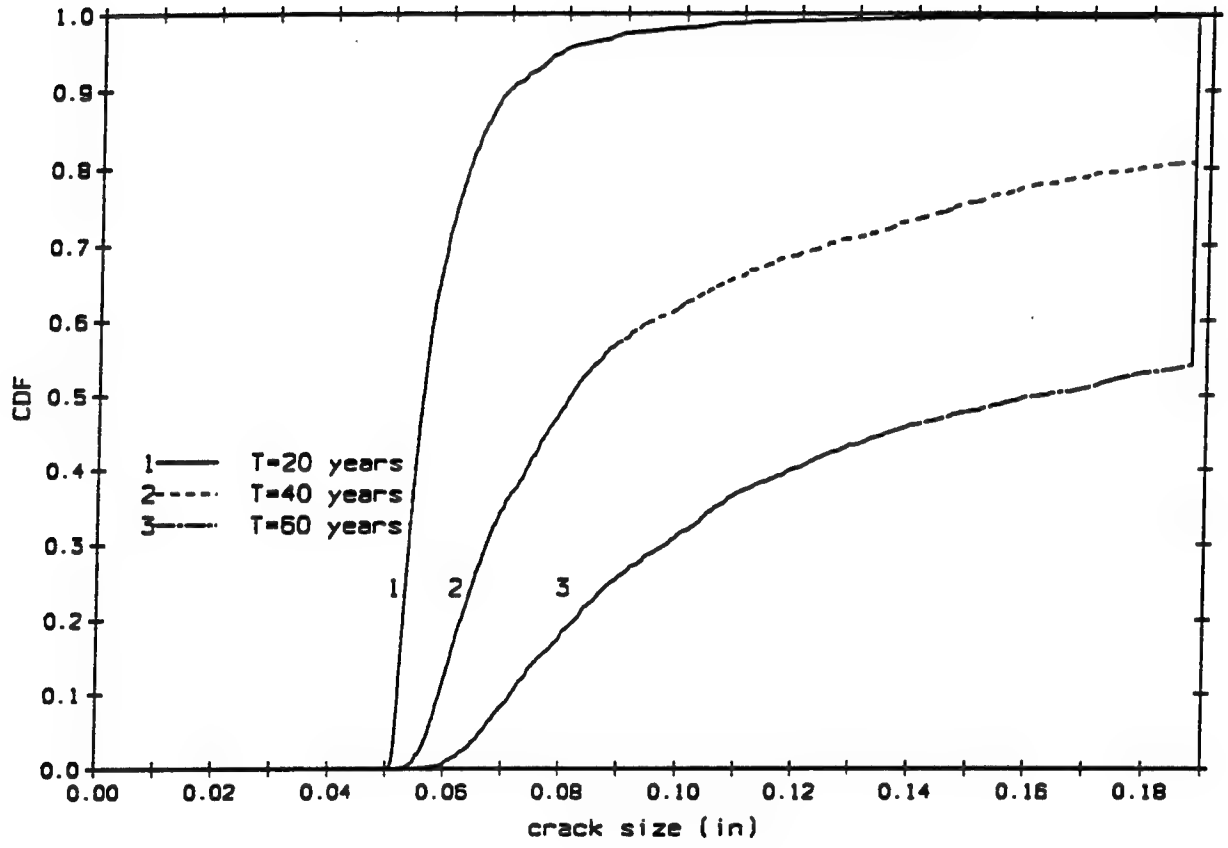

Figure 5.10: CDFs at different times

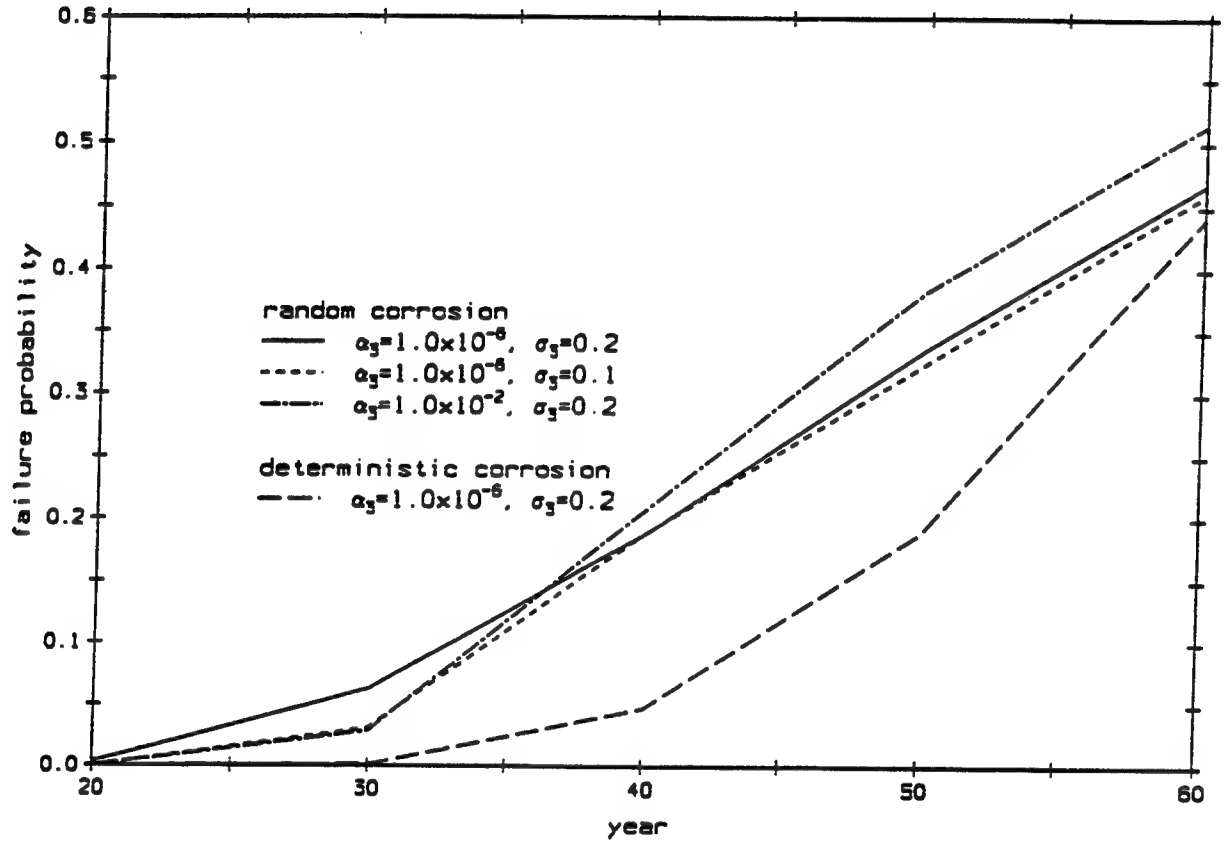

Figure 5.11: Failure probability versus time

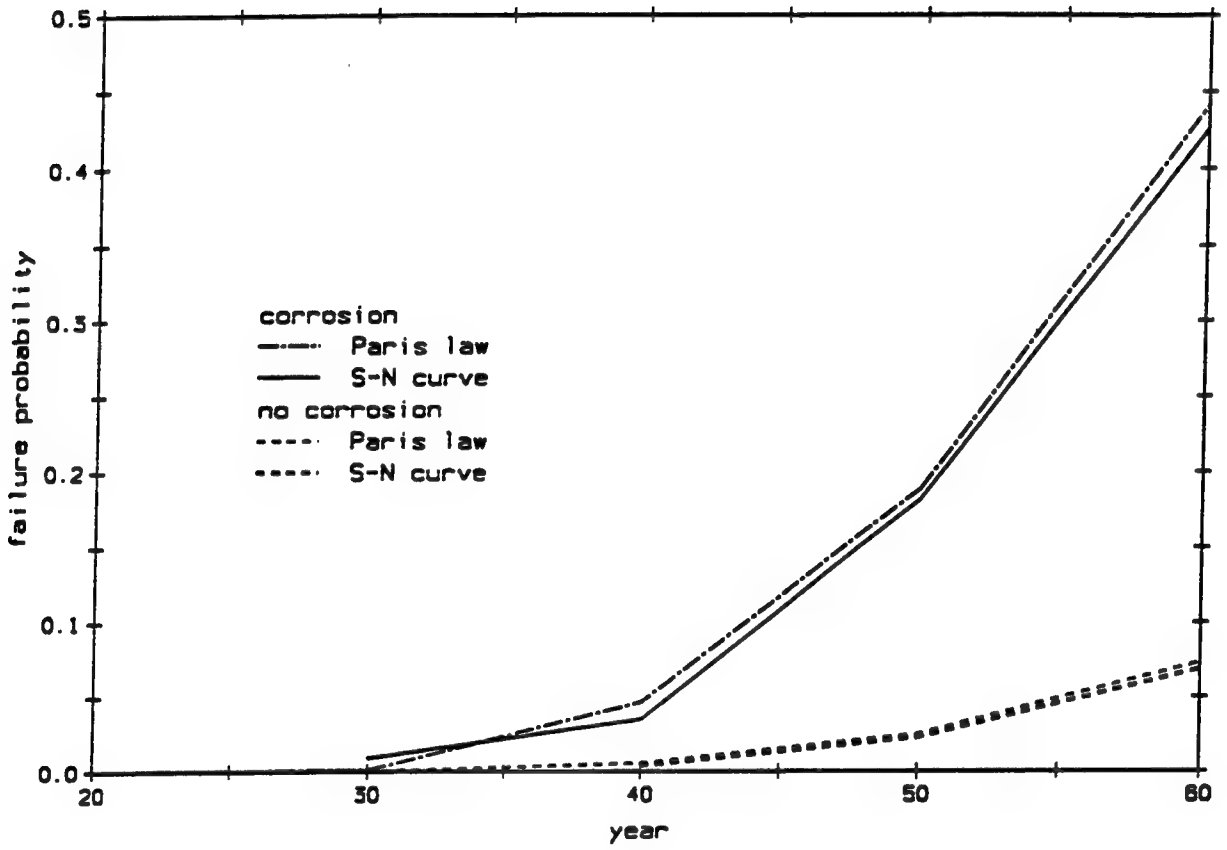

Figure 5.12: The effect of corrosion on time-dependent reliability

Chapter 6

Non-destructive Evaluation

The need for reliable inspection tools to detect and quantify fatigue cracks in steel structures without impairing their function in service is evident. For example, a study by Chase (1994) showed that almost half of the bridges in the United States have steel girders, and fatigue cracks are a major problem in them. Inspections of miter gates at locks and dams typically reveal extensive fatigue cracking in the downstream girder flanges, which are subjected to tension (U.S. Army Corps of Engineers, 1992). Non-destructive evaluation techniques (NDE) facilitate inspection and play an important role in structural reliability assessment as well as in repair decisions, especially when combined with methods of failure analysis derived from fracture mechanics. A summary of different performance characteristics of several commonly used NDE techniques, such as sensitivity to the flaw size and adaptability to field in civil structures is given in Table 6.1 (Chase, 1994).

This chapter reviews the performance of different NDE techniques, characterizes the uncertainties that are inherent in flaw detection and measurement, and identifies the factors that appear to be particularly important in in-service condition assessment and reliability evaluation. A guideline for repair is suggested. Examples of condition assessment based on MT and UT are illustrated.

6.1 Mathematical tools for NDE characterization

Two issues are of primary concern for reliability-based condition assessment: flaw detection and flaw measurement.

6.1.1 Probability of flaw detection

Probabilistic characteristics of each NDE technique determine the quality of the information gained regarding the in-service crack size from the inspection data. Some authors have postulated that the detection probability is independent of flaw size. This is counter-intuitive, inasmuch as large flaws seem more likely to be detected than small ones. A probability of detection (POD) curve for a particular NDE method can be obtained by introducing flaws of various sizes, a, into test specimens, asking inspectors to examine the specimens in a controlled experiment, and plotting the $POD(a)$ based on these experimental observations. Generally, $POD(a)$ increases with increasing flaw size. Each NDE device has an inherent minimum resolution and thus a threshold of detection, a_{th}. The POD curve will be nonzero for $a > a_{th}$. Conversely, the situation may arise where a flaw is indicated when none is present. This situation is described by the false call probability (FCP), i.e. $POD(a = 0) > 0$. The FCP is significant for non-visually-assisted techniques, such as UT, EC and RT. To obtain a complete picture of the flaw detection capacities of a particular NDE method, POD curves should be developed from tests which include both blank and flawed specimens.

Several POD models have been proposed; their parameters can be estimated through regression analysis of experimental data, as shown in Figure 6.1. Berens (1989) suggested that a log-logistic function is suitable for fitting such data:

$$POD(a) = (1 + \exp(-(\frac{\pi}{\sqrt{3}}(\frac{\ln a - \mu}{\sigma}))))^{-1}; \qquad a > 0 \tag{6.1}$$

where μ and σ are parameters depending on factors, such as equipment, field conditions and inspector training. Parameter $\mu = lna_{0.5}$, where $a_{0.5}$ is the median flaw size satisfying $POD(a_{0.5}) = 0.5$; σ is related to the steepness of the $POD(a)$ curve, a smaller value of σ being associated with a steeper $POD(a)$ curve. The log-logistic model is similar to a lognormal distribution.

Others have suggested that the POD can be modeled by the exponential distribution (e.g., Tsai and Wu, 1993),

$$POD(a) = \begin{cases} 1 - exp(-c(a - a_{th})) & a \geq a_{th} \\ 0 & a < a_{th} \end{cases} \tag{6.2}$$

in which a_{th} =minimum detectable flaw and c =constant, both of which depend on the NDE device and its resolution. If NDE were perfect, every flaw above the threshold of detection, a_{th}, would be detected, and $POD(a)$ would take on the appearance of a Heaviside function,

$$POD(a) = H(a - a_{th}) \tag{6.3}$$

Such is not the case, of course; however, one would like c to be as large as possible in order to approach this condition.

Eqn 6.1 and 6.2 both are consistent with intuition, in that large flaws almost certainly will be detected while very small flaws will almost certainly be missed, assuming that the entire component is inspected. Considering that even very large flaws may not be detected with certainty, an alternative expression for the probability of detection was proposed (Staat, 1993):

$$POD(a) = (1-p)(1-exp(-ca)) \qquad a \geq 0 \tag{6.4}$$

Note that this $POD(a)$ is asymptotic to $1-p$ for large values of a. There is no threshold of detection in this model, i.e., flaws larger than zero have a finite POD. A model combining the best features of both Eqns 6.2 and 6.4 (and also more constants that must be determined experimentally) would be,

$$POD(a) = (1-p)(1-exp(-c(a-a_{th}))) \qquad a \geq a_{th} \tag{6.5}$$

The probability of detecting flaws smaller than a_{th} would be zero, while the probability of detecting very large flaws would be $1-p$; typically p would be on the order of $0.01-0.05$.

One disadvantage of the models represented by Eqn 6.2-6.5 is that none of them incorporates the false call probability. Taking this into account, Heasler, Taylor and Doctor (1993) proposed a logistic model using a instead of $\ln a$ in Berens's model.

$$POD(a) = (1+\exp(-(\alpha+\beta a)))^{-1} \tag{6.6}$$

Thus,

$$FCP = POD(a=0) = (1+\exp(-\alpha))^{-1} \tag{6.7}$$

A comparison of the above POD curves is presented in Figure 6.2.

6.1.2 Flaw measurement error

Error in flaw sizing is also an important issue. The relationship between the actual and measured flaw size is generally described by a linear function determined by regression analysis. There are two types of regression analysis. One is conducted with given measured size, a_m, and variable true size, A, (e.g. Rummel, et al, 1989),

$$A = \beta_1 + \beta_2 a_m + \epsilon \tag{6.8}$$

The random variable, ϵ, describes replicate experimental errors with respect to A, and is assumed to be approximately normally distributed with standard deviation varying with different NDE procedures and inspection teams. Coefficients of these models are obtained from regression analysis. The regression analysis conducted in terms of A on a_m is most useful because the true size needs to be estimated from an inspection for reliability assessment. An alternative proposed regression model is in terms of A_m (or $\log A_m$) on a (or $\log a$) (e.g. Heasler et al, 1990; 1993),

$$\log A_m = \beta_1 + \beta_2 \log a + \epsilon \tag{6.9}$$

$$A_m = \beta_1 + \beta_2 a + \epsilon \tag{6.10}$$

or

$$A_m = \begin{cases} \beta_1 + \beta_2 a + \epsilon & a \geq c_{th} \\ c_{th} & \text{otherwise} \end{cases} \tag{6.11}$$

in which c_{th} represents the resolution limit, the smallest flaw that can be sized by the NDE equipment tested. Eqn 6.9 employs a log transformation of the data to stabilize the errors. On the other hand this implies that errors are proportional to flaw size (with zero error for zero flaw size), which generally is not the case. While Eqn 6.10 implies that the error does not change with size, negative values in measured size may occur if the standard deviation of ϵ is relatively large. Eqn 6.11 implies that a measured flaw size can never be smaller than the resolution limit. Eqns 6.9-6.11 presume that the true size is given, and the measured size is an estimate; this is characteristic of laboratory test programs, but is contrary to the needs of reliability assessment.

The role of NDE in time-dependent reliability analysis is examined in section 6.3.

6.2 Performance of NDE techniques

6.2.1 Visual inspection (VT)

The oldest and still most widely used NDE method for steel miter gate structures is visual inspection. Underwater inspections for cracks usually are performed visually, supplemented by magnetic particle inspection (MT) after cleaning (Kishi, 1988). Visual inspection can identify regions of corrosion, or peeling or blistering of coatings that may indicate damage to the substrate. Special attention must be paid to welds and to heat-affected zones of weldments.

Liquid penetrant (PT)

Liquid penetrant is effective in locating surface flaws in essentially nonporous materials. The fluorescent or visible penetrant seeps into various types of minute surface openings by capillary action. Indications of defects thus are given. The advantage of this method is that it depends neither on ferromagnetism (as does, for example, MT) nor on defect orientation as long as only surficial flaws are considered. The major limitation of PT is that it cannot detect subsurface flaws and can be excessively influenced by the surface roughness or porosity. Studies of application of PT to the detection of fatigue cracks in steel bridges have revealed that this method is good for crack lengths greater than approximately 10 mm in welds and 24 mm in other types of joints such as bolted, riveted and eyebar joints(Chase, 1994).

Examining the data by Rummel, Hardy and Cooper (Metals Handbook, 1989) from an analysis of data from 328 fatigue cracks in 118 aluminum alloy specimens, it is found that the POD curve (Section 6.1.1) for PT is close to the exponential form,

$$POD = 1 - exp(-c(a - a_{th})); \qquad a \geq a_{th} \tag{6.12}$$

where the parameters are estimated as $c \simeq 2/mm$ and $a_{th} \simeq 0.5mm$, as shown in Figure 6.3. No false call data were included in the analysis, and thus the false call probability equals zero. The flaw measurement error (Section 6.1.2) is described by a linear function of the actual flaw size A in terms of measured flaw size, a_m;

$$A = b_1 + b_2 a_m + \epsilon \tag{6.13}$$

where the parameters are estimated as $b_1 \simeq 0$, $b_2 \simeq 0.9$ and $\sigma_\epsilon \simeq 0.638mm$ assuming that the data falls in a 98% interval.

Data on crack detection in 4330 vanadium modified heat treated steel (Packman et al, 1969) imply a typical PT POD:

$$POD = \frac{1}{1 + exp(-(a_1 + a_2 a))} \tag{6.14}$$

as illustrated in Figure 6.4, where the parameters are estimated as $a_1 \simeq -2.2$, and $a_2 \simeq 0.47/mm$. The corresponding FCP is about 10%. No sizing data could be located for steel.

Magnetic particle inspection (MT)

MT is utilized to reveal surface and subsurface discontinuities in ferro-magnetic materials. When the material is magnetized, a leakage field is generated by magnetic discontinuities that lie in a direction generally transverse to the direction of the magnetic

field. The leakage field gathers and holds some of the finely divided ferro-magnetic particles applied over the surface. This forms an outline of the discontinuity and indicates its location, size and shape.

MT is capable of detecting fine, sharp and shallow surface cracks in ferro-magnetic materials, but is not good for wide and deep defects. It cannot be used for nonferro-magnetic materials. The magnetic field must be in a direction that intercepts the principal plane of discontinuity for a good result. Thin coatings of paint and other nonmagnetic coverings adversely affect the sensitivity. MT is effective in detecting surficial defects in excess of about 5 mm long in welds and greater than 25 mm in bolted or riveted joints (Chase, 1994).

Studies by Packman et al (1969) indicated that a typical MT POD for cracks in 4330 vanadium modified steel is of the form of Eqn 6.14, as shown in Figure 6.4, where $a_1 = -2.94$, and $a_2 = 1.42/mm$. The corresponding FCP is about 5%. No data could be located for sizing error, but it has been claimed that MT is quite good at quantifying crack size (Chase, 1994).

6.2.2 Ultrasonic inspection (UT)

UT is used to detect both surface and internal discontinuities in materials. Beams of high frequency sound waves introduced into the material attenuate due to wave scattering and are partially or completely reflected at interfaces. The reflected beam is displayed and analyzed to define the presence and location of defects such as cracks or voids. UT can also be used to measure thickness and extent of corrosion by monitoring the transit time of a sound wave through the component or the attenuation of the energy. UT can be performed under water.

The principal advantages of UT are its portability, superior penetrating power and volumetric scanning ability, which allows the detection of interior flaws. UT is sensitive to crack length approximately greater than 5 mm in welds and 10 mm in bolted or riveted joints, and its complexity and operator dependence are moderate (Chase, 1994). Its disadvantage is that defects are difficult to detect in portions of structure where the surface is rough or irregular or where flaws are very small, thin or not homogeneous.

Research has been in progress for several years to determine reliability of in-service ultrasonic inspection techniques, with the aim of establishing reliability of the inspection process for pressure vessels and piping systems in nuclear power plants (Heasler, et al, 1993; Heasler, et al, 1996). Data are being obtained from an international

round-robin program on ultrasonic inspection capabilities involving teams from the United States, several European countries and Japan. The types of cracks implanted into the test specimens include fatigue and stress corrosion cracks. The materials employed are clad ferritic steel, cast stainless steel and wrought stainless steel. In civil engineering structures, ferritic steel is of major interest. A typical POD curve for crack depth in ferritic steel developed as part of this program is in the form of Eqn 6.14, with (a_1, a_2) ranging from $(-1.7, 0.173/mm)$ to $(-18.2, 4.268/mm)$, corresponding to a FCP ranging from 15% to 0. The POD curve corresponding to $(-18.2, 4.268/mm)$ is plotted in Figure 6.4. The sizing data for crack depth exhibits considerable scatter. This implies that while UT is good at locating cracks, it may not be suitable for quantifying crack size as shown in Figure 6.5. Moreover, false call probabilities tend to be higher for volumetric inspection methods such as UT, values as high as 27% being reported by some investigators (Heasler, et al, 1990)

6.2.3 Eddy current (EC)

EC is effective in detecting defects at or within a few millimeters of the surface. It is based on the principle of electromagnetic induction. Taking a pipe as an example, a current is created in the pipe by encircling it with induction coils. The presence of a crack in the pipe impedes the current flow and changes its direction, causing changes in the associated electromagnetic field which can be monitored. Thus surface discontinuities having a combination of predominantly longitudinal and radial dimensional components can readily be detected.

Surface discontinuities can be detected by EC with high speed and low cost. If a coating is present, it need not be removed. However, the sensitivity of this method to defects beneath the surface is decreased. Also, laminar defects may not alter the flaw enough to be detected. Defects less than 6 mm (1/4 inch) at the toe of a weld reportedly cannot be detected by EC (Shah, et al, 1994). EC is effective in detecting fatigue cracks with lengths greater than approximately 10 mm in welds and greater than 25 mm in bolted or riveted joints (Chase, 1994).

Research on the ability of eddy-current inspection techniques to detect flaws in steel steam generator tubes (Bowen, et al, 1989) indicated a typical POD curve that is close to Eqn 6.14, with $a_1 = -2.94$ and $a_2 = 9$ and a is percentage of specimen thickness. The typical parameters of the sizing regression of A on A_m are $b_1 = -34\%$, $b_2 = 1.7$, $\sigma_\epsilon = 13\%$, with crack size measured in term of the percentage of the wall thickness. The slope deviates from 1, and the intercept does not equal 0, indicating measurement bias for small flaw sizes. Although the relative value of crack size to wall thickness may affect the accuracy of the inspection, the absolute crack size has

more significant effects on the inspection result. Thus, it is recommended that data for POD and sizing error be provided in the absolute sense. A POD curve assuming that the wall thickness is 25.4 mm is plotted in Figure 6.4. This POD is qualitatively consistent with the results reported by Shah, et al (1994) and Chase (1994).

6.2.4 Acoustic emission (AE)

Sudden movement in stressed materials produces acoustic stress waves. The stress waves can be detected on the surface of the structure by one or more piezoelectric transducers. One source of AE is defect-related active deformation processes such as fatigue crack growth. Thus, AE offers the possibility of monitoring growing defects during service. Research has been conducted to relate AE energy counts to stress intensity factor and strain energy release rate (Yeh, Enneking and Tsai, 1994). However, difficulties still remain in using acoustic transducers to locate or size growing defects accurately due to the noise resulted from various sources. Efforts have been made (Ghorbanpoor, 1994) to improve signal discrimination techniques for AE evaluation of steel bridges. AE is effective for fatigue cracks in steel bridges greater than 10 mm in welds and 20 mm in joints, respectively. More specific information on detection probability or measurement error for AE could not be located. The technique is still relatively new in its application to civil structures.

6.2.5 Radiography (RT)

RT methods are based on the differences in absorption of penetrating radiation, such as X-ray or γ-ray, by different portions of a component. The images produced can be analyzed to locate flaws. RT can detect internal flaws which are not too small in relation to section thickness. Planar defects cannot be detected unless their principal plane is essentially parallel to the radiation beam. In contrast to the other methods above, access to both sides of the component is required. Safety protocols also must be followed. RT is relatively expensive. This technique is effective in detecting cracks greater than approximately 10mm in welds and bolted and riveted joints (Chase, 1994).

A typical POD curve for X-ray inspection obtained by Rummel, Hardy and Cooper (1989) from data on 328 fatigue cracks in 118 aluminum alloy specimens can be modeled by Eqn 6.12, with $a_{th} = 0.5mm$ and $c = 0.36/mm$. The slope is low compared with that of the PT as shown in Figure 6.3. The sizing data exhibit considerable scatter, as shown in 6.6.

6.2.6 Summary

Most of the available data for describing NDE capacities quantitatively have been obtained from laboratory experiments. In-service data are generally insufficient for providing statistical information. For surface or near-surface cracks, MT demonstrates good performance as far as detecting and sizing accuracy are concerned. Furthermore, it can be applied both in air and underwater. For internal cracks, UT is a good choice for locating cracks, but may not be as good for measuring crack size. POD data regarding different types of cracks (e.g. fatigue or stress corrosion cracks) in different materials (e.g. ferritic or wrought stainless steel) using UT are available only for laboratory conditions. Most POD data are applicable to welded connections, but it is not clear how to apply them to bolted, riveted or eyebar connections, for which NDE data are more limited. Some studies on field inspection of different joint details have provided qualitative information regarding detection capacities, but quantitative data are not available (e.g. Chase, 1994).

6.3 Role of NDE in reliability-based condition assessment

While the analytical models of structural deterioration presented in Chapters 3 and 4 provide a forecast of the structure behavior and a basis for estimating when inspection might be required, periodic non-destructive inspection gives additional information on the in-service condition of the structure. Since there are errors and uncertainties inherent in the inspection process, as described in the preceding sections, decisions regarding maintenance or repair should be based on the analytical predictions, inspection data and uncertainties in the inspection techniques. Accordingly, if a flaw is detected and the measured size is greater than some predetermined (see below) critical value, c_{cr}, the component should be repaired. If, however, no flaw is detected or if the measured flaw size is less than c_{cr}, the decision to continue service should be based on the uncertainties associated with the inspection and the prior knowledge of the probability density function (PDF) of crack size. In order to provide guidelines for this decision process, this section examines the role played by NDE in the reliability-based condition assessment of structures.

Suppose a crack is detected during NDE and the measured size is $A_m = c$. If the inspection were perfect, the actual crack size A would be equal to c. However, the measurement is uncertain. The relationship between actual and measured crack size is assumed to be given by Eqn 6.13, where ϵ is normally distributed with zero mean

and standard deviation σ_ϵ. Let D be the event that a crack is detected. Assume the probability distribution of the true crack size is normal, with mean equal to $b_1 + b_2 c$ and standard deviation equal to σ_ϵ,

$$P(A \leq a | (A_m = c) \cap D) = \Phi(\frac{a - b_1 - b_2 c}{\sigma_\epsilon}) \tag{6.15}$$

where $\Phi(\bullet)$ is the standard normal CDF.

If the safety margin is $M = a_{cr} - A$, in which a_{cr} =critical crack size, a repair action should be taken when $P(M < 0) = p_{cr}$, that is,

$$1 - P(A \leq a_{cr}) = 1 - \Phi(\frac{a_{cr} - \mu_A}{\sigma_A}) = p_{cr} \tag{6.16}$$

Combining Eqns 6.15 and 6.16, we obtain a linear function of c_{cr}, the critical measured size, versus a_{cr}, the critical true size,

$$c_{cr} = \frac{1}{b_2} a_{cr} - \frac{b_1 + \Phi^{-1}(1 - p_{cr})\sigma_\epsilon}{b_2} \tag{6.17}$$

The slope of this function is the inverse of the slope of the sizing regression line, b_2. The intercept is $-\frac{b_1 + \Phi^{-1}(1-p_{cr})\sigma_\epsilon}{b_2}$. The parameter b_1 makes c_{cr} shift down if $b_1 > 0$, and up if $b_1 < 0$. The contribution of σ_ϵ, the measure of sizing scatter, is proportional to $-\Phi^{-1}(1 - p_{cr})$, which is greater than 0 if $p_{cr} > 0.5$, and less than or equal to 0 otherwise. For the special case in which $p_{cr} = 0.5$, σ_ϵ has no influence on c_{cr}, which means that the decision is made based only on the mean performance of sizing. For perfect sizing, $c_{cr} = a_{cr}$.

It should be noted that the values of a_{cr} and p_{cr} depend on factors such as the redundancy of the structure and inspection period. For example, if the structure is highly redundant, damage to one element does not affect significantly the performance of the whole structure, and the values of a_{cr} and p_{cr} can be set relatively high. Determination of a_{cr} and p_{cr} is beyond the scope of this study, which focuses on identification of significant factors for reliability analysis.

In order to identify c_{cr}, it is important to have accurate information for the regression of A on a_m. Laboratory studies have been conducted to measure cracks in aluminum specimens (e.g. Rummel et al, 1989; Berens; 1989). However, measurement error statistics representative of cracks in steel components in service (e.g., bridges, miter gates, offshore platforms) could not be located for common NDE techniques used in field inspection. Moreover, although extensive laboratory studies have assessed the inspection performance of UT and EC on steel (e.g., Heasler, et al; 1993; Bowen et al, 1989), the regression analysis of these experimental data was expressed

in terms of A_m on a. This presentation does not match the needs of reliability-based structural condition assessment, where the true flaw size is required for calculating fatigue failure probability. Furthermore, the statistics of A_m on a cannot be simply converted to those of A on a_m (Benjamin and Cornell, 1970).

If no crack is detected, it does not necessarily mean that no crack is present. Let $f_A(a)$ be the prior PDF of crack size. The conditional posterior CDF of crack size (following inspection) is,

$$P(A \leq a|\bar{D}) = \frac{P(A \leq a \cap \bar{D})}{P(\bar{D})} \tag{6.18}$$

in which

$$P(A \leq a \cap \bar{D}) = \int_0^a P(\bar{D}|A = a) f_A(a) da \tag{6.19}$$

$$= \int_0^a (1 - POD(a)) f_A(a) da \tag{6.20}$$

and

$$P(\bar{D}) = \int_0^\infty (1 - POD(a)) f_A(a) da \tag{6.21}$$

The posterior CDF of crack size thus is,

$$P(A \leq a|\bar{D}) = \frac{\int_0^a (1 - POD(a)) f_A(a) da}{\int_0^\infty (1 - POD(a)) f_A(a) da} \tag{6.22}$$

and the posterior PDF is,

$$f''_A(a) = \frac{\partial P(A < a|\bar{D})}{\partial a} \tag{6.23}$$

$$= \frac{(1 - POD(a)) f_A(a)}{\int_0^\infty (1 - POD(a)) f_A(a) da} \tag{6.24}$$

If the CDF of crack size, $F_A(a)$, is available instead of $f_A(a)$, Eqn 6.22 can be re-written as,

$$P(A < a|\bar{D}) = \frac{(1 - POD(a)) P_A(a) + \int_0^a \frac{\partial POD(a)}{\partial t} F_A(a) da}{(1 - POD(\infty)) + \int_0^\infty \frac{\partial POD(a)}{\partial t} F_A(a) da} \tag{6.25}$$

The posterior PDF, which is determined by the POD and the prior PDF, can be used as the basis of decision-making regarding repair. If no repair is made, the posterior PDF can be substituted in the time-dependent reliability assessment as the

initial condition to determine remaining service life or safety margin. For the special case when the detection is perfect, which implies that there is no crack if none is detected, the POD curve is a step function at zero, and the posterior PDF would be a Dirac delta function at $a = 0$. On the other hand, if the POD is nearly zero, the posterior PDF is nearly the same as the prior PDF, which implies that the inspection is not informative; in this case, the decision to repair or continue service must rely only on the prior distribution.

In general, a repair decision might be based on the following decision tree:

$$\text{inspection} \begin{cases} \text{detection} \begin{cases} A_m \geq c_{cr} & \text{repair} \\ A_m < c_{cr} & \text{no repair} \end{cases} \\ \text{no detection} \begin{cases} \text{POD nearly perfect} & \text{no repair} \\ \text{POD good to medium} & \text{consider posterior PDF} \\ \text{POD poor} & \text{based on prior PDF} \end{cases} \end{cases}$$

In field applications to civil structures, MT and UT are common. The impact of these NDE techniques on reliability-based condition assessment is considered in the following illustrations.

6.4 Illustrations of NDE effects on reliability

6.4.1 Crack measurement using MT

This section illustrates the impact of measurement errors on reliability. Assume that MT is used to inspect a steel miter gate similar to the Emsworth gate. The sizing parameters of MT are not available, but it is known that the sizing error is small. Thus, it is assumed that $b_1 = 0$, $b_2 = 1.0$ and σ_ϵ =0.95 mm (0.0375 in), around 10% of the flange thickness. Assume $a_{cr} = 4.8mm$ (around 0.1875 in), which is half of the flange thickness. The required value of c_{cr} changes when the value of p_{cr} varies, based on Eqn 6.17, as shown in Figure 6.7. The slope of c_{cr} is very sensitive to p_{cr} when $p_{cr} \leq 0.2$, and is nearly constant in the region of $0.2 \leq p_{cr} \leq 0.5$. Moreover, for small values of p_{cr}, the critical measured crack size, c_{cr}, is smaller than the critical true crack size, a_{cr}; this implies that critical situation may occur even though the measured crack size is smaller than a_{cr}.

When p_{cr} is fixed and a_{cr} is changed, the value of c_{cr} changes as shown by the family of c_{cr} versus a_{cr} curves in Figure 6.8. The relationship between c_{cr} and a_{cr} is linear with slope 1.0 and negative intercept, implying that the critical measured size is smaller than the critical true size.

To examine the effect of the NDE measurement parameters on the time-dependent structural reliability, the failure probabilities of a structural element similar to Vertical Beam No. 7 on the Emsworth Lock (cf Figure 5.1) are studied for five different cases, shown in Table 6.2. All reliability calculations were performed using the method in Section 5.3 and 5.4, assuming an AASHTO Category E detail. The first case represents the situation when no NDE is involved; here, the failure probability with respect to time is the same as predicted in Chapter 5. The other four cases assume that the structure is inspected at $T = 40$ years, with measured size $c = 2.54$ mm (0.1 in). The second case assumes that the gate is fully repaired, and the failure probability becomes very small immediately right after the repair. The damage process then develops subsequently with similar probabilistic characteristics as in the first case, except that the time shifts, as shown in Figure 6.9. The third to fifth cases assume that no repair action is taken. The third case represents an unbiased estimate of the true crack size and small variance (10% of the flange thickness), the fourth represents biased estimation, and the fifth represents an unbiased estimate but large variance (20% of the flange thickness), as indicated by the NDE parameters in Table 6.2. Based on Eqn 6.15, the CDFs of the true crack size at $t = 40$ years were estimated. These CDFs are normal distribution functions, and the possibility exists that the values of crack size fall outside the physical limit (0, flange thickness). To avoid this unreasonable situation, the CDFs were truncated and were later taken as the CDFs of the initial crack size for subsequent crack propagation analysis. The failure probabilities shown in Figure 6.9 for Cases 3-5 were updated assuming $a_{cr} = 4.8$ mm (0.1975 in). The failure probability for these three cases all are larger than the second case because no repair is performed. Among these three cases, the failure probability is the greatest when the scatter of NDE measurement is the largest (Case 5), and the smallest when the slope of the regression line of A on a_m is smaller than 1.0 (Case 4). The differences in failure probability with respect to different NDE measurement parameters are significant. Accordingly, the reliability forecast is strongly dependent on the quality of the data that describe the probabilistic characteristics of the NDE measurement.

6.4.2 Crack detection using UT

This section illustrates the effect of flaw detectability on reliability. The component inspected is ferritic steel. The crack growth law is

$$dA/dt = \nu C(Y\Delta\sigma\sqrt{\pi A})^m X(t) \tag{6.26}$$

where $C = 3.6\times10^{-10}$ (corresponding to English units), $Y = 1.12$, $m = 3$, $\Delta\sigma = 20$ ksi (138 MPa) (deterministic) (Barsom and Rolfe, 1987) and $\nu = 4$ cycle/hr. The noise

X is assumed to be an uncorrelated process, with a lognormal marginal distribution. The mean and standard deviation for $\log_{10} X$ are (0, 0.1). At the time of an inspection (at which t is set equal to zero), the crack size is a random variable with prior PDF $\mathcal{N}(15, 3)$ mm. The prior PDF and CDF of the initial crack size are plotted in Figure 6.10 and 6.11.

The NDE technique is UT with POD function defined by Eqn 6.14 (Heasler et al, 1993). Parameter a_1 is related to the FCP, and is non-dimensional and negative. Bigger absolute values of a_1 correspond to smaller FCP and smaller PODs for small cracks. The steepness of the POD is determined by a_2; the larger the a_2, the steeper the curve. Three POD curves are illustrated in Figure 6.12, PODs 1 and 2 have the same FCP, 0.15, but different steepness parameters. PODs 1 and 3 have the same steepness parameter but different FCPs. The parameters (a_1, a_2) are $(-1.7, 0.3/mm)$, $(-1.7, 0.15/mm)$, and $(-7, 0.3/mm)$, respectively. The first two POD curves are typical for UT inspection under controlled laboratory conditions of thermal fatigue cracks in clad ferritic steel components. (Heasler, et al, 1996); the first represents good inspection performance, and the second represents medium inspection performance. The third is an assumed curve, used simply to represent poor inspection performance. Assuming that no flaw was detected, the posterior CDFs and PDFs at $t = 0$ for three different POD curves are plotted in Figures 6.10 and 6.11 based on Eqns 6.24 and 6.22 as a comparison with the prior PDFs and CDFs. Note that the PDFs are shifted toward smaller flaw sizes because no flaw was detected. Taking these posterior PDFs as the PDFs for the initial crack size at $t = 0$, the posterior CDFs at $t = 10,000$ hr are calculated and are plotted in Figure 6.13, along with the CDF computed from the prior at $t = 0$. Crack growth statistics were computed using the procedure described in Section 4.1 in all cases. The crack size distributions at $t = 10,000$ hr clearly are affected by different values of FCP and steepness parameter, and differences between them increase when time increases. The posterior distribution of crack size converges to the prior distribution as the performance of the NDE technique becomes poorer (the worst one is POD 3). Although no flaw was detected at $t = 0$, there is still a high probability that a crack exits when the inspection performance is not informative (e.g., POD 3). In this case, the condition of the structure should not be judged simply from the inspection data, but also should be based on the prior distribution.

	Defect Characteristics	Sensitivity	Accessibility	Instrument Complexity	Operator Dependence
VT	surface underwater	good	fair	low	high
MT	surface sub-surface ferromagnetism underwater	excellent	fair	low	high
EC	surface sub-surface	good	excellent	medium	medium
UT	surface internal underwater	excellent	fair	medium	medium
RT	surface internal	fair	poor	medium	high
AE	growing defect	good	excellent	high	low

Table 6.1: NDE techniques

Case	inspection/repair	NDE measurement parameters		
		b_1	b_2	σ
1	no/no			
2	yes/full			
3	yes/no	0	1.0	0.0375
4	yes/no	0	0.7	0.0375
5	yes/no	0	1.0	0.075

Table 6.2: Parameters with respect to different NDE measurement errors

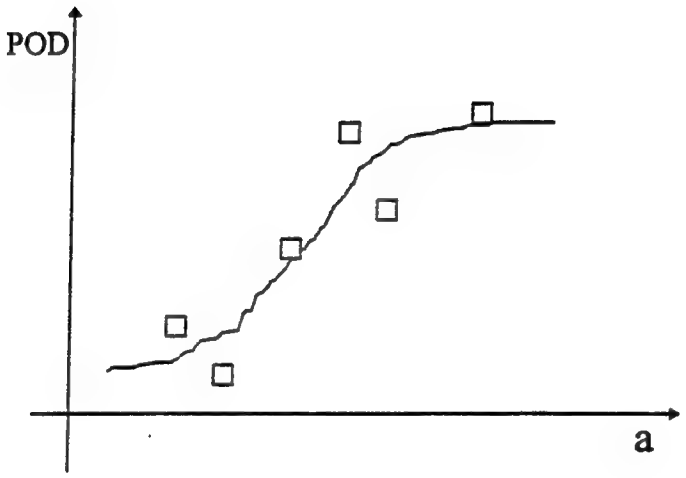

Figure 6.1: Fitting flaw detection data with a POD curve

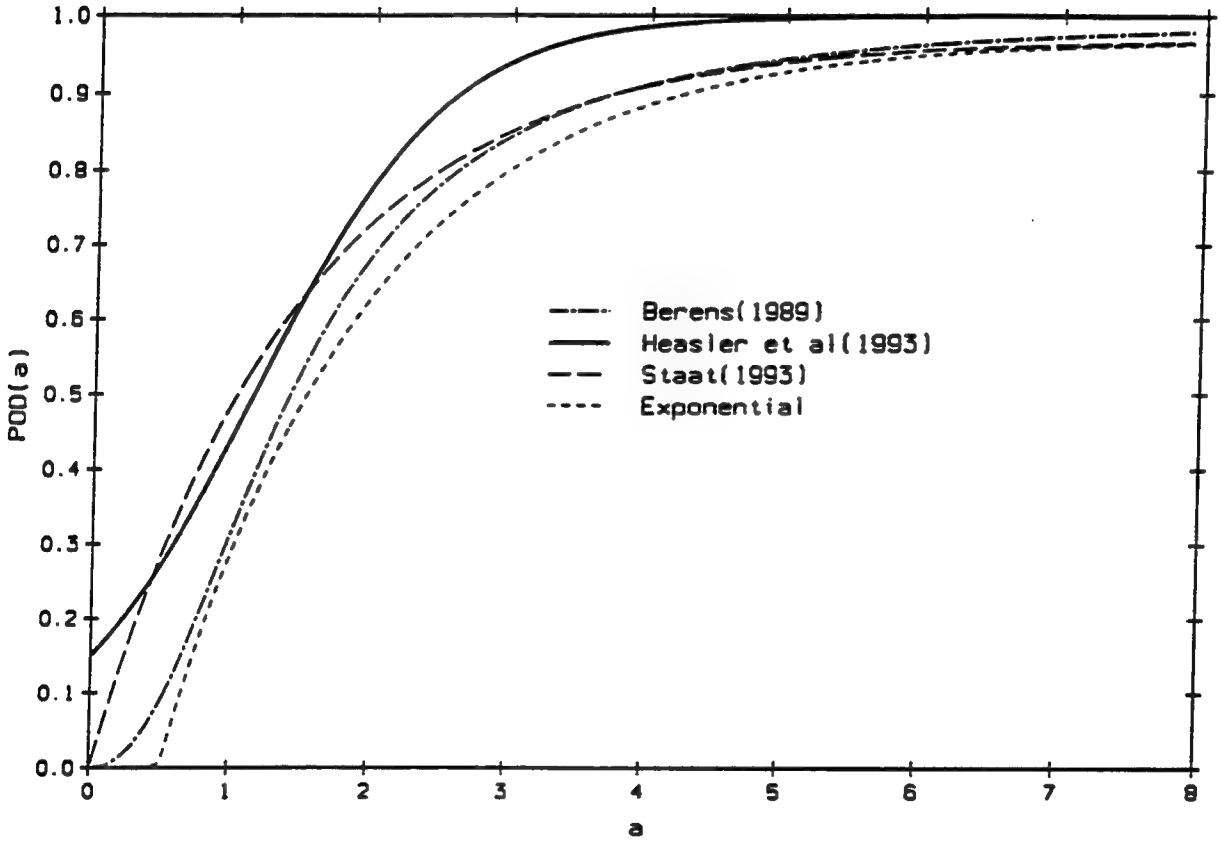

Figure 6.2: Illustration of different POD models

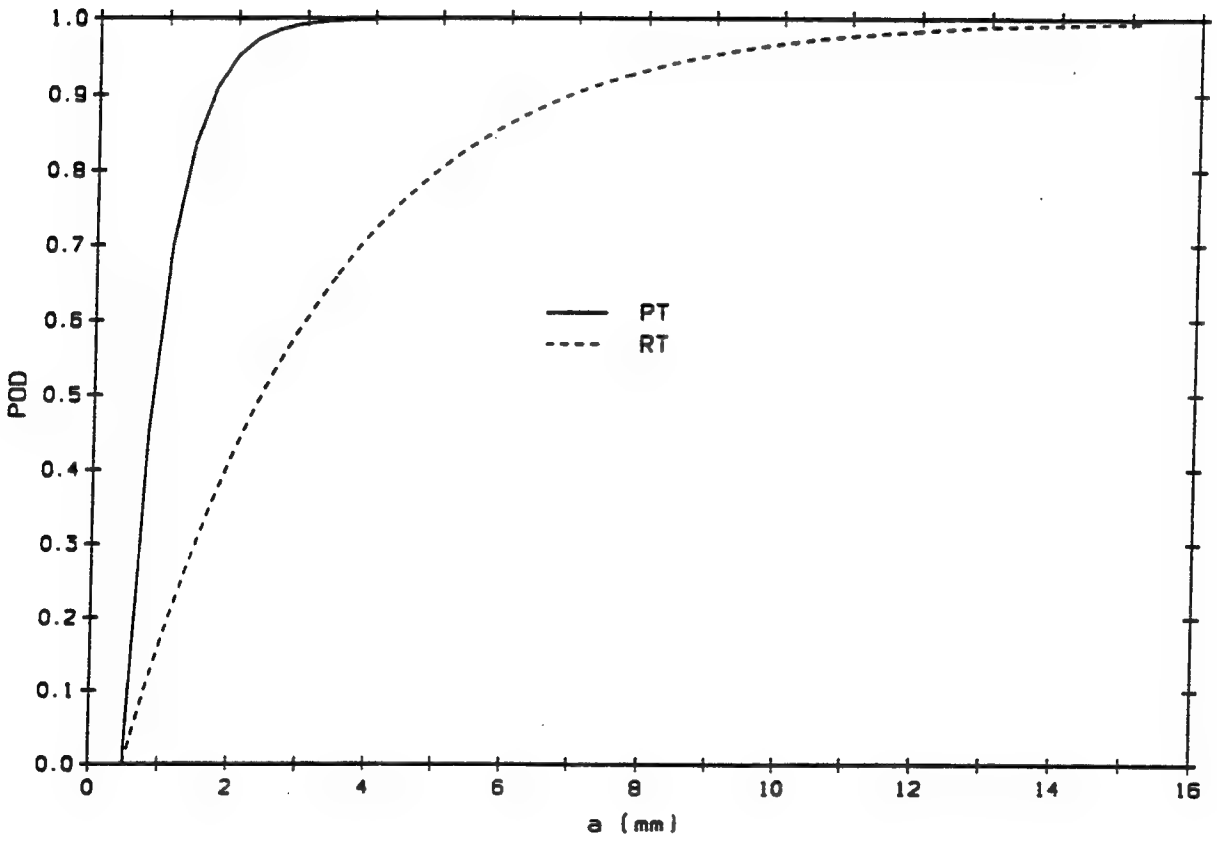

Figure 6.3: POD by PT and RT for aluminum specimens

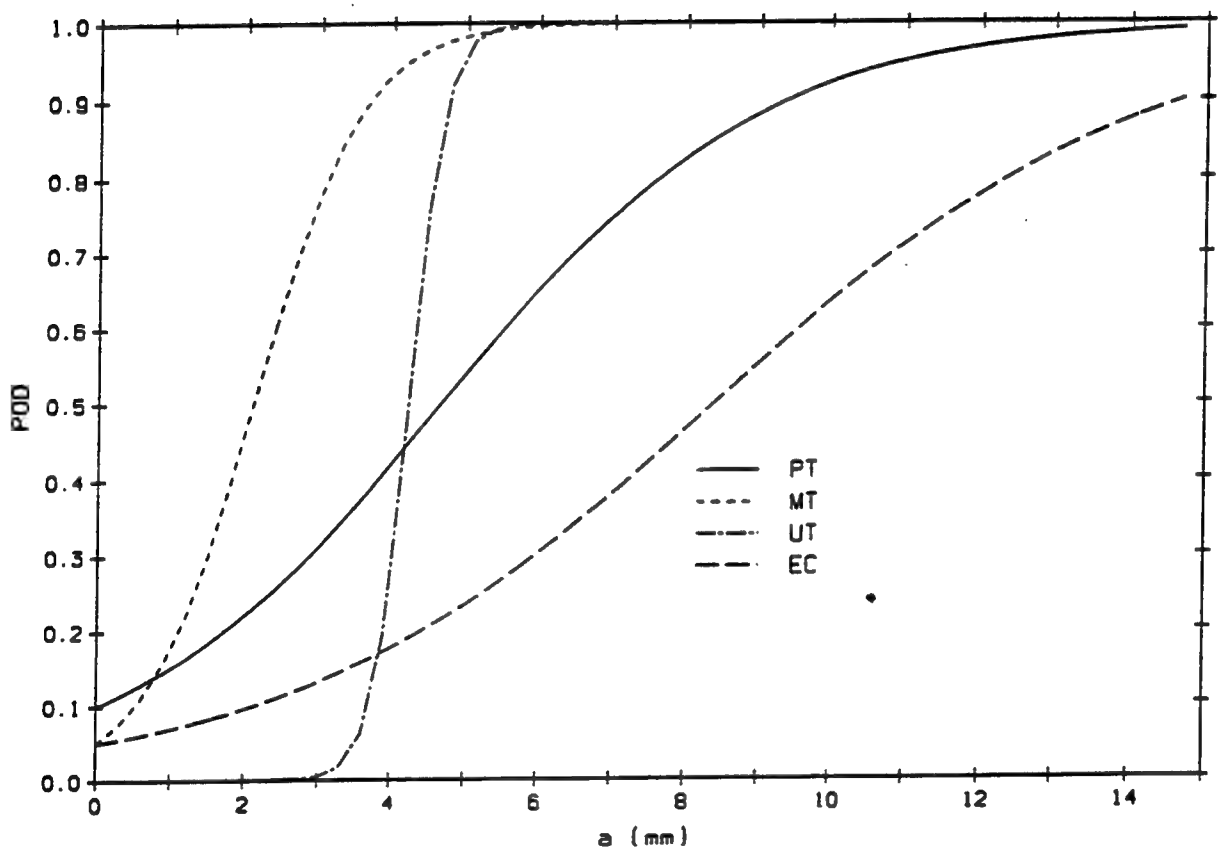

Figure 6.4: POD by NDT for steel specimens

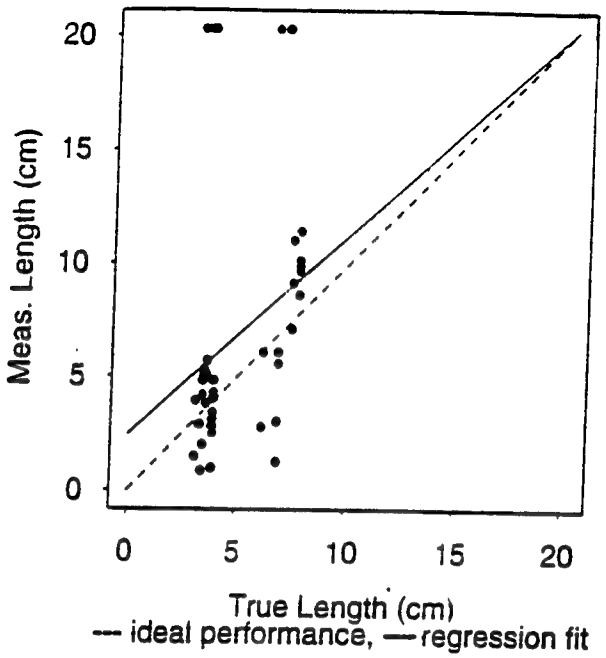

Figure 6.5: Measurement error using UT (Heasler and Doctor, 1996)

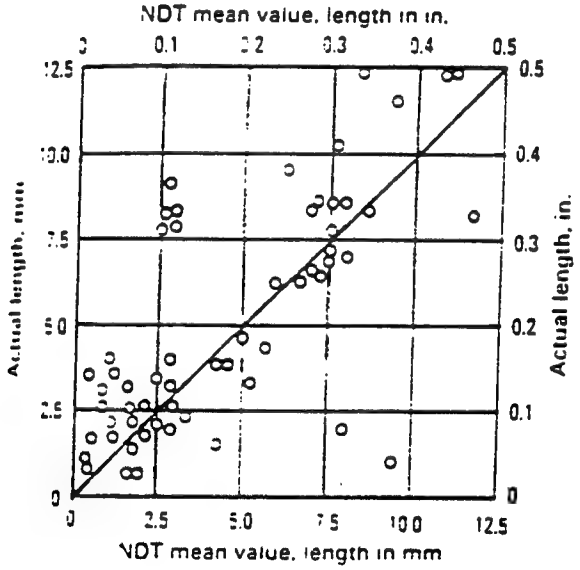

(b) RT

Figure 6.6: Measurement error using RT (Rummel et al, 1989)

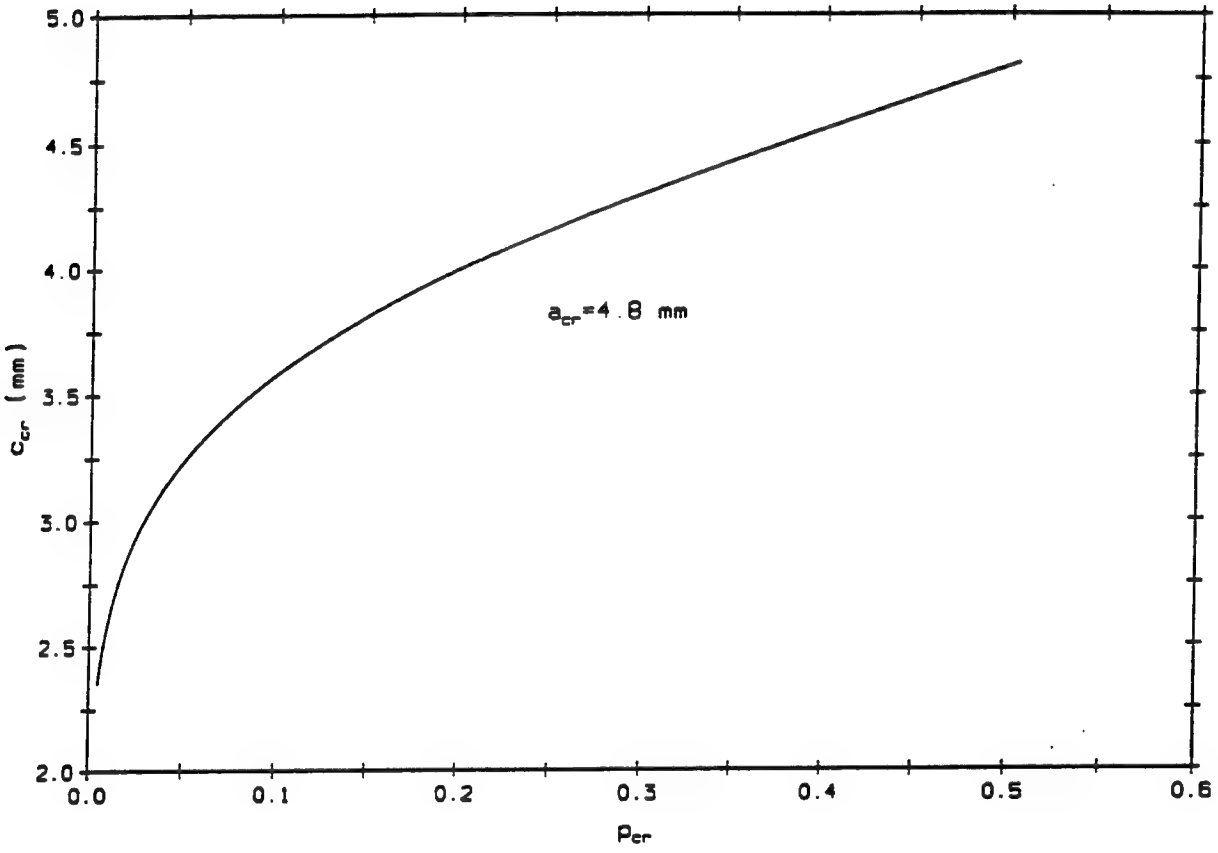

Figure 6.7: c_{cr} versus p_{cr}

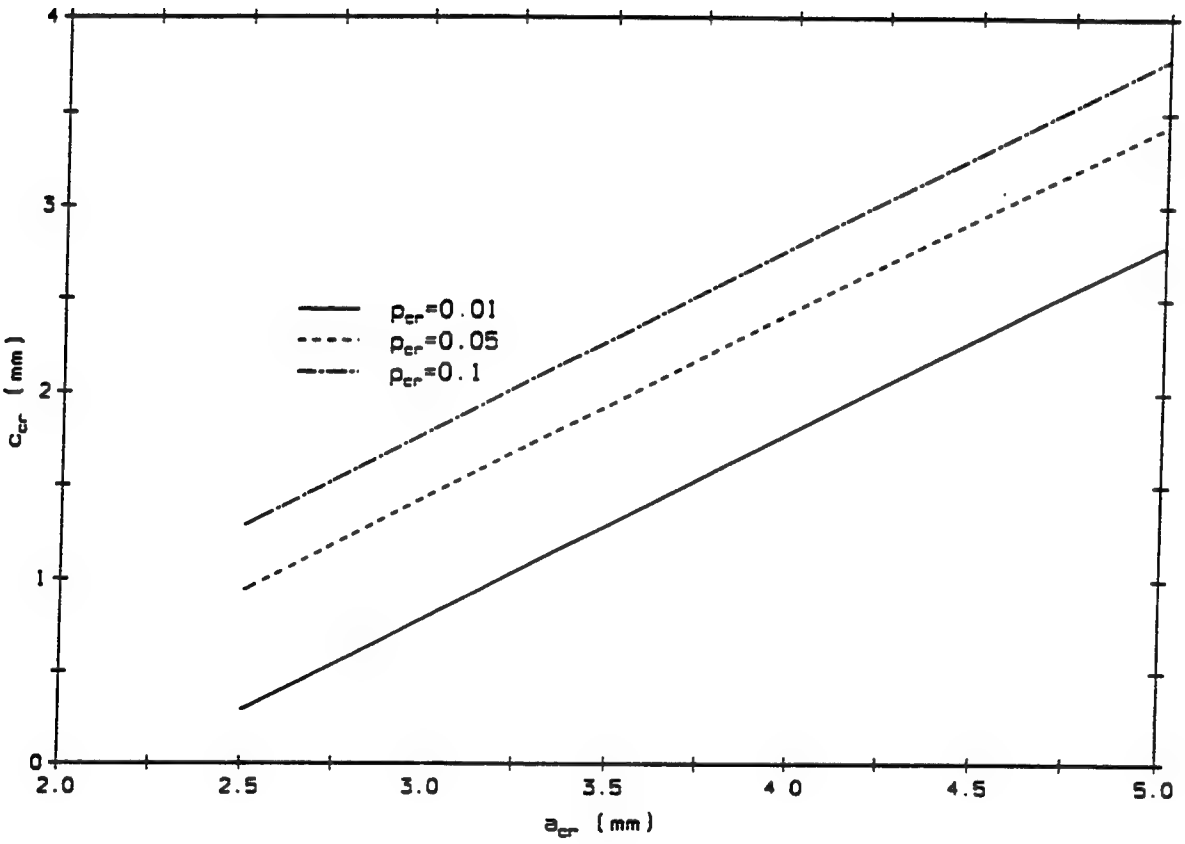

Figure 6.8: c_{cr} versus a_{cr}

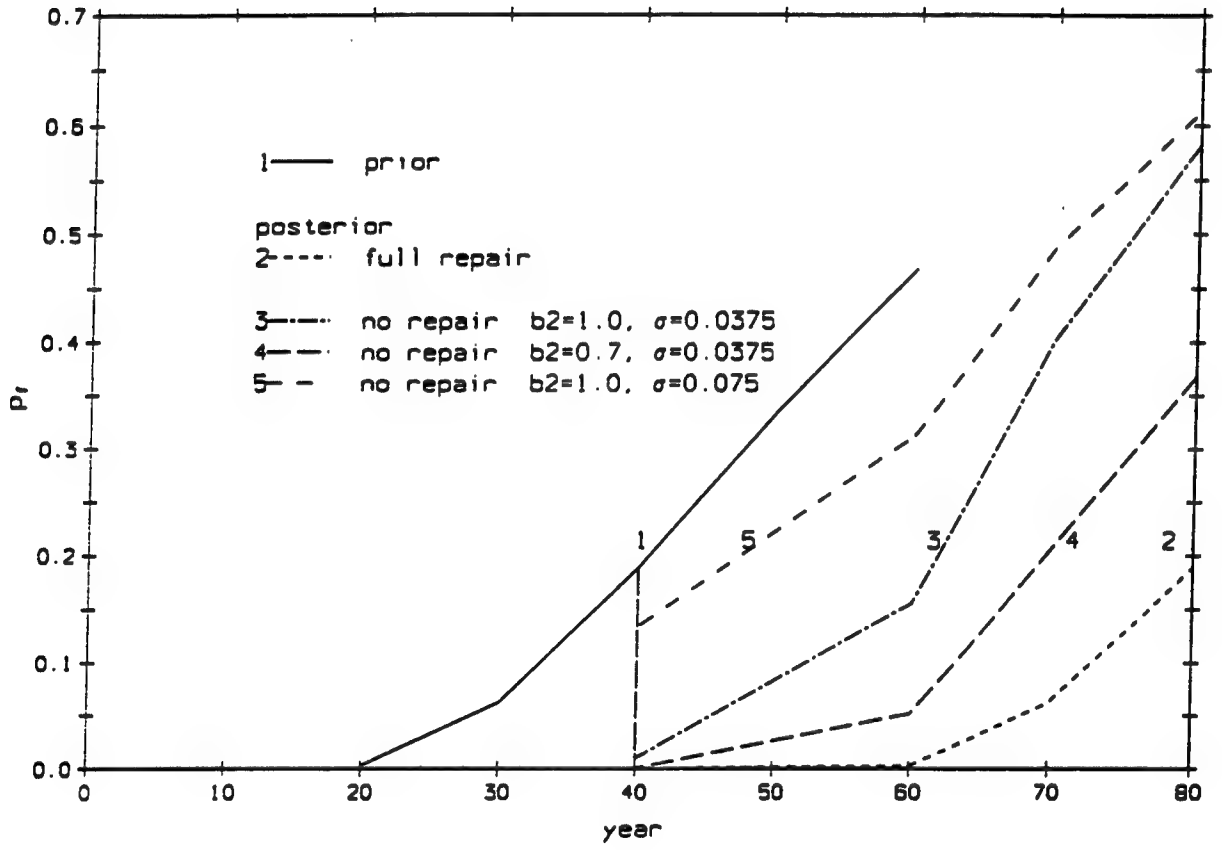

Figure 6.9: Updating failure probability

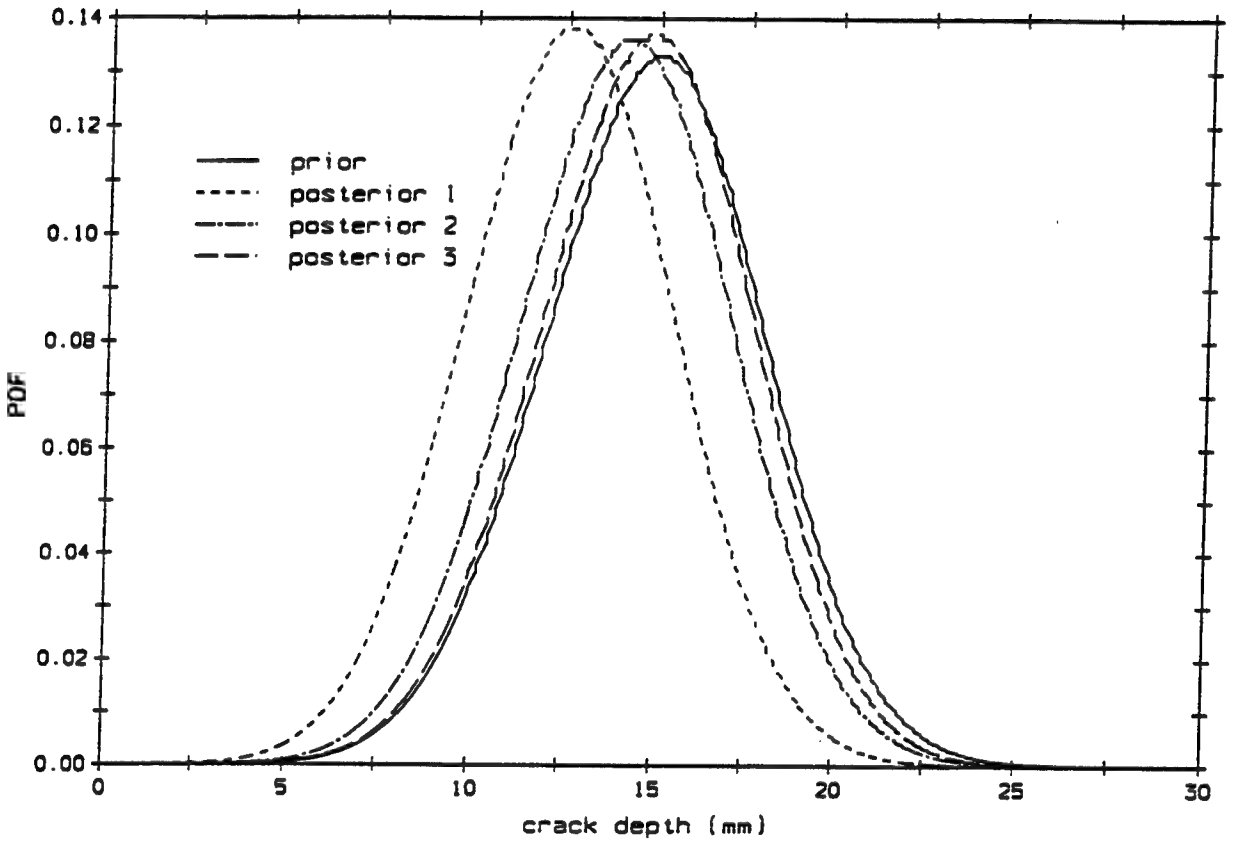

Figure 6.10: Prior and posterior PDFs of crack size at t=0

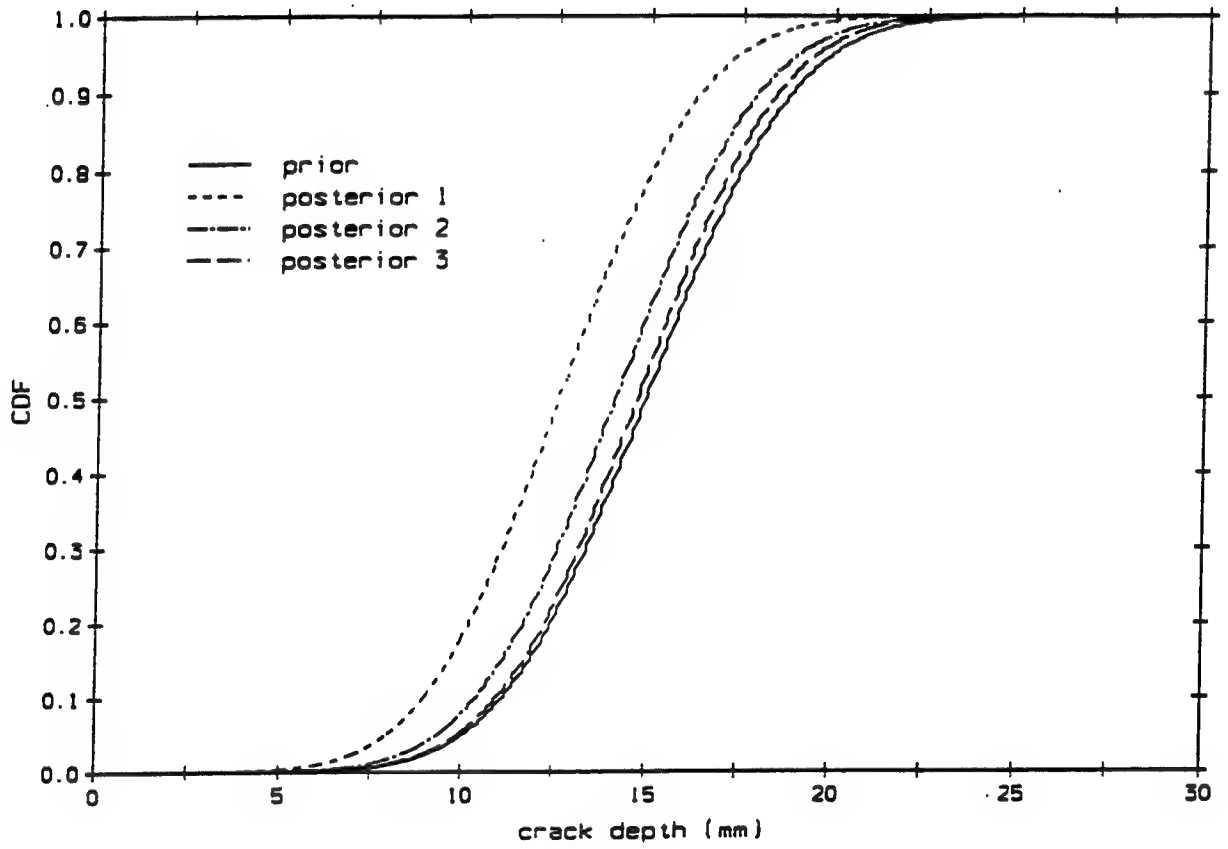

Figure 6.11: Prior and posterior CDFs of crack size at t=0

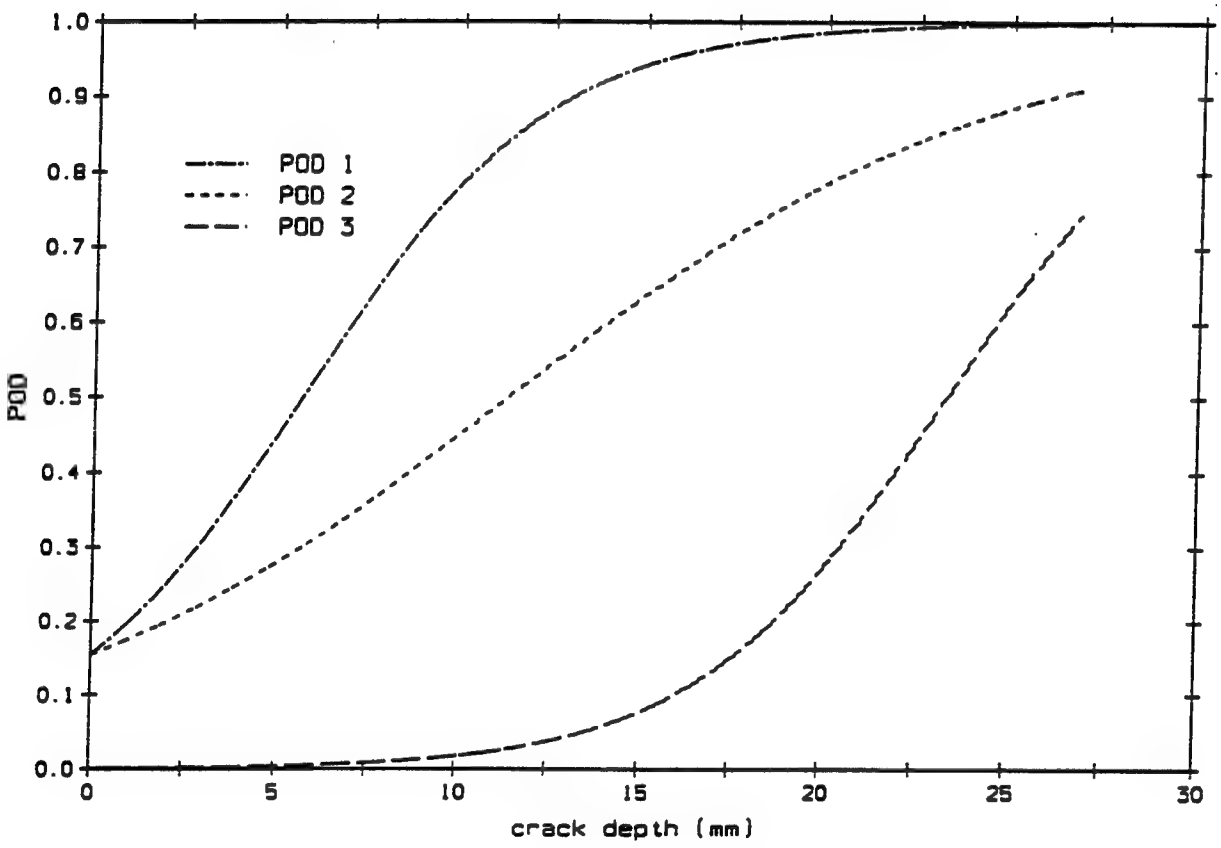

Figure 6.12: POD curves for UT

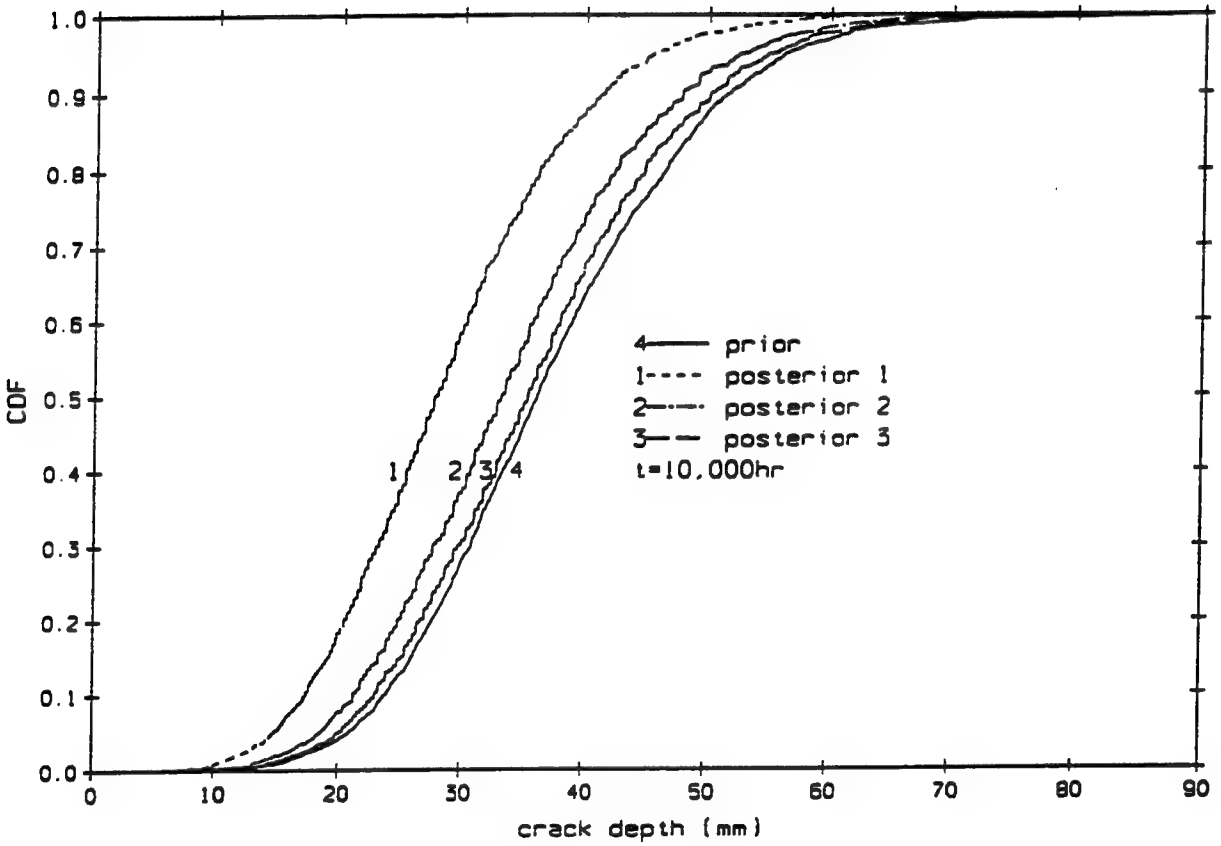

Figure 6.13: Prior and posterior CDFs of crack size at t=10,000hr

Chapter 7

Summary, Conclusions and Recommendations

7.1 Summary and conclusions

This report presented a methodology for evaluation of fatigue reliability in steel civil structures, taking into account uncertainties in materials, environment and loads. The role of NDE in reliability-based structural condition assessment was also investigated.

The crack growth model was formulated using linear fracture mechanics and Paris' law. The study of stochastic crack growth involved two aspects: the first is the model of uncertainty in fatigue crack growth under service load conditions, while the second is the efficient computation of the probability laws describing crack evolution in time. Contributions to the uncertainty in crack growth arise from the statistical nature of the crack growth law under constant amplitude loading and randomness in variable amplitude loading. The uncertainty in the crack growth under constant amplitude cycling is modeled by a time (or cycle)-dependent random noise process with arbitrary (generally non-Gaussian) marginal distribution and correlation structure. This random noise process depicts the inherent variability in crack growth that is apparent when growth is modeled by empirical laws such as the Paris equation. Wide-band variable amplitude random stresses are modeled by an approximation based on the rainflow analysis of stress cycle identification.

The proposed method generalizes the results of previous studies (e.g., Lin and Yang, 1985, Spencer, et al, 1989) by allowing specific marginal distributions and correlation structures of randomness in crack growth to be considered and loadings to

be modeled as random processes. The statistical nature of crack growth under constant amplitude loading is modeled by a combination of time domain and frequency domain analyses. The noise is transformed into a Gaussian process, which is generated by a system of time-dependent linear differential equations. These differential equations, along with the crack growth law, take the form of an Ito stochastic differential equation, which models the evolution of crack size as one component of a vector Markov diffusion process. The probability distribution of crack size at any time is then calculated analytically (e.g. numerical integration of the Fokker-Plank-Kolmogorov equation) or by simulation (e.g. Euler scheme). These approaches give consistent results. However, the simulation approach is more straightforward and computationally efficient. The method is validated by comparison of the results with previous studies by Lin and Yang (1985). Application of the method to the reliability analysis of crack growth in the steel miter gates at Emsworth Lock and Dam on the Ohio River results in predictions of fatigue damage that are consistent with the observed performance of the gates during a 60-year service life (Ellingwood, Zheng and Bhattacharya, 1996).

Deterministic models of crack growth rate based on parameters obtained from the customary regression analysis of $log da/dN$ on $log \Delta K$ can result in an unconservative estimate of crack growth. Stochastic models of crack growth compensate for this underestimation. Different correlation structures in the growth rate noise result in significant differences in the dispersion in crack size but relatively small differences in the mean value of crack size. Strongly correlated noise results in the highest dispersion, but slightly smaller mean value of crack size at a given time. The nature of this correlation may have a significant impact on estimated fatigue reliability. Whether taking the noise as a random variable is a more conservative approach to estimate the failure probability depends on the critical crack size. The probability distribution of crack size also depends strongly on what assumptions are made regarding the marginal distribution of the noise term when the correlation length is long. The effect of marginal distribution of the noise becomes negligible when its correlation length is very small, say 1% of the time of interest.

Crack growth due to wide-band stress processes is assessed by identifying the stress ranges from rainflow analysis, a method which has been widely applied in cycle counting for stress-life or strain-life approaches to fatigue analysis. Rainflow analysis of the stress history does not preserve the correlation structure of the process and the loading sequence is randomized. Therefore, samples of the stress range obtained from the rainflow analysis can be envisioned as samples from a stress process that is uncorrelated with respect to time. The marginal distribution of the stress process can be estimated from a long history of stress under the assumption that the process is ergodic. The validity and efficiency in computation of this approach is demonstrated

by comparison of the results with extensive direct simulation.

A sensitivity study was conducted to assess the relative importance of uncertainty in load and in crack growth noise on fatigue reliability. This study showed the variability of load can be a dominant factor for crack dispersion when the noise is an uncorrelated process. However, when the noise becomes highly correlated, its statistical characteristics become a critical factor.

Reliability-based condition assessment of structures in-service assisted by NDE was also investigated. Comparison of the performance of different NDE techniques in detecting and sizing cracks reveals that for surface or subsurface cracks, MT demonstrates good performance as far as detecting and sizing accuracy are concerned; for internal cracks, UT is a good choice for locating cracks, but may not be good at sizing crack depth. Considerable uncertainties are associated with both flaw detection and measurement, and these uncertainties have significant impact on the time-dependent reliability analysis. As a result, decisions regarding maintenance or repair should rely on the probabilistic information of the NDE technique, outputs of inspection and prior CDF of flaw size. If a flaw is detected, the critical measured size on which a repair action should be based is judged by the critical true crack size, the sizing accuracy and a target p_f. The critical measured size is a linear function of the critical true size, the slope and intercept being determined by the NDE sizing performance. The smaller the sizing bias and variance are, the closer the measured size approaches the true crack size. If no flaw is detected, any decision to repair should be based on the NDE detection performance, described by the POD curve. If the performance is perfect and no flaw is detected, no repair is needed. On the other hand, if the detection performance is poor, the decision to repair should be based on the prior PDF of crack size. If the POD is somewhere in between, the repair decision should depend on both the POD of the NDE methods and the prior PDF of crack sizes estimated from the stochastic crack growth model.

7.2 Recommendations

Studies of stochastic crack growth herein showed that different correlation structures and marginal distributions of the noise in crack growth rate result in estimates of failure probability that may differ significantly, particularly in the latter stage of service life. Fatigue experiments should be conducted to define the characteristics of the correlation and marginal distribution of the random crack growth rate noise term for different service environment and materials under constant amplitude loadings to improve the stochastic representation of service life.

The stochastic models of uncertainty in this study are applied to the deterministic crack growth rate model based on linear elastic fracture mechanics. A similar approach should be investigated for the cases when plastic fracture mechanics model might be used (e.g., large scale yielding of the region around the cracks may occur when unusual loadings, such as impact loads due to vessel collision, contribute significantly to structural deterioration). More complex loadings may be investigated through stochastic finite element analysis.

This study focused on stochastic fatigue damage from a single crack due to mechanical fatigue. Interaction of fatigue damage with other factors, such as corrosion, requires further investigation. Since most civil structures are highly redundant systems, the presence of one crack does not necessarily lead to failure of the whole structure. A study of the interaction of multiple cracks based on stochastic finite element analysis and system reliability analysis is recommended.

Although POD and crack sizing accuracy play an important role in condition assessment, data to describe POD and sizing error for common NDE techniques, especially MT and PT, for fatigue field service conditions and different steel structural details are limited. A more systematic study should be conducted to identify probabilistic characteristics of commonly used NDE techniques for detection and measurement of cracks in typical structural details in different field conditions. Reliability analysis requires that the regression analysis on sizing be conducted in terms of A on A_m, not vice versa. The probability of detection and sizing error should be presented as a function of absolute size instead of relative size. False call probabilities should be determined.

In service condition assessment and maintenance policies for civil facilities can be optimized using the time-dependent fatigue reliability analysis tools presented herein. Such optimization studies require accurate estimates of fatigue probabilities and costs of inspection, maintenance and repair, and functional failure. While this research focused on the first aspect, efforts also should be made to define these costs. The availability of this information would lead to improved facility management policies.

Bibliography

[1] American Association of State Highway and Transportation Officials (AASHTO), *Standard Specifications for Highway Bridges*, 14th ed., AASHTO, Washington, D.C, 1989.

[2] American Institute of Steel Construction (AISC), *Allowable Stress Design Manual of Steel Construction*, 9th ed., AISC, Chicago, IL, 1989.

[3] ASCE, Committee on Fatigue and Fracture Reliability of the Structural Division, "Fatigue Reliability 1-4", *Journal of the Structural Division*, ASCE, Vol. 108, No. ST1, pp. 3-88, January 1982.

[4] ASM, *Metals Handbook*, 9th ed., ASM International, Vol.17, 1989.

[5] Ang, A.H. and Tang, W.H., *Probability Concepts in Engineering Planning and Design, Vol I–Basic Principles*, John Wiley & Sons, Inc, New York, NY, 1975.

[6] Arnold, L., *Stochastic Differential Equations: Theory and Applications*, John Wiley & Sons, Inc, New York, NY, 1974.

[7] Barsom, J.M. and Rolfe, S. T., *Fracture and Fatigue Control in Structures: Applications of Fracture Mechanics*, 2nd ed., Prentice-Hall, Inc., Englewood Cliffs, New Jersey, 1987.

[8] Basquin, O.H., "The Exponential Law of Endurance Tests", *Proceedings of the American Society for Testing and Materials*, ASTM, Vol 10, pp. 625-630, 1910.

[9] Benjamin, J.R. and Cornell, C.A., *Probability, Statistics and Decision for Civil Engineers*, McGraw-Hill Publishing Co., New York, NY, 1970.

[10] Berens, A.P., "NDE Reliability Analysis", *Metals Handbook*, 9th ed., ASM International, Vol.17, pp. 689-701, 1989.

[11] Bowen, W.M., Heasler, P.G. and White, R.B., "Evaluation of Sampling Plans for In-service Inspection of Steam Generator Tubes", NUREG/CR-5161, U.S. Nuclear Regulatory Commission, Washington, DC, 1989.

[12] Box, G.E.P. and Draper, N.R., *Empirical Model-Building And Response Surfaces*, John Wiley & Sons, Inc, New York, NY, 1987.

[13] Chase, S.B., "A New Fatigue Crack Detection System", *Structural Materials Technology: an NDT conference*, Atlantic City, New Jersey, Technomic Pub. Co., pp. 334-338, 1994.

[14] Clark, W.G., Jr. and Hudak, S.J. Jr., "Variability in Fatigue Crack Growth Rate Testing", *Journal of Testing and Evaluation*, ASTM, Vol. 3, No. 6, pp. 454-476, 1975.

[15] Cramer, H. and Leadbetter, M.R., *Stationary and Related Stochastic Processes*, John Wiley & Sons, Inc., New York, NY, 1967.

[16] Coffin, L.F., "A Study of the Effects of Cyclic Thermal Stresses on a Ductile Metal", *Transactions of the American Society of Mechanical Engineers*, ASME, Vol. 76, pp. 931-950, 1954.

[17] Ditlevsen, O, "Random Fatigue Crack Growth–a First Passage Problem", *Engineering Fracture Mechanics*, Pregamon Press Ltd, Vol. 23, No. 2, pp. 467-477, 1986.

[18] Dowling, N.E., "Fatigue Life Prediction for Complex Load Versus Time Histories", *Transactions of the ASME*, ASME, Vol. 105, pp. 206-214, July 1983.

[19] Dowling, N.E., "Fatigue Failure Predictions for Complicated Stress-strain Histories", *Journal of Materials*, ASTM, Vol. 7, No. 1, pp. 71-87, 1972.

[20] Dowling, N.E. and Begley, J.A., "Fatigue Crack Growth During Gross Plasticity and the J-integral", *Mechanics of Crack Growth*, ASTM, Special Technical Publication 590, pp. 82-103, 1976.

[21] Dowling, N.E., "Crack Growth During Low Cycle Fatigue of Smooth Axial Specimens", *Cyclic Stress-Strain and Plastic Deformation Aspects of Fatigue Crack Growth*, ASTM, Special Technical Publication 637, pp. 97-121, 1977.

[22] Downing, S.D. and Socie, D.F., "Simple Rainflow Counting Algorithms", *International Journal of Fatigue*, Butterworth & Co Ltd, Vol. 4, pp. 31-40, January 1982.

[23] Elber, W., "The Significance of Fatigue Crack Closure", *Damage Tolerance in Aircraft Structures*, ASTM, Special Technical Publication 486, pp. 230-242, 1971.

[24] Elber, W., "Fatigue Crack Closure under Cyclic Tension", *Engineering Fracture Mechanics*, Pregamon Press Ltd, Vol. 2, pp. 37-45, 1970.

[25] Elderton, W.P. and Johnson, N.L., *Systems of Frequency Curves*, Cambridge University Press, Cambridge, UK, 1969.

[26] Ellingwood, B., Zheng, R. and Bhattacharya, B., *Reliability-based Condition Assessment of Steel Miter Gates*, Final Report Submitted to Black and Veatch Engineers, May 1996.

[27] Forman, R. G., Kearney, V. E. and Engle, R. M., "Numerical Analysis of Crack Propagation in Cyclic-loaded Structures", *Journal of Basic Engineering*, ASME, Vol. 89, No. 3, pp. 459-464, 1967.

[28] Fuchs, H.O., Nelson, D.V., Burke, M.A. and Toomary, T.L., "Shortcuts in Cumulative Damage Analysis", *Fatigue under Complex Loading: Analyses and Experiments, Advance in Engineering*, SAE, Vol 6, pp. 145-162, 1977.

[29] Ghorbanpoor, A., "An Assessment of the Current Acoustic Emission Evaluation of Steel Bridges", *Structural Materials Technology: an NDT conference*, Atlantic City, New Jersey, Technomic Pub. Co., pp. 114-118, 1994.

[30] Grigoriu, M., *Applied Non-Gaussian Process.* PTR Prentice Hall, Englewood Cliffs, NJ, 1995.

[31] Grigoriu, M., "Crossing of Non-Gaussian Translation Process", *Journal of Engineering Mechanics*, ASCE, Vol 110, No 4, pp. 610-620, 1984.

[32] Hartle, R., Amrhein, W. and Wilson, K. III et al, *Bridge Inspector's Training Manual 90*, FHWA-PD-91-015, National Technical Information Service, Springfield, Virginia, 1991.

[33] Heasler, P. G. and Doctor, S. R., *Piping Inspection Round Robin*, NUREG/CR-5068, US Nuclear Regulatory Commission, Washinton, D.C, 1996.

[34] Heasler, P. G., Taylor, T.T., Spanner, J.C. et al., *Ultrasonic Inspection Reliability for Intergranular Stress Corrosion Cracks*, NUREG/CR-4908, US Nuclear Regulatory Commission, Washington, D.C, 1990.

[35] Heasler, P.G., Taylor, T.T. and Doctor, S.R., *Statistically Based Reevaluation of PISC-II Round Robin Test Data*, NUREG/CR-5410, US Nuclear Regulatory Commission, Washington, DC, 1993

[36] Hibberd, R. D. and Dover, W. D., "The Analysis of Random Load Fatigue Crack Propagation", *Advances in Fracture Research, Fracture 77, ICF-4, Proceedings of the 4th International Conference on Fracture*, University of Waterloo, Canada, Vol. 2B, pp. 1187-1194, June 1977.

[37] Hovey, P. W., Gallagher, J. P. and Berens, A. P., "Estimating the Statistical Properties of Crack Growth for Small Cracks", *Engineering Fracture Mechanics*, Pregamon Press Ltd, Vol. 18, No. 2, pp. 285-294, 1983.

[38] Irwin, G. R., "Analysis of Stresses and Strains Near the End of a Crack Traversing a Plate", *Journal of Applied Mechanics*, ASME, Vol. 24, pp. 361-364, 1957.

[39] Kishi, T., "Nondestructive Evaluation of Civil Structures in Japan", *Proceedings of the International Workshop on Nondestructive Evaluation for Performance of Civil Structures*, California, pp 63-79, 1988.

[40] Kloeden, P.E. and Platen, E., *Numerical Solution of Stochastic Differential Equations*, Springer-Verlag Berlin Heidelberg, 1992.

[41] Lin, Y.K. and Yang, J.N., "A Stochastic Theory of Fatigue Crack Propagation", *AIAA Journal*, AIAA, Vol. 23, No.1, pp. 117-124, 1985.

[42] Lin, Y.K., *Probabilistic Theory of Structural Dynamics*, McGraw Hill, 1967.

[43] Lutes, L. D., Corazao, J., Hu, S. J. and Zimmerman, J., "Stochastic Fatigue Damage Accumulation", *Journal of Structural Engineering*, ASCE, Vol. 110, No. 11, pp. 2585-2601, 1984.

[44] Madsen, H.O., "Random Fatigue Crack Growth and Inspection", *Structural Safety and Reliability, Proceedings of ICOSSAR'85*, Kobe, Japan, Elsevier, Amsterdam, Netherlands, Vol. 1, pp. 475-484, 1985.

[45] Madsen, H.O., Krenk, S. and Lind, N.C., *Methods of Structural Safety*, Prentice-Hall, Englewood Cliffs, New Jersey, 1986.

[46] Manson, S. S., "Behavior of Materials under Conditions of Thermal Stress", *National Advisory Commission on Aeronautics: Report 1170*, Lewis Flight Propulsion Laboratory, Cleveland, 1954.

[47] Matsuishi and Endo, "Fatigue of Metals Subjected to Varying Stress", Paper Presented to Japan Society of Mechanical Engineers, Fukuoka, Japan, March 1968.

[48] Miner, M.A., "Cumulative Damage in Fatigue", *Journal of Applied Mechanics*, ASME, Vol 12, pp. 159-164, 1945.

[49] Myers, R.H., *Response Surface Methodology*, Allyn and Bacon, Inc, Boston, MA, 1971.

[50] Nelson, D.V., "Review of Fatigue-crack-growth Prediction Methods", *Experimental Mechanics*, Society for Expeimental Stress Analysis, pp. 41-49, February 1977.

[51] Nelson, D.V. and Fuchs, H.O., "Predictions of Cumulative Fatigue Damage Using Condensed Load Histories", *Fatigue under Complex Loading: Analyses and Experiments, Advance in Engineering*, SAE, Vol. 6, pp. 163-187, 1977.

[52] Ortiz, K. and Kiremidjian, A.S., "A Stochastic Model for Fatigue Crack Growth Rate Data", *Journal of Engineering for Industry*, Transactions of the ASME, Vol. 109, pp. 13-18, 1987.

[53] Packman, P. F., Pearson, H. S., Owens, J. S. and Young, G., "Definition of Fatigue Cracks Through Nondestructive Testing", *Journal of Materials*, ASTM, Vol. 4, pp. 666-700, 1969.

[54] Paris, P. C., Gomez, M. P. and Anderson, W. P., "A Rational Analytic Theory of Fatigue", *The Trend in Engineering*, Office of Engineering Research, University of Washington, Vol. 13, 1961, pp. 9-14.

[55] Parzen, E., *Stochastic Processes*, Holden-Day, Inc., San Francisco, California, 1965.

[56] Rashe, D. and Morrow, J., "Mechanics of Materials in Low Cycle Fatigue Testing", Manual on *Low Cycle fatigue Testing*, STP 465, ASTM, Philadelphia, PA, 1969.

[57] Rice, J. R., "A Path Independent Integral and the Approximate Analysis of Strain Concentrations by Notches and Cracks", *Journal of Applied Mechanics*, ASME, Vol 35, pp. 379-386, 1968.

[58] Rice, S. O., "Mathematical Analysis of Random Noise", *Bell System Technical Journal*, Vol. 23, 1944 and Vol. 24, 1945, Reprinted in *Selected Papers on Noise and Stochastic Processes*, Dover Publications, Inc., New York, N.Y., pp. 123-244, 1954.

[59] Rummel, W.D., Hardy, G.L. and Cooper, T.D., *Metals Handbook*, 9th ed., ASM International, Vol.17, pp. 674-688, 1989.

[60] Shah, V.N. Smith, S.K. and Sinha, U.P., "Insight for Aging Management of Light Water Reactor Components-steel Containment." NUREG/CR-5314, Vol. 5, US Nuclear Regulatory Commission, Washington, DC, 1994.

[61] Shinozuka and Deodatis, "Simulation of Stochastic Processes by Spectral Representation", *Applied Mechanics Reviews*, ASME, Vol. 44, No 4, pp. 191-203, April 1991.

[62] Sobczyk, K., and Spencer, B.F. Jr., *Random Fatigue: From Data to Theory*, Academic Press, Inc., San Diego, CA, 1992.

[63] Sobczyk, K., *Stochastic Differential Equations, with Applications to Physics and Engineering*, Kluwer Academic Publishers, Netherlands, 1991.

[64] Soong, T.T. and Grigoriu, M., *Random Vibration of Mechanical And Structural Systems*, P T R Prentice Hall, Englewood Cliffs, New Jersey, 1993.

[65] Spencer, B.F., Jr. and Tang, J., "Markov Process Model for Fatigue Crack Growth", *Journal of Engineering Mechanics*, ASCE, Vol. 114, No. 12, pp. 2134-2157, 1988.

[66] Spencer, B.F., Jr., Tang, J. and Artley, M.E., "A Stochastic Approach to Modeling Fatigue Crack Growth", *Journal of the AIAA*, AIAA, Vol 27, No 11, pp. 1628-1635, 1989.

[67] Staat, M., "Sensitivity of and Influences on the Reliability of an HTR-module Primary Circuit Pressure Boundary", Trans., 12th International Conference on Structural Mechanics in Reactor Tech., Elsevier, Amsterdm, the Netherlands, Vol. M., pp. 147-152, 1993.

[68] Suresh, S., *Fatigue of Materials*, Cambridge University Press, Cambridge, UK, 1991.

[69] Tsai, C. H. and Wu, W. F., "Application of Probabilistic Fracture Mechanics to Risk Assessment of Pressure Vessels", Trans., 12th International Conference on Structural Mechanics in Reactor Tech., Elsevier, Amsterdm, the Netherlands, Vol. M., pp. 135-140, 1993.

[70] Tucker, M. J., Challenor, P. G. and Carter, D. J. T., "Numerical Simulation of A Random Sea: A Common Error and Its Effect Upon Wave Group Statistics", *Applied Ocean Research*, CML publications, England, Vol. 6, No. 2, pp. 118-122, 1984.

[71] Ude, T., "Statistics by Simulation from Second-order Models for Responses of Floating Structures", Proceedings of the 10th ASCE Engineering Mechanics Special Conference, Boulder, Co., pp. 1292-1295, May 1995.

[72] U.S. Army Corps of Engineers, Waterways Experiment Station (1995), *Loading Cycles for the Fatigue Reliability Analysis of Miter Gates*, Technical Report ITL-95, Washington, D.C., Sept. 1995.

[73] U.S. Army Corps of Engineers, *Structural Inspection and Evaluation of Existing Welded Lock Gates*, Technical Letter No. 1110-2-346, Washington, D.C., Sept. 1993.

[74] U.S. Army Corps of Engineers, *Reliability Assessment of Navigation Structures*, Technical Letter No. 1110-2-532, Washington, D.C., May 1992.

[75] Veers, P.S., *Fatigue Crack Growth Due to Random Loading*, SANDIA Report 87-2039, Sandia National Laboratory, Albuquerque, New Mexico, 1987.

[76] Virkler, D.A., Hillberry, B.M. and Goel, P.K., "The Statistical Nature of Fatigue Crack Propagation". *Journal of Engineering Materials and Technology*, ASME, Vol. 101, pp. 148-153, 1979.

[77] Walker, K., "The Effect of Stress Ratio During Crack Propagation and Fatigue for 2024-T3 and 7075-T6 Aluminum", *Effects of Environment and Complex Load History for Fatigue Life*, ASTM, Special Technical Publication 462, pp. 1-14, 1970.

[78] Wheeler, O. E., "Spectrum Loading and Crack Growth", *Journal of Basic Engineering*, ASME, Vol. 94, pp. 181-186, 1972.

[79] Winterstein, S. R., "Nonlinear Vibration Models for Extremes and Fatigue", *Journal of Engineering Mechanics*, ASCE, Vol. 114, No. 10, pp. 1772-1790, 1988.

[80] Wirsching, P.H. and Light, M.C., "Fatigue under Wide Band Random Processes", *Journal of the Structural Division*, ASCE, Vol. 106, No. ST7, pp.1598-1607, 1980.

[81] Yang, J.N., Salivar, G.C. and Annis, C.G., "Statistical Modeling of Fatigue Crack Growth in a Nickel-based Superalloy", *Engineering Fracture Mechanics*, Pregamon Press Ltd, Vol. 18, No 2, pp. 257-270, 1983.

[82] Yeh, J.C. Enneking, J.A. and Tsai, C.L., "Study of Acoustic Emission Characteristics for Fracture Assessment of Structural Weldment", *Review of Progress in Quantitative Nondestructive Evaluation*, Plenum Press, New York, Vol. 13, pp. 477-483, 1994.

[83] Yen, B.T., Huang, T., Lai, L.Y. and Fisher, J.W., *Manual for Inspecting Bridges for Fatigue Damage Conditions*, Dept. of Civil Engineering Report No 511-1, Lehigh University, Bethlehem, PA, 1990.

REPORT DOCUMENTATION PAGE

Form Approved
OMB No. 0704-0188

1. AGENCY USE ONLY *(Leave blank)*	2. REPORT DATE	3. REPORT TYPE AND DATES COVERED
	September 1998	Final report

4. TITLE AND SUBTITLE
Stochastic Fatigue Crack Growth in Steel Structures Subjected to Random Loading

5. FUNDING NUMBERS

6. AUTHOR(S)
Ruohua Zheng, Bruce R. Ellingwood

7. PERFORMING ORGANIZATION NAME(S) AND ADDRESS(ES)
The Johns Hopkins University
Department of Civil Engineering
Baltimore, MD 21218

8. PERFORMING ORGANIZATION REPORT NUMBER

9. SPONSORING/MONITORING AGENCY NAME(S) AND ADDRESS(ES)
U.S. Army Engineer Waterways Experiment Station,
3909 Halls Ferry Road, Vicksburg, MS 39180-6199;
U.S. Army Corps of Engineers, Washington, DC 20314-1000

10. SPONSORING/MONITORING AGENCY REPORT NUMBER
Contract Report ITL-98-1

11. SUPPLEMENTARY NOTES
Available from National Technical Information Service, 5285 Port Royal Road, Springfield, VA 22161.

12a. DISTRIBUTION/AVAILABILITY STATEMENT
Approved for public release; distribution is unlimited.

12b. DISTRIBUTION CODE

13. ABSTRACT ***(Maximum 200 words)***

Fatigue crack growth can be a significant problem in steel structures that are subjected to a large number of repeated load cycles during their service lives. Uncertainty in fatigue behavior arises from the random nature of the service load, environmental conditions, material properties and other factors. Stochastic approaches to model this uncertainty can lead to improved fatigue-resistant design or in-service inspection and maintenance policies. This report generalizes the stochastic model of uncertainty in crack growth under constant amplitude loading by introducing a random noise process with arbitrary (generally non-Gaussian) marginal distribution and correlation structure. A computationally efficient method based on the rainflow method of stress identification is proposed for handling broad-band stress processes in analyzing stochastic crack propagation. The impact of uncertainty in flaw detection and measurement capabilities on in-service structural condition assessment and reliability-based service life prediction also is investigated.

The proposed method is applied in a time-dependent reliability analysis of a steel miter gate at the Emsworth Lock and Dam that suffered severe deterioration from corrosion-fatigue. The predicted fatigue behavior is consistent with observations of damage over a sixty-year service life, providing some confirmation of the use of stochastic fatigue analysis in structural condition assessment and service life prediction.

14. SUBJECT TERMS

Broad-band stress	Rainflow method	Stochastic methods
Crack growth	Random loads	Stress identification
Fatigue	Random noise	Time-dependent
Flow detector	Steel structures	Uncertainty

15. NUMBER OF PAGES
157

16. PRICE CODE

17. SECURITY CLASSIFICATION OF REPORT	18. SECURITY CLASSIFICATION OF THIS PAGE	19. SECURITY CLASSIFICATION OF ABSTRACT	20. LIMITATION OF ABSTRACT
UNCLASSIFIED	UNCLASSIFIED		